Fall 1994

Passive radiosonde transducer design for remote pressure sensing applications

Yang Gao
New Jersey Institute of Technology

Copyright Warning & Restrictions

The copyright law of the United States (Title 17, United States Code) governs the making of photocopies or other reproductions of copyrighted material.

Under certain conditions specified in the law, libraries and archives are authorized to furnish a photocopy or other reproduction. One of these specified conditions is that the photocopy or reproduction is not to be "used for any purpose other than private study, scholarship, or research." If a, user makes a request for, or later uses, a photocopy or reproduction for purposes in excess of "fair use" that user may be liable for copyright infringement,

This institution reserves the right to refuse to accept a copying order if, in its judgment, fulfillment of the order would involve violation of copyright law.

Please Note: The author retains the copyright while the New Jersey Institute of Technology reserves the right to distribute this thesis or dissertation

Printing note: If you do not wish to print this page, then select "Pages from: first page # to: last page #" on the print dialog screen

ABSTRACT

PASSIVE RADIOSONDE TRANSDUCER DESIGN FOR REMOTE PRESSURE SENSING APPLICATIONS

by
Yang Gao

Intracranial pressure can be measured to accuracies within 1 milliTorr using passive microtransponders that are micromachined using silicon as a base technology. These microtransponders can operate with either a dual-oscillator or a phase-locked loop frequency scanned control system.

The current work describes the design of a totally implantable microsensor for biomedical applications with the aim to monitor and measure the epidural intracranial pressure . The implanting microsensor is basically an RLC device in which capacitance varies with fluid pressure. The resonant frequency of RLC Series connected device varies with chemically etched diaphragm electrode spacing and thereby measures the variations with pressure changes in the fluid pressure . The small pressure changes are recorded by an external receiver unit which drives the implanted sensor into oscillator by means of an RF magnetic field.

The pressure measurement system is expected to measure pressure with an accuracy of 1 Torr over the range 1 to 760 Torr. The microsensor is expected to measure pressure at distances up to 2 meters from the power source loop in any environment that is nonconductive and nonmagnetic. The one application of the present thesis is for the chronic measurement of intercranial fluid pressure following brain surgery and for eschemic brain conditions.

PASSIVE RADIOSONDE TRANSDUCER DESIGN FOR REMOTE PRESSURE SENSING APPLICATIONS

by
Yang Gao

A Thesis
Submitted to the Faculty of
New Jersey Institute of Technology
in Partial Fulfillment of the Requirements for the Degree of
Master of Science in Electrical Engineering

Department of Electrical and Computer Engineering

October 1994

APPROVAL PAGE

PASSIVE RADIOSONDE TRANSDUCER DESIGN FOR REMOTE PRESSURE SENSING APPLICATIONS

Yang Gao

Dr. William N. Carr, Thesis Committee Chairperson — Date
Professor
Department of Electrical and Computer Engineering, NJIT

Dr. Kenneth Sohn, Committee Member — Date
Professor
Department of Electrical and Computer Engineering, NJIT

Dr. Durga Misra, Committee Member — Date
Associate Professor
Department of Electrical and Computer Engineering, NJIT

BIOGRAPHICAL SKETCH

Author: Yang Gao

Degree: Master of Science in Electrical Engineering

Date: October 1994

Undergraduate and Graduate Education:

- Master of Science in Electrical Engineering,
  New Jersey Institute of Technology, Newark, NJ, 1994

- Bachelor of Science in Electrical Engineering,
  Beijing Polytechnic University, China, 1989

Major: Electrical Engineering

This thesis is dedicated to
My Parents and Sister
for their love

ACKNOWLEDGMENT

I have a chance here to express my sincere gratitude to many people who assisted me during my thesis work, especially to my graduate advisor Dr. William N. Carr for his guidance an inspiration. Without his support, the thesis would not be done.

My thanks are due to the thesis committee.

I would also like to express my appreciation to my friends at NJIT, who gave me their kindly assistance. I am indebted to my elder sistor, Min Gao, who encouraged me at every stage of my life. I feel particularly indebted to Guang Yang, Subramanyam Chamarti, Chao Ye, Chao Sun and Jing zhu who helped me a lot for my thesis.

Finially, a sincerely thank you to my parents. They are always my support.

TABLE OF CONTENTS

LIST OF TABLES

LIST OF FIGURES

CHAPTER 1

INTRODUCTION AND HISTORY OF BIOSENSORS

The most pervasive silicon sensor is the pressure sensor, and the highest volume application is the disposable blood pressure sensors. In this device, a thin pressure sensitive diaphragm area is etched into a small silicon chip (typically less than 2 mm. square). Piezoresistors are defined and diffused into the surface of the diaphragm, and these resistors change value in proportion to the stress applied due to pressure on the diaphragm. Pressure is measured by the amount of this resistance change. Typically this chip is mounted on a ceramic substrate (usually with thick film laser-trimmed calibration resistors) and encapsulated in plastic to form the sensor body. Similar devices are used to measure respiratory, dialysis, urinary or other pressures.

1.1 Abstract

Over the past several decades, a number of intracranial pressure measurement devices have been developed, the majority of which have been implanted with leads protruding out from the cranial cavity. Pioneering work in this field was done by Dr. Carter Collins in the 1960s using pillbox devices with dimensions in the centimeter range. The method has the advantage of high degree of miniaturization of the device physical size, so that it can be totally implanted inside the skull to track the ICP. Microelectronics technology has been used, as recent studies in biomaterials has proved silicon sensors are biocompatible[1]. Moreover microengineering provides drastic reduction in device dimensions for easy implantation anywhere in human body.

Resonant RLC devices based on silicon technology in which the capacitance varies with external fluid static pressure have been reported by [2], [3]. The resonant frequency

of the RLC series connected device varies with static fluid pressure as the capacitance diaphragm electrode spacing is varied.

This thesis presents the design and simulation of a totally implantable microsensor for chronic biomedical application.

Chapter 2 dwells with the basic theory of the sensor-based system. The block diagram approach for the realization of the passive radiosonde systems are also dealt in the same chapter.

Chapter 3 will present theory of the resonance devices. To present a model that includes a magnetic field created by the rf power source loop antenna, the voltage induced in the resonant passive device, and the magnetic field created by the resonance current at the frequency f_O and the voltage pickup in the loop receiving antenna of the radio receiver. In particular chapter 4 deal with the mathematical modeling of inductance and chapter 5 with the capacitance modeling.

Chapter 6 describe the performance of the passive radiosonde system using PSPICE modeling. The results are also included in the same chapter.

We conclude in chapter 7 along with a brief summary. The softwares used for the design of the passive radiosonde system and mentor graphic design layout are presented in the Appendix A, B, C respectively.

1.2 Academic Activity

Optical, electrochemical, piezoelectric and thermometric biosensors are being actively pursued in a large number of laboratories throughout world. These are being coupled individually or in combinations with both catalytic (e.g. enzymes, cells, tissues) and affinity (e.g. antibody, nucleic acids, cell receptors) systems. The medical applications fall into two principal categories: in vitro diagnostics and in vivo monitoring. The bulk of the activity is concentrated on the former goal, but the challenge of continuous in vivo monitoring forms a significant part of many programs. Enzyme electrode technology has advanced

significantly in the last decade and work is now focused on refining the specificity, sensitivity and general operational characteristics of devices. Mediator technology has had a significant impact on the chemistry employed in amperometric sensors at the expense of more traditional hydrogen peroxide based systems, although there is significant interest in other ways of reducing the operating potential of enzyme electrodes.

1.3 Silicon Sensor Technology

Silicon microstructure technology provides a basis for manufacture high performance sensors at a low cost and in high volume. In addition, silicon devices are typically small, rugged, stable and unaffected by biological fluids. The basic technology involves photopatterning and chemically etching wafers of silicon to create three-dimensional structures. Recent process enhancements include:

1. Detailed modeling, which allows design of higher performance parts.

2. Electrochemical etch stops, which permit very precise dimensional control.

3. Fusion bonding, so that multiple layers can be etched and then fused together to form very complex three dimensional structures.

1.4 Passive Sensor and its Applications

Passive sensor is that which does not need its own power supply which has the advantage of avoiding both lifetime reduction and problems resulting from an inductive energy transmission into the implant. The function of passive sensor system is based on the coupling of two components either by induction or by electromagnetic or ultrasonic wave fields, so that the information receiver changes a characteristic parameter according to the variations of the second, implanted component's condition.

The various applications of biosensor systems are as follows:

1. Patient monitoring where freedom of movement is desired, such as in obtaining an exercise electrocardiogram.

2. Patient monitoring in an ambulance and in other location away from the hospital.

3. Research on unrestrained, unanesthetized animals in their natural habit.

4. Collection of medical data from a home or office.

5. Radio frequency transmissions for monitoring astronauts in the space.

6. Use of telephone links for transmission of electrocardiograms or other medical data.

CHAPTER 2

DESCRIPTION OF THE SENSOR-BASED SYSTEM

2.1 Introduction

This chapter establishes the perspectives of elements of intracranial pressure and its measurement techniques. The varied sensors based intracranial pressure measurement techniques are compared. A detailed description of the improved tracking system is presented.

2.2 Intracranial Pressure Monitoring

Intracranial hypertension is a syndrome that results from tumor, trauma hydrocephalus or massive lesions brought by abscess or injection. The increased fluid pressure inside the skull that results can be deceiving and devastating. Hence a continuous, accurate knowledge of intracranial pressure would be of great value as a guide for therapy and as an index of the clinical state in many neurosurgical cases, particularly in monitoring pressure changes in acute head injury cases. Our research focuses on the development of totally implantable microsensors for biomedical applications including chronic intracranial monitoring. The present work design and fabricates an implantable silicon sensor based on microelectronics technology. Silicon has become a synonym for integrated circuit technology, thanks to its spectacular electronic properties and equally amazing mechanical properties. Silicon can be micromachined into the tiniest electromechanical systems even built. Microsensors and microactuators intended for biomedical applications have become an important research area.

2.2.1 Concepts of Intracranial Pressure

Intracranial pressure is a generic term to designate any pressure measured in the cranial cavity. The concept of ICP is based on the relationships among three volumes, blood, brain, and cerebrospinal fluid(CSF), enclosed within a skull. If one or more of these three volumes increase without a concomitant fall in the other volumes, an increase in ICP results[4].

The goal of all intracranial therapies is maintenance of cerebral blood flow to provide adequate oxygen and glucose to the brain. Increases in ICP can reduce cerebral blood flow. Because it is not practical to monitor cerebral blood flow at the bedside, a calculated pressure, cerebral perfusion pressure(CPP), is used to reflect cerebral blood flow. CPP equals arterial pressure(MAP) minus ICP.

Once ICP rises to arterial pressure levels, blood flow through the brain reduces, and death occurs. Patients at risk of such a condition occurring include those with severe head trauma, space-occupying mass lesion, hydrocephalus, encephalitis, Rey's syndrome, and cerebral hemorrhage.

2.2.2 Totally Implantable Radiosonde

Fig. 2.1 shows the different sites of the cranial compartment. The passive pressure sensor that is totally implanted works on the principle of radio frequency coupling. The figure also shows the incision made to implant the radiosonde. Fig. 2.2 shows the section of cranial compartment after healup. Fig. 2.3 is the equivalent circuit diagram of the passive radiosonde.

2.2.3 Fully Implanted ICP Monitoring

Invasive intracranial pressure monitoring and the data it provides has advantages especially as a treatment and prognostic indicator[5]. The most common complication

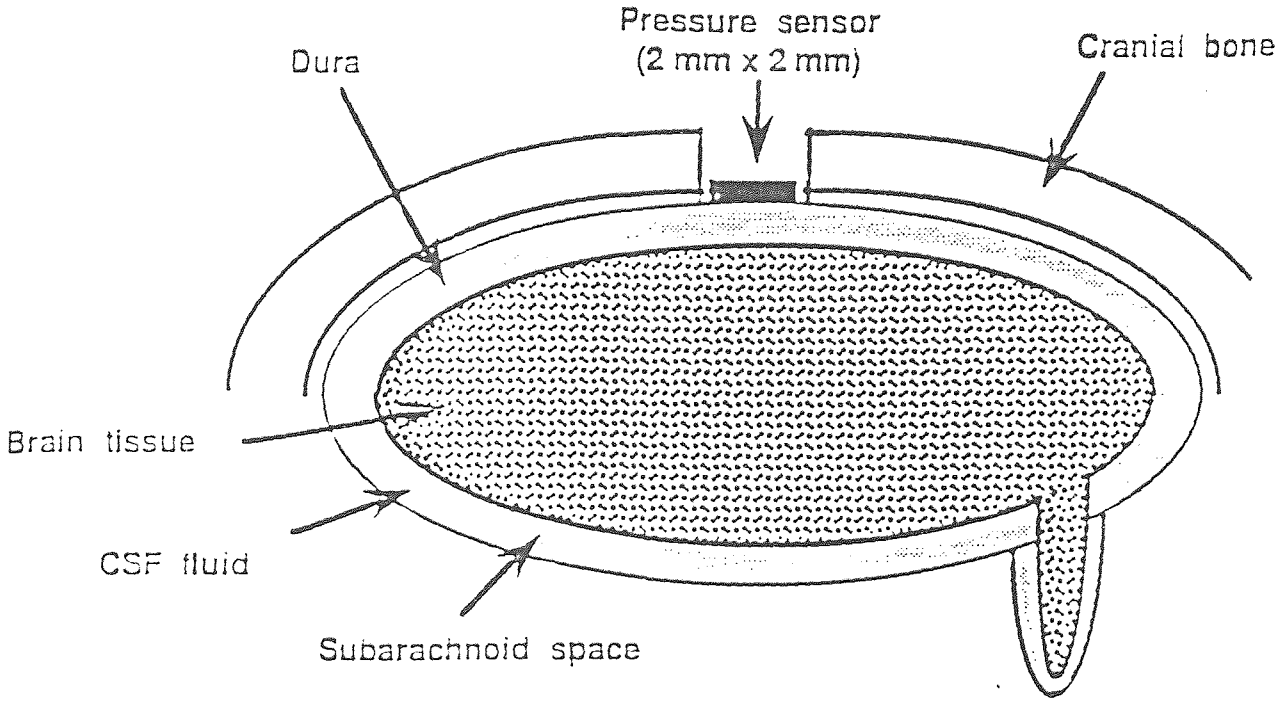

Figure 2.1 Cranial compartment showing the implanted pressure sensor

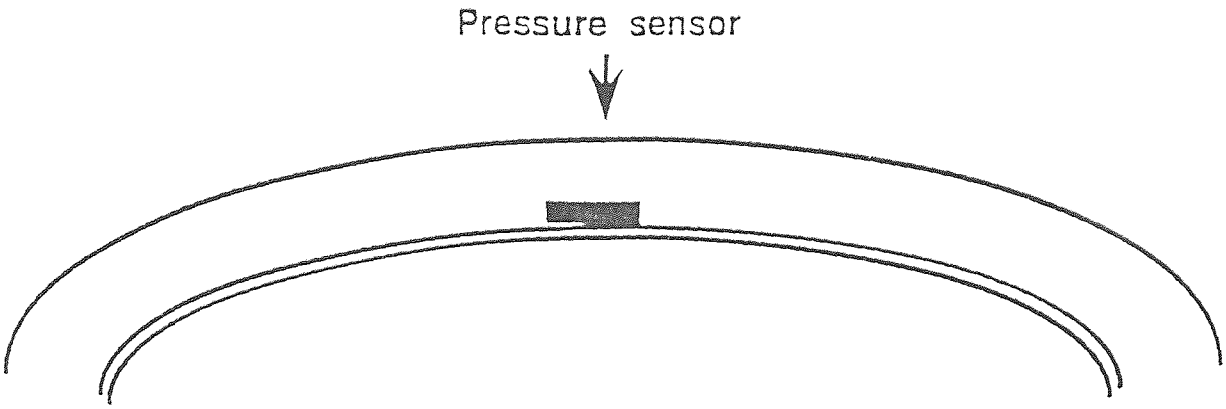

Figure 2.2 Showing the healup of incision after craniotomy

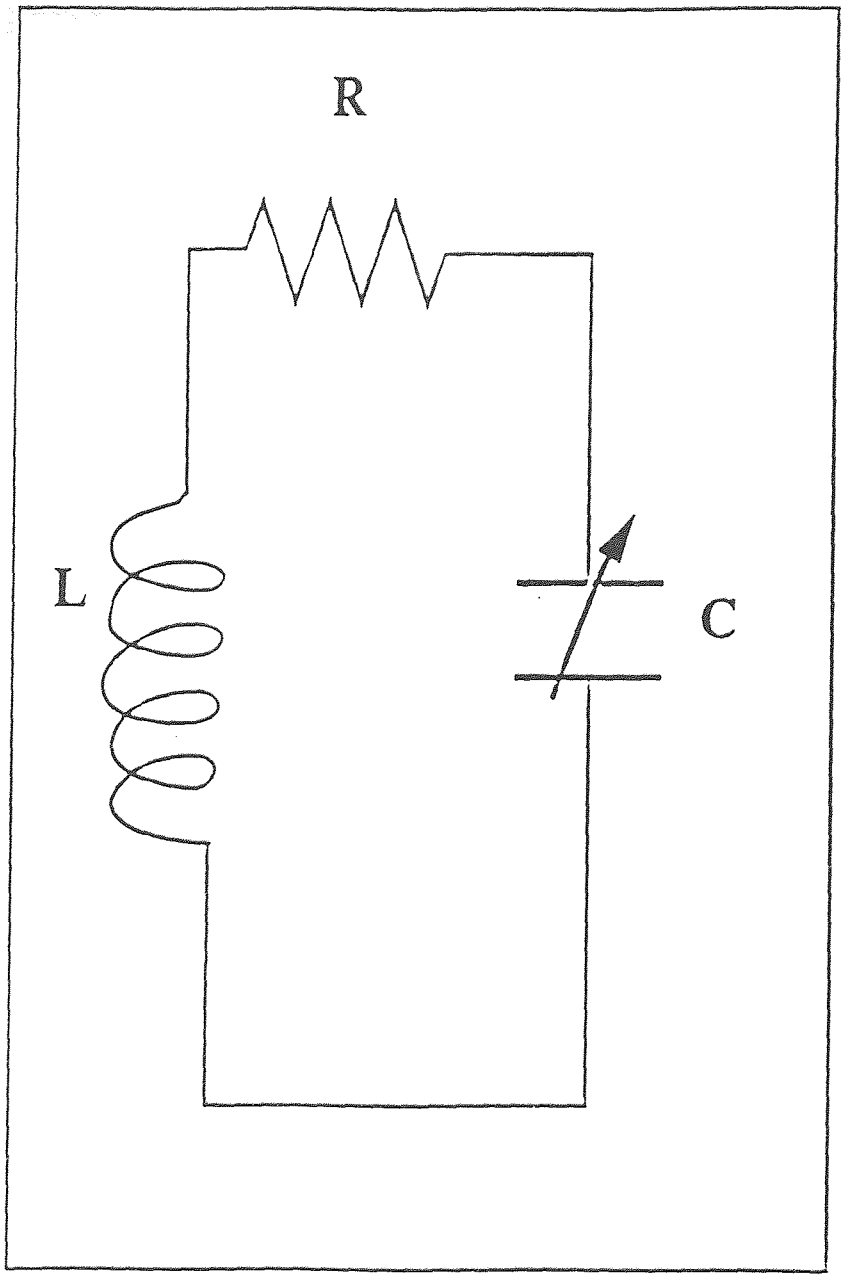

Figure 2.3 Equivalent circuit diagram of the passive radiosonde

associated with ICP monitoring is infection. The factor most consistently associated with ICP monitor-related infection was the duration of monitoring.

Invasive monitoring of ICP is becoming the standard of care for management of acute neuralgic and neurosurgical patients. As a result of microelectronics technology, a new totally implantable silicon microsensor has been designed and fabricated for facilitating chronic measurement of ICP thus by reducing the risk of infection to a greater extent.

2.3 The Passive Sensor-based System

Intracranial pressure can be measured to accuracies within 1 MilliTorr using passive microtransponders based on the current silicon micromachining technology. These microtransponders can operate with either a dual-oscillator or a phase-locked loop frequency scanned control systems.

2.3.1 Design of Passive Pressure Sensors

The basic passive pressure sensor consists of a chemically etched diaphragm with an integral plane coil. The variables for the design of inductance include track width, spacing between the tracks and the number of turns of the coil. In this design aluminum and copper metallization are used for a spiral square geometry that is compatible with our CAD design tools. The capacitance of the microsensor is based on the distance of separation between the internal plates that vary with biofluid pressure. The inductance and capacitance used for fabrication are 100 nanoHenries and 10 picoFarads respectively which provide a resonant frequency of 161MHz. The quality factor around 500 results in higher circulating currents in the sensors.

In this research we have designed four microtransponder devices. Device A(Fig. 2.4) is a very simple parallel resonant circuit that has a resonant frequency varying with environment fluid pressure. Device B(Fig. 2.5)is a series connected circuit which operates

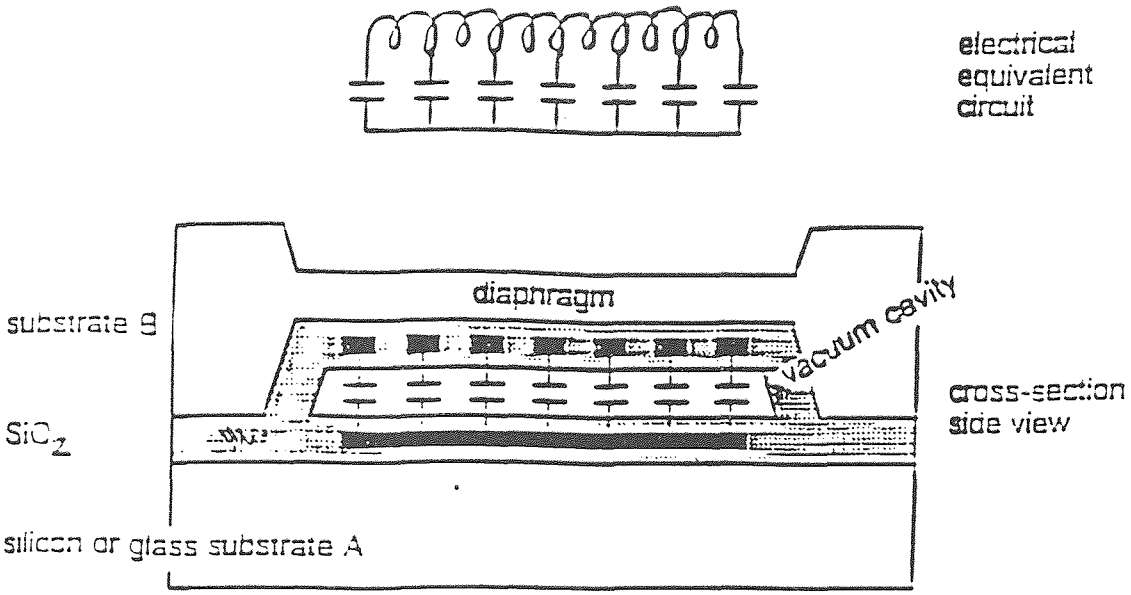

Figure 2.4 Wafer bonded microtransponder A

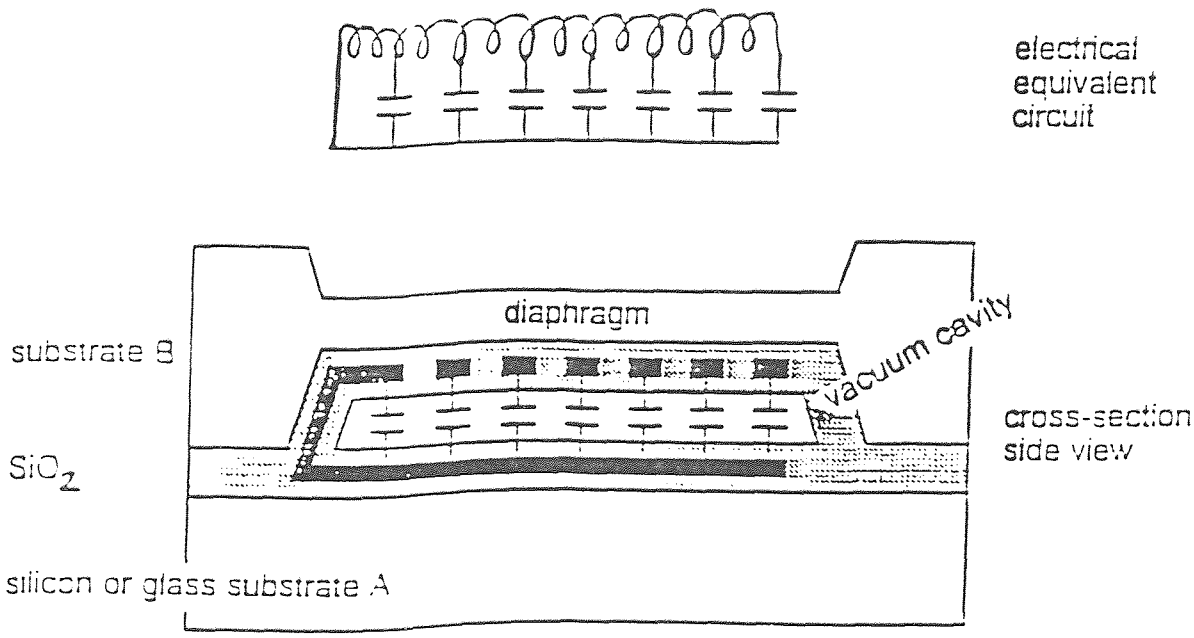

Figure 2.5 Wafer bonded microtransponder B

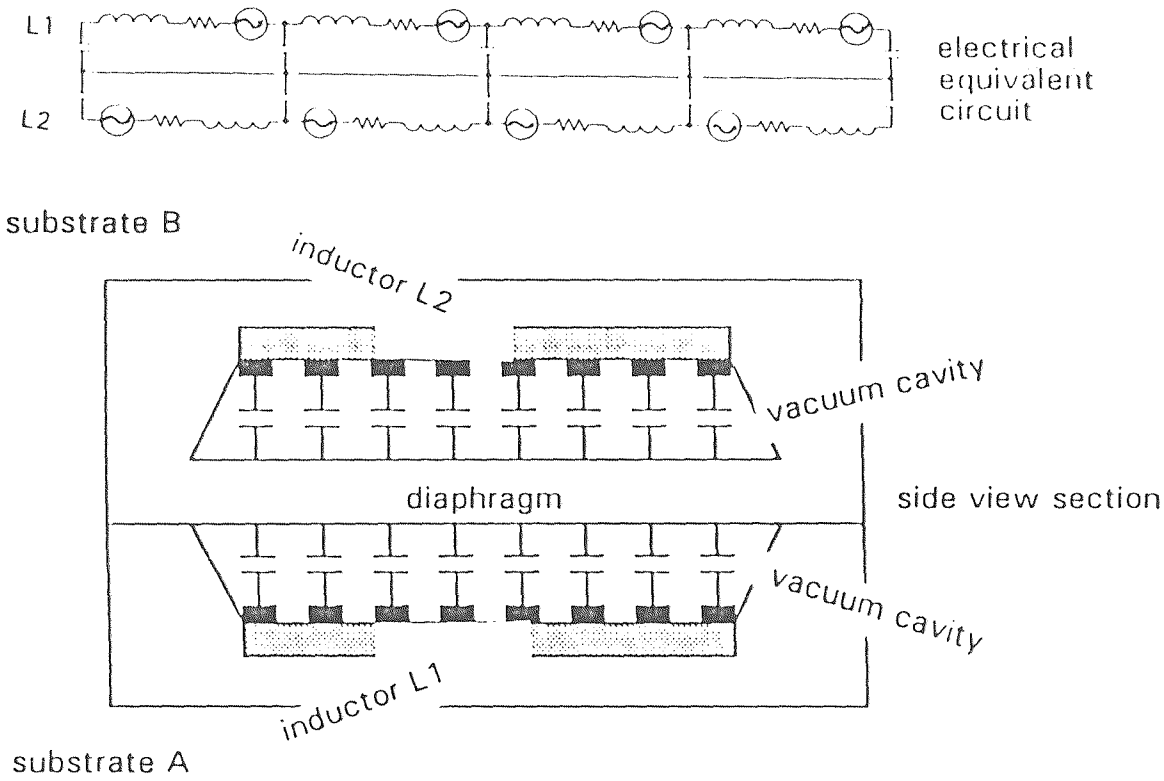

Figure 2.6 Wafer bonded microtransponder C

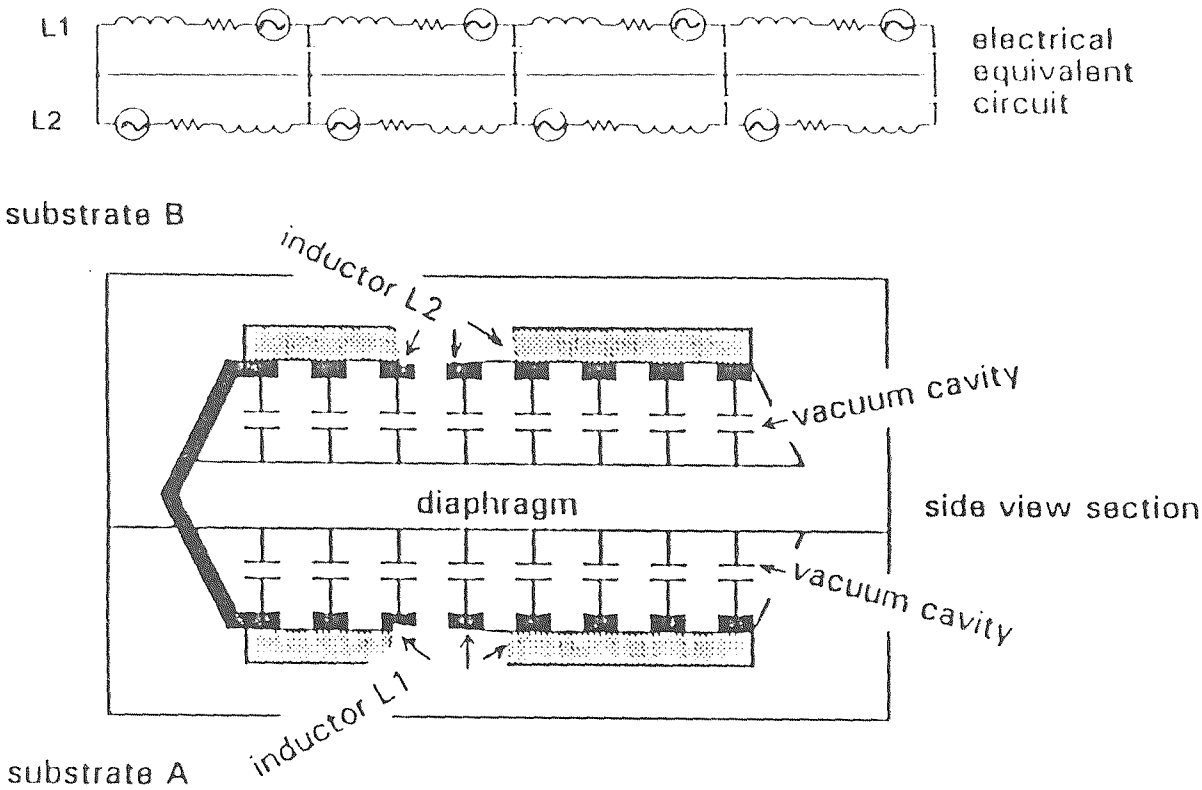

Figure 2.7 Wafer bonded microtransponder D

with a basic resonant circuit also varying with fluid pressure. The basic theory of device C (Fig. 2.6) and device D(Fig. 2.7) are the same as device A and device B respectively except the sensitivities are much higher. Also the devices C and D have a major disadvantage in the form of the complexity in device design and fabrication technology and they also need advanced micromachining technologies.

2.3.2 Design of Phase Locked Loop System and its Operation

The system design consists of an implantable pressure sensor and a receiver to detect and measure biofluid pressure variations. The implanting microsensor is basically a series connected RLC circuit in which capacitance varies with biofluid pressure. The resonant frequency of RLC circuit varies chemically etched diaphragm electrode spacing that is linear function of the biofluid pressure.

The basic principle involved in detecting the signal from the passive radiosonde is by FM detection. A simple method of converting frequency variations to voltage variations is by FM reactance technique. In FM reactance principle the reactance varies with the frequency. An alternating current, such as an r-f signal or i-f signal, flowing through an inductor will remain at a constant value if neither the voltage nor the frequency is varied. However, since reactance varies with the frequency, the current flowing through an inductor will vary in amplitude when the frequency of the applied signal varies, even though the amplitude of the voltage remains constant. The amount of change in the amplitude of the current is dependent upon the shift in frequency because of the basic resonant characteristics of the pressure sensors and other tuned circuits. Since an FM signal varies in frequency above and below the center frequency by an amount depending upon the amplitude of the modulating signals, applying a frequency modulated signal to an inductor will convert frequency deviations to amplitude changes in the current. These amplitude changes in current when made to flow through an resistor will produce corresponding voltage changes across the terminals of the resistor. The ideal response

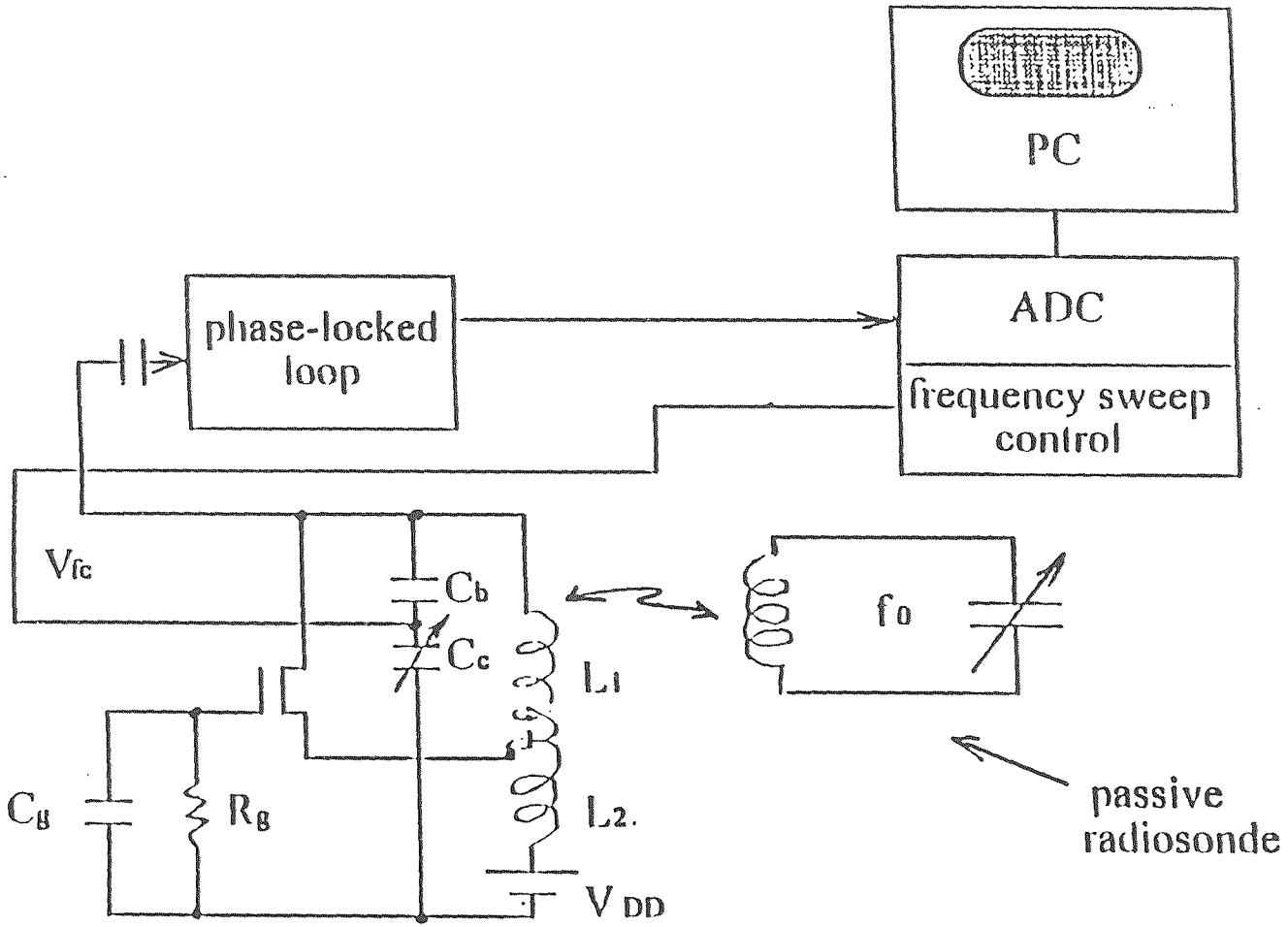

Figure 2.8 Phase locked loop system

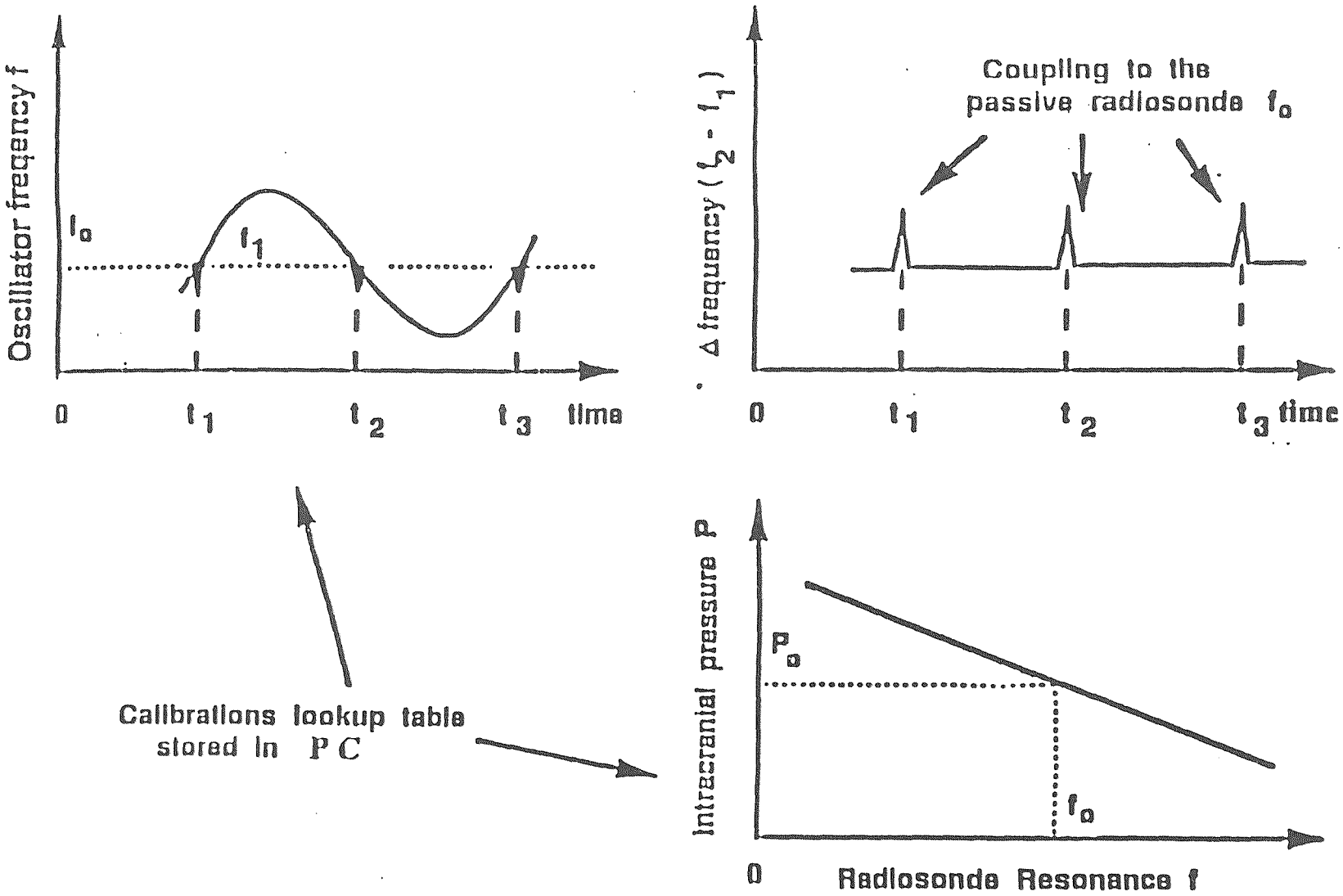

Figure 2.9 Selected signal levels for the phase locked loop system

curve of an FM detector shows that each frequency variation produces a definite value of voltage and also that a linear relationship exists between the frequency and the voltage. This linear relationship is essential in order to produce distortionless conversion.

The basic system operates with a very simple LC-resonant passive radiosonde microsensor. The LC-resonant circuit is excited by the magnetic field created by the remote transmitter as shown in Fig 2.8, Without the influence of the passive microsensor radiosonde, the oscillator maintains a fixed frequency f_1, as it is tandem-tuned over a frequency range. The f_1 provides a steady signal to the analog-to-digital converter unless the specific resonant frequency f_0 of the microsensor is matched at time t_2, when $f_1=f_0$. A sudden shift in f_1 occurs at time t_2 and a 'blip' occurs in the ADC output. This 'blip' can be decoded into a specific, unique gauge pressure in the remote electronics. That is basic system operation principle and is summarized furthering Fig.2.9.

2.3.3 Design of Dual Tracking Hartley Decode System and Its Operation

A phase sensitive endoradiosonde absorption detector was decided to be more useful. An external inductively coupled oscillator detector of the Hartley type has been chosen for detecting the passive radiosonde at a distance. Fig. 2.10 shows the improved model of the complete receiver unit system to detect the radiating signal from the passive radiosonde. The system is employed two Hartley oscillators, one acting as a reference oscillator. The Hartley oscillator is chosen because of the fact that the operating range falls in the lower frequency ranges. The other blocks of the diagram are the signal conditioning block(low pass or band pass filter), the phase detection block(reactance phase demodulator), an A/D converter for interfacing to a datalogging machine(IBM/AT).

The dual tracking Hartley decode system was designed and the operation of the systems is characterized by the graphs shown in Fig. 2.11. Both the oscillators track each other with a constant frequency. As long as the frequency f_1 of the Hartley oscillator is different from the resonant frequency f_0 of the implanted radiosonde, f_2-f_1 is a constant.

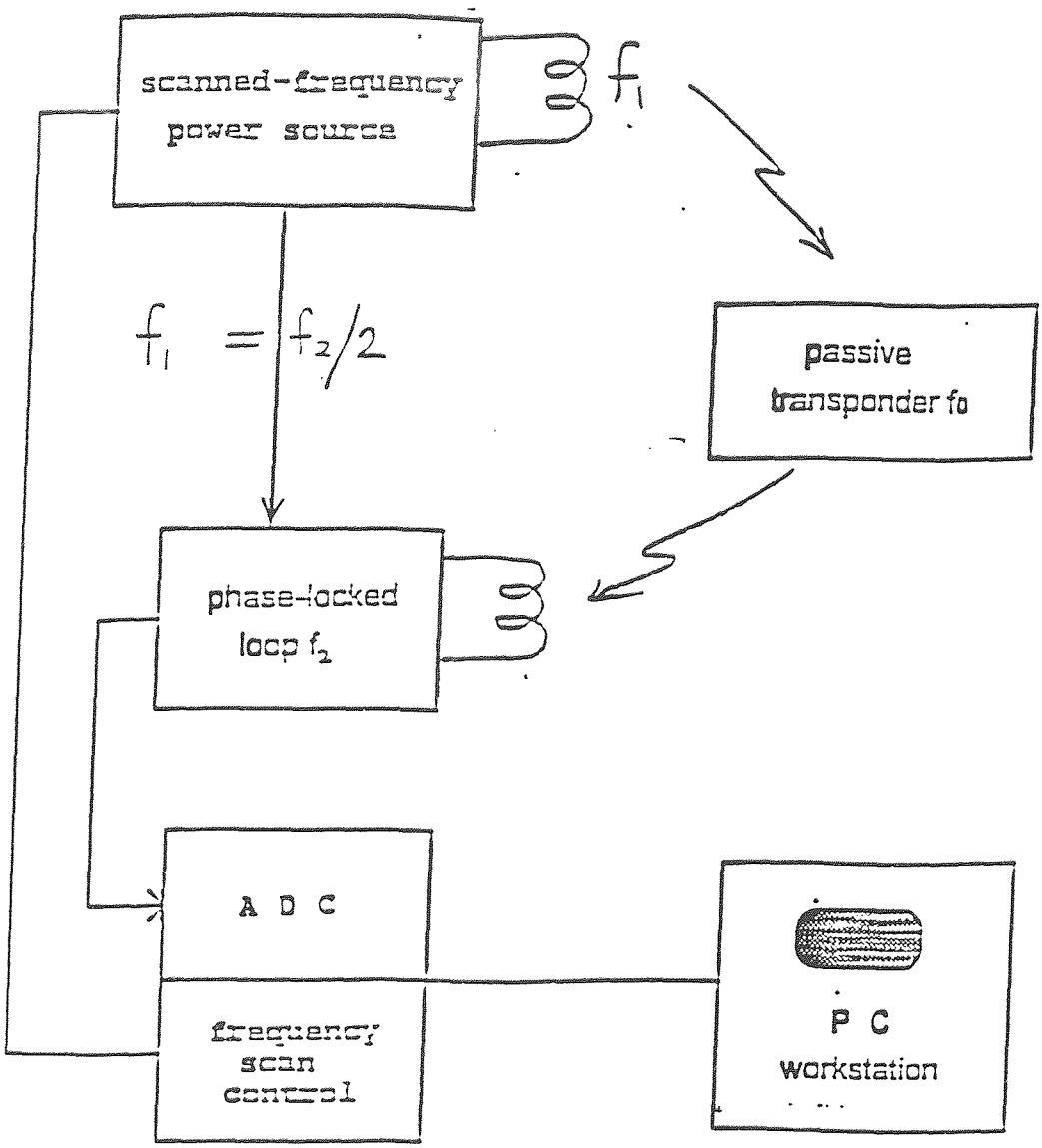

Figure 2.10 Dual tracking hartley decode system

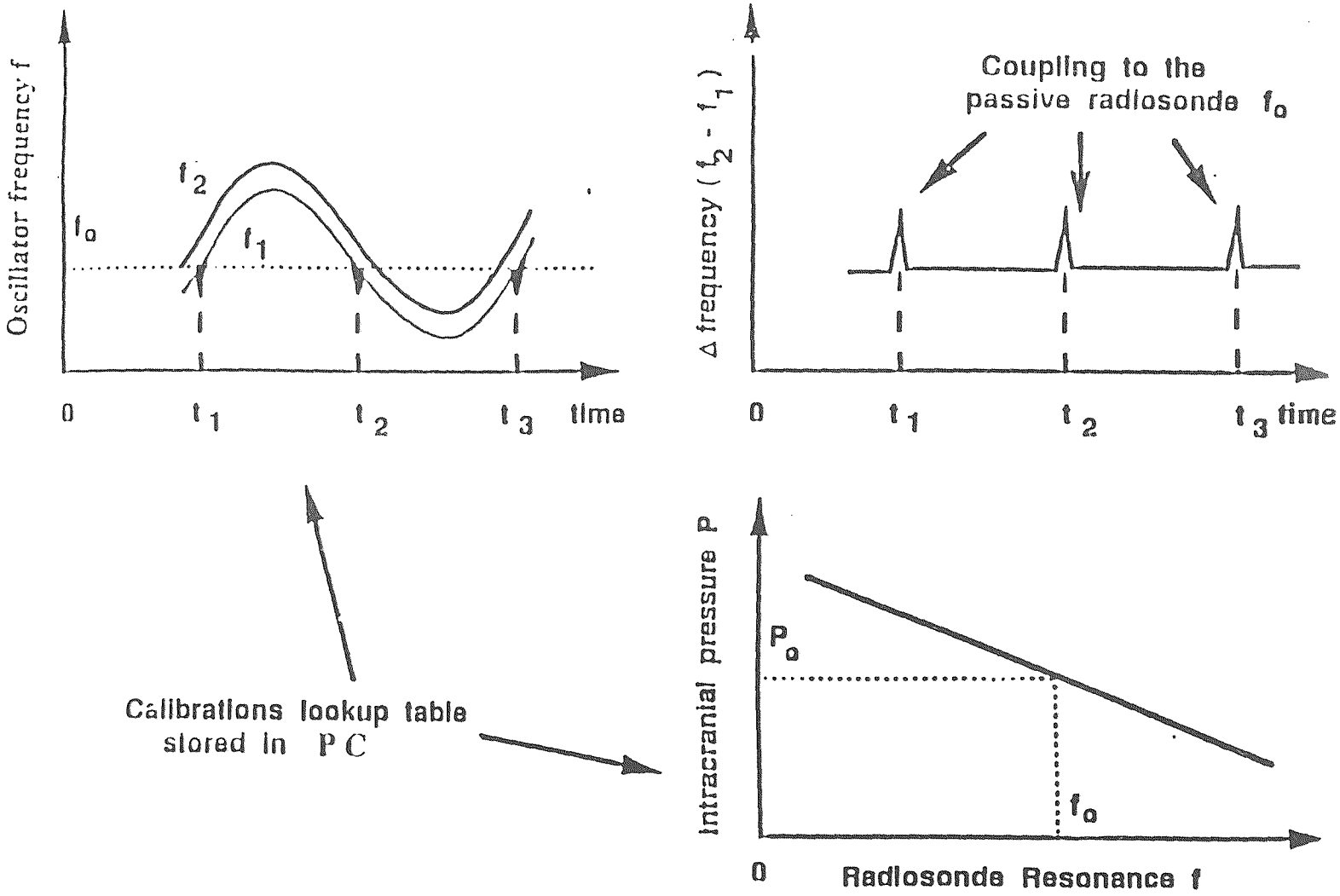

Figure 2.11 Selected signal levels for dual tracking hartley decode system

By repeatedly sweeping the external oscillator frequency, the energy absorbed by the passive radiosonde at its resonant frequency which changes with time is tracked and is received by the Q-sensitive telemetry receiver unit. Whenever the external oscillator frequency $f_1=f_0$, the resonant frequency f_1 changes due to the coupling. This is detected by the phase reactance demodulator circuitry. The momentary shift in the phase is converted to a digital signal by using an A/D converter. A calibrated look up table is stored in the computer, the direct reading of the intracranial pressure as a function of radiosonde frequency is continuously logged in and the reading of the ICP is directly shown on the PC monitor. This way the systems continuously monitors and tracks the ICP in the skull.

CHAPTER 3

BASIC THEORY AND SIMULATION TOOLS

This chapter starts with the description of electronic circuit equivalent for pressure sensor and its detection system. In the process all the mathematics required to simulate entire detection system is also taken care of.

3.1 Basic Device

The principle of operation of pressure sensor is based on resonant circuit. In general there are two types of resonant circuits possible known as series resonant circuit and parallel resonant circuit. With the resonance nature the impedance becomes either maximum or minimum depending upon the type of resonant circuit. So the corresponding electrical parameter of measurement can be either current or voltage. The resonant frequency of operation is a function of L and C of the pressure sensor used

$$f_0 = \frac{1}{2\pi\sqrt{LC}}$$

In a pressure sensor the inductance is realized using square spiral geometry and its simulations whose results are discussed in chapter 4. Capacitance is a parallel plate type whose design is given in chapter 5. Capacitance is a function of distance of separation between plate [6].

The separated distance of a pressure sensor between plates varies with amount of pressure applied the diaphragm of the second wafer as shown in Fig. 2.10. All the possible types of pressure sensors discussed in chapter 2 are resonant circuits with the resonant frequency being a function of inductance and capacitance only. It is worthwhile to note that the Quality factor of the device decides the bandwidth of the resonant circuit

used and also the quality factor of the circuit decides amount of power dissipated per unit cycle in the inductance.

3.2 RF Coupled Detection

The block diagram of the RF Coupled detection is shown in Fig. 2.10. In this the implanted sensor is the pressure sensor with the coil being a spiral structure of square geometry acting as an inductor. The Q-sensitive oscillator has a coil that is acting like an antenna to receive and track the signal generated by the pressure changes in the form of frequency changes of the implanted pressure sensor. The amount of coupling between the coils (oscillator coil and inductor coil of pressure sensor) is important parameter which decides the sensitivity of the whole system. Coupling Coefficient is function of distance separation between the coils and orientation of the two coils. The amount of signal reception for inductive coupling is mathematically derived in the following section.

3.3 Induction Coupling

A current carrying small inductor coil can induce a magnetic flux into near loop antenna. The magnetic induced magnetic field can be estimated by Biot Savart's Law Which states that the magnetic field induced at any point P2 produced by a current carrying differential element Idl at a point P1 is given by

$$B = \frac{\mu_0}{4\pi}\int \frac{I\,\overline{dl} \times \overline{aR}}{R^2}$$

where

I = Filamentary current

dl = vector length of current path P1

aR = unit vector of points joining P1 to P2

R = distance of separation between P1 & P2

Applying the above principle to a side of the rectangular loop carrying current I shown in Fig. 3.1 we have

$$d = R \cot \phi$$

$$dB = \frac{\mu_0 I}{4\pi R} \sin\phi d\phi \overline{a\theta}$$

$$B = \frac{\mu_0 I}{4\pi R}(\cos\phi_1 - \cos\phi_2)\overline{a\theta}$$

For a rectangular loop carrying current I has four side, by superposition principle

$$B = \frac{\mu_0 I}{4\pi R}\sum_{i=1}^{4} (\cos\phi_{i1} - \cos\phi_{i2})\overline{a\theta_i}$$

Where ϕ is the angle between the planes and is well known to be a function of direction cosines. The direction cosines for the Fig. 3.2 are calculated and cosines of the angles between planes are given by following equations

$$\cos\phi_{11} = \frac{(X_0 + l)}{\sqrt{(X_0 + l)^2 + (Y_0 + a)^2 + Z_0^2}}$$

= Angle between AE and AB

$$\cos\phi_{12} = \frac{(X_0 - l)}{\sqrt{(X_0 - l)^2 + (Y_0 + a)^2 + Z_0^2}}$$

$$\cos\phi_{22} = \frac{(Y_0 - a)}{\sqrt{(X_0 - l)^2 + (Y_0 + a)^2 + Z_0^2}}$$

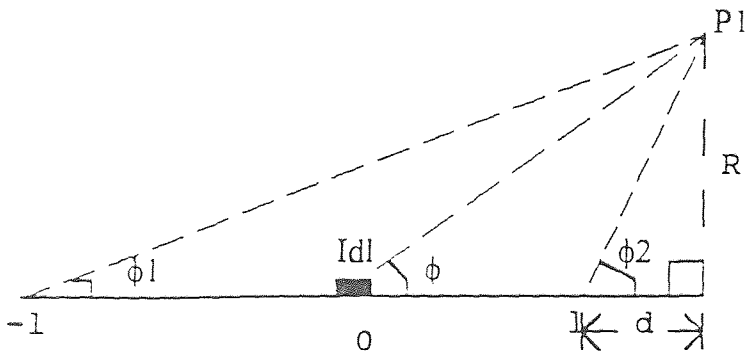

Figure 3.1 Magnetic fluxdensity at a point p1 due to the current carrying element Idl

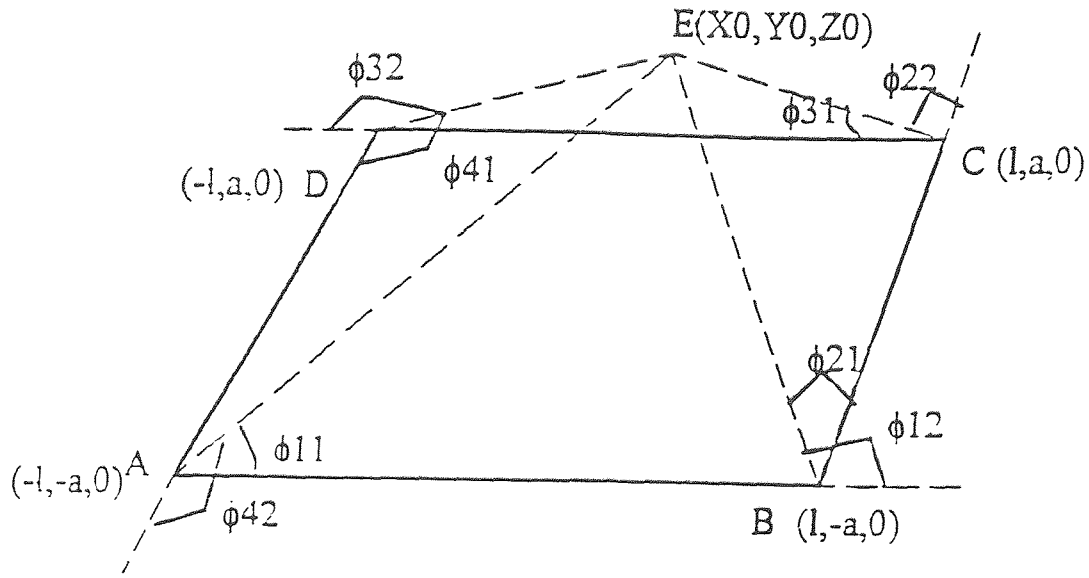

Figure 3.2 Voltage induced into the square loop antenna from a small current carrying

$$\cos\phi_{31} = \frac{-(X_0 - l)}{\sqrt{(X_0 - l)^2 + (Y_0 + a)^2 + Z_0^2}}$$

$$\cos\phi_{21} = \frac{(Y_0 + a)}{\sqrt{(X_0 - l)^2 + (Y_0 + a)^2 + Z_0^2}}$$

$$\cos\phi_{32} = \frac{-(X_0 + l)}{\sqrt{(X_0 + l)^2 + (Y_0 - a)^2 + Z_0^2}}$$

$$\cos\phi_{41} = \frac{-(Y_0 - a)}{\sqrt{(X_0 + l)^2 + (Y_0 - a)^2 + Z_0^2}}$$

$$\cos\phi_{42} = \frac{-(Y_0 + a)}{\sqrt{(X_0 + l)^2 + (Y_0 + a)^2 + Z_0^2}}$$

The distance of separation between E and AB ,BC, CD and AD lines is given as R_1, R_2, R_3 and R_4 respectively are given by the following expressions.

$$R_1 = \sqrt{(Y_0 + a)^2 + Z_0^2}$$

$$R_2 = \sqrt{(X_0 - l)^2 + Z_0^2}$$

$$R3 = \sqrt{(Y_0 - a)^2 + Z_0^2}$$

$$R_4 = \sqrt{(X_0 + l)^2 + Z_0^2}$$

The resultant unit vectors are given by

$$a_{\theta 1} = -\frac{Z_0}{\sqrt{Z_0^2 + (Y_0 + a)^2}}\bar{Y} + \frac{(Y_0 + a)}{\sqrt{Z_0^2 + (Y_0 + a)^2}}\bar{Z}$$

$$a_{\theta 2} = \frac{Z_0}{\sqrt{Z_0^2 + (X_0 - 1)^2}}\bar{Y} + \frac{(1 - X_0)}{\sqrt{Z_0^2 + (X_0 - 1)^2}}\bar{Z}$$

$$a_{\theta 3} = \frac{Z_0}{\sqrt{Z_0^2 + (Y_0 - a)^2}}\bar{Y} + \frac{(a - Y_0)}{\sqrt{Z_0^2 + (Y_0 - a)^2}}\bar{Z}$$

$$a_{\theta 4} = -\frac{Z_0}{\sqrt{Z_0^2 + (X_0 - 1)^2}}\bar{Y} + \frac{(1 + X_0)}{\sqrt{Z_0^2 + (X_0 - 1)^2}}\bar{Z}$$

So the overall magnetic flux density is given as

$$B = \sum_{i=1}^{4} \frac{\mu_0 I}{4\pi R_i}(Cos\phi_{i1} - Cos\phi_{i2})a_{\theta i}$$

and so the magnetic flux density as a vector form can be given as

$$\bar{B} = B_x\bar{X} + B_y\bar{Y} + B_z\bar{Z}$$

The induced voltage due to the flux density is calculated by the help of Faraday's law which is given by

$$V = -\frac{\partial}{\partial t}\int B \bullet dS$$

Where 'S' is any surface bonded by the coil and does not change with time Therefore the voltage induced in the coil can be considered as at the steady state conditions and is given by

$$V = -\omega \int B \bullet dS$$

$$V = -\omega A(B_x \cos\alpha + B_y \cos\beta + B_z \cos\gamma)$$

Where A = area of cross section

ω = frequency in radians

α, β, γ are the angles between and X,Y and Z axes respectively.

Applying reciprocity theorem voltage induced by the small current carrying coil into the receiving antenna is given as

$$V = -\omega A(B_x \cos\alpha + B_y \cos\beta + B_z \cos\gamma)$$

The results show that the maximum voltage can be induced in the antenna when current carrying conductor is parallel to the Z-axis , i.e., when $\gamma = n\pi$ where n=0,1,2, With this electromagnetic theory and the mathematical equations developed in this section the RF coupling between the pressure sensor and receiving system we are ready to analyze the whole system.

This RF coupled system is also known as dual tracking Hartley decode system. Even though there are many techniques available to track a passive frequency modulated endoradiosonde but this system is proved to be more sensitive and accurate when the pressure sensor and RF coupled system separated by a distance of 5 mm to 1 centimeter.

An external inductively coupled oscillator detector system has Hartley oscillator detector which is used for tracking oscillator frequency for detecting the passive radiosonde at a distance of 0.5 cm. The whole system is shown in Fig. 2.10.

The system operates with two Hartley oscillators in which one constantly operates at f2 and the other oscillator operate at a frequency depending on the coupling between the pressure sensor and the resonant oscillator circuit. By repeatedly sweeping external

oscillator frequency the energy absorbed by the passive radiosonde at its resonant frequency which changes with time is tracked and received by the Q-sensitive telemetry receiver unit. The difference between these two signals is signal conditioned by passing through a low pass/band pass filter and using a reactance phase demodulator (which is also known as FM Detector) and is fed as a digital signal to the computer after passing through the A/D converter and interface circuitry called as Data Acquisition system. An FM detector has a definite voltage corresponding to each frequency input signal and this linear relationship is crucial for the whole system detection capability. So the band of frequency of operation is limited to this linear range of this FM detection system. At any other frequency the reactance modulator will be in nonlinear range and the system reception will be poor and therefore the accuracy of measurement will be less and the whole system becomes less sensitive.

The digital signal received by the PC will be read as ICP reading by using the look up table of calibrated system readings. So the digital signal at the PC is function of the frequency of reception which in turn is function of Pressure sensor frequency of operation and the amount of coupling between the two coils. The graphs corresponding to this method are all shown in Fig. 2.11.

CHAPTER 4

SIMULATION RESULTS FOR INDUCTANCE MODELLING

This chapter deals with the design and simulation of spinal inductance.

4.1 Mathematical Concept for Inductance Calculation

The square spinal inductance is shown in Fig. 4.1. Computer calculation of spinal inductance for square geometries is based on Grover method[7]. The total inductance is a function of the length, width, thickness, spacing between tracks and the number of turns of square spinal inductor.

The total inductance is given by

$L_T = L_O + M_+ + M_-$

where

L_T = total inductance of the coil in nonohenries

L_O = total self inductance of all the segments used in the coil

M_+ = total mutual inductance of the segments having current flow in same direction

M_- = total mutual inductance of the segments having current flow in opposite direction

The self inductance of a conductor segment of rectangular cross section is given by

$L_O = 0.002l\{\ln(2l/(W+T)+0.50049+(W+T)/3l\}$

where

l = length of conductor segment

W = width of conductor segment

T = thickness of conductor segment

With the skin depth into consideration at 161MHz in around 6.25*2=13.5 micron, a conductor of width 10μ is chosen so that skin depth is taken care of. In general by

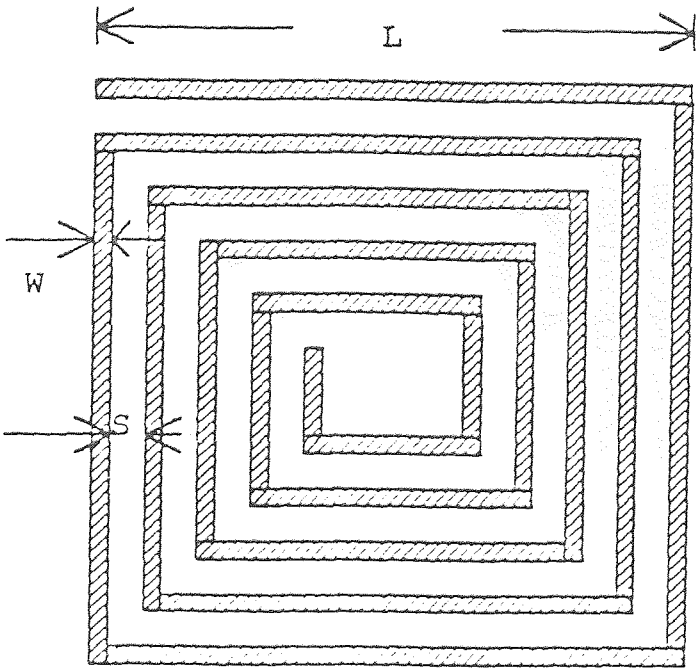

Figure 4.1 Spiral inductor of square geometry

increasing the width of inductor the resistance of conductor decreases and a high quality factor is obtained for the coil.

The mutual inductance between current flowing conductors 1 and 2 is given by

$$M_{+} = \frac{d\phi_{12}}{di_1}$$

$$M_{-} = \frac{d\phi_{21}}{di_2}$$

In general, at the same frequency of operation and mutual inductance is vectorial sum of M_+ & M_-.

The mutual inductance between two parallel conductors are a function of length, and geometric mean distance between conductors.

$M = 2lQ$

where

Q = mutual inductance parameter

$= \ln\{[(l/(GMD)+[1+l^2/GMD^2]^{1/2}\}-[1+GMD^2/l^2]^{1/2}+[GMD/l]$

where

$\ln GMD = \ln d -\{[1/12(d/w)^2]+[1/60(d/w)^4]+[1/168(d/w)^6]+ \bullet \bullet \bullet$

where M_+ and M_- are positive and negative values respectively.

d = distance between tracks

w = track width

Using the above concept, mutual inductances for current flowing in the same direction and for opposite direction are calculated .

All the formulas have been used for simulation of inductance using Sigmaplot software in PC. Simulation program and result have been shown in nest two pages. From the results we can observe that positive mutual inductance M_+ is much higher than M_-.

The M_- is smaller because the distance of separation is much higher between two conductors having opposite current directions.

4.2 Solid Modeling Spiral Inductance

We use Maxwell 2D to calculate the inductance of this model(Fig. 4.2-4.5). The procedure for modeling inductance is described in detail in Appendix A, B.

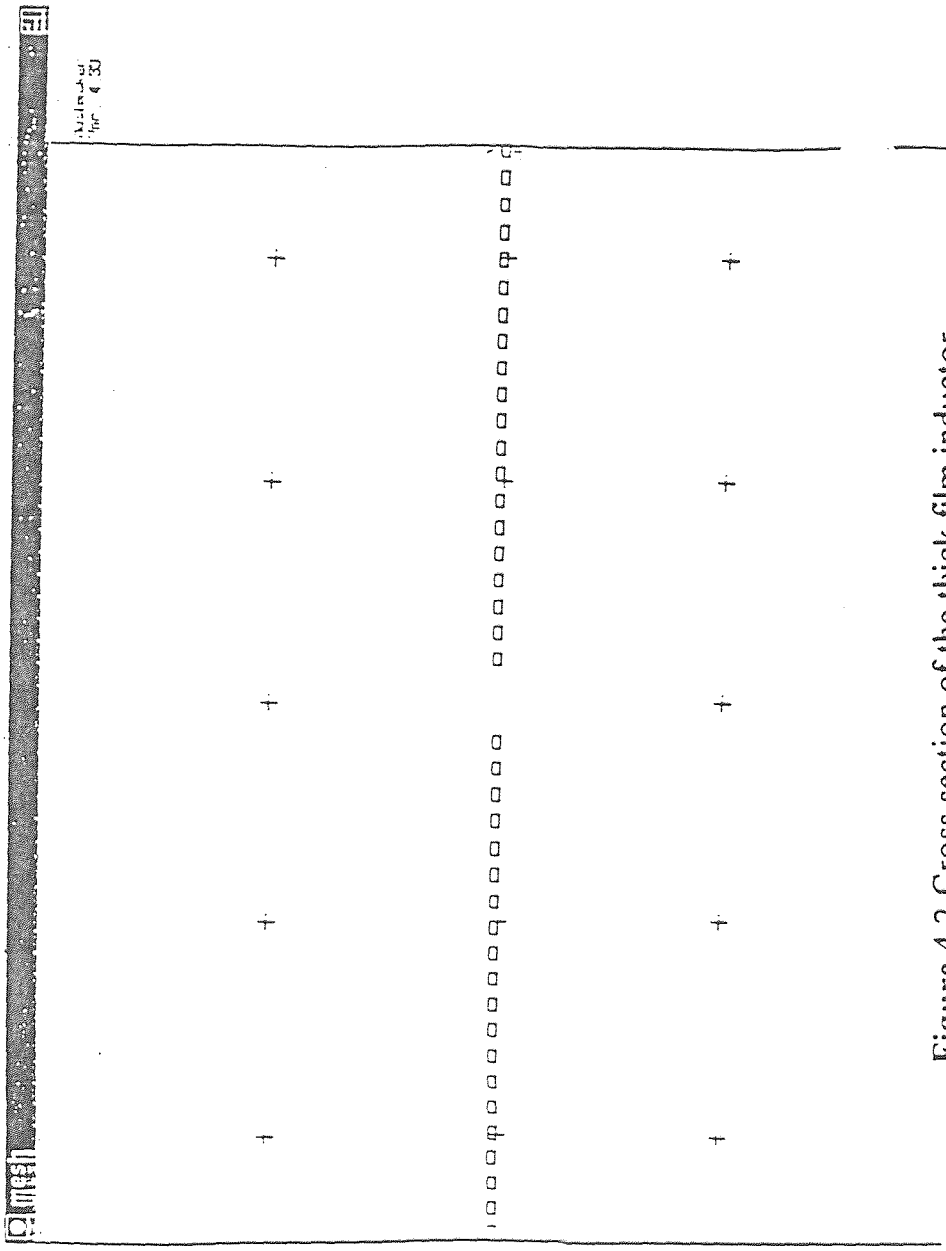

Figure 4.2 Cross section of the thick film inductor located above the conducing substrate

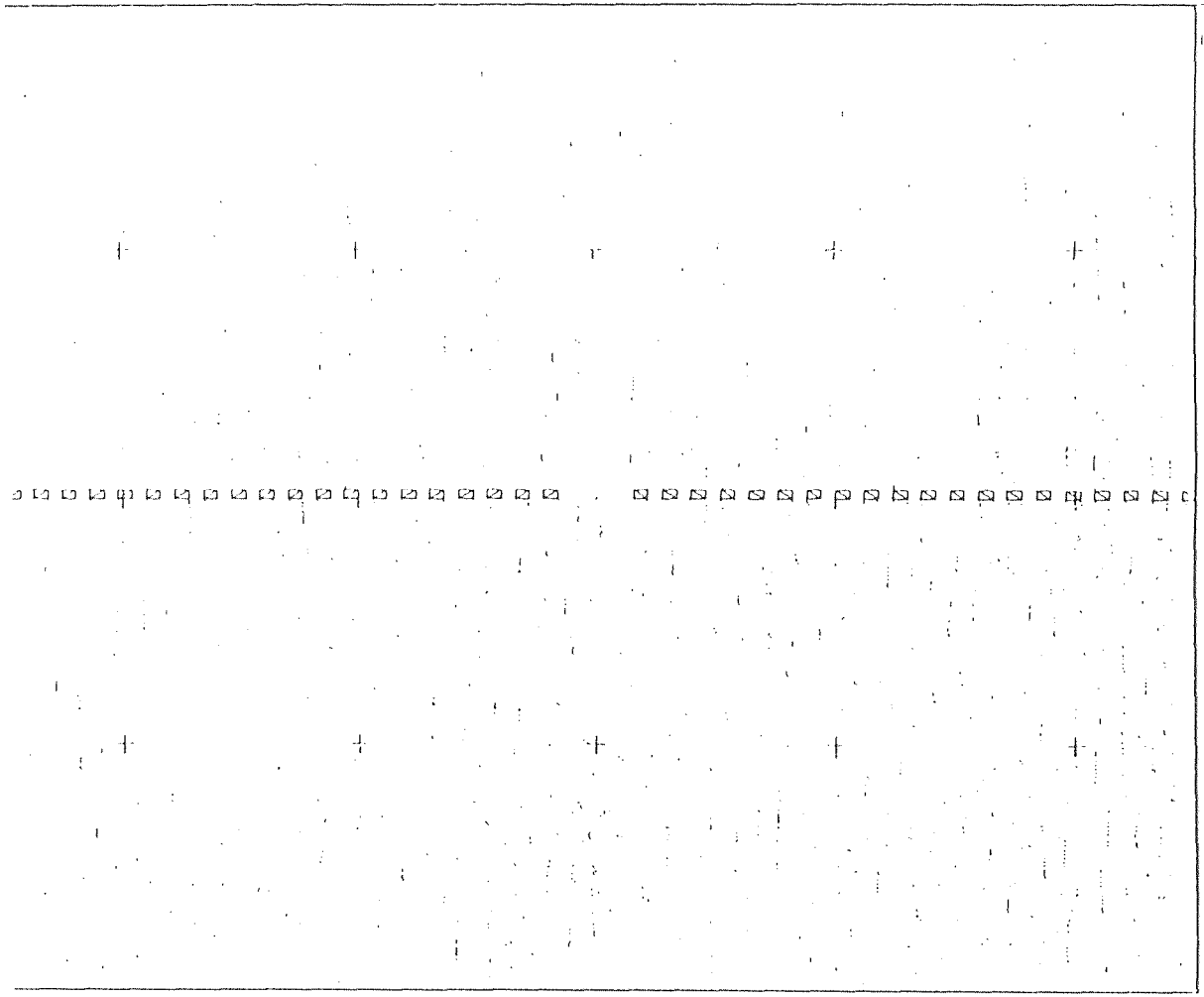

Figure 4.3 Mash for the microtransponder

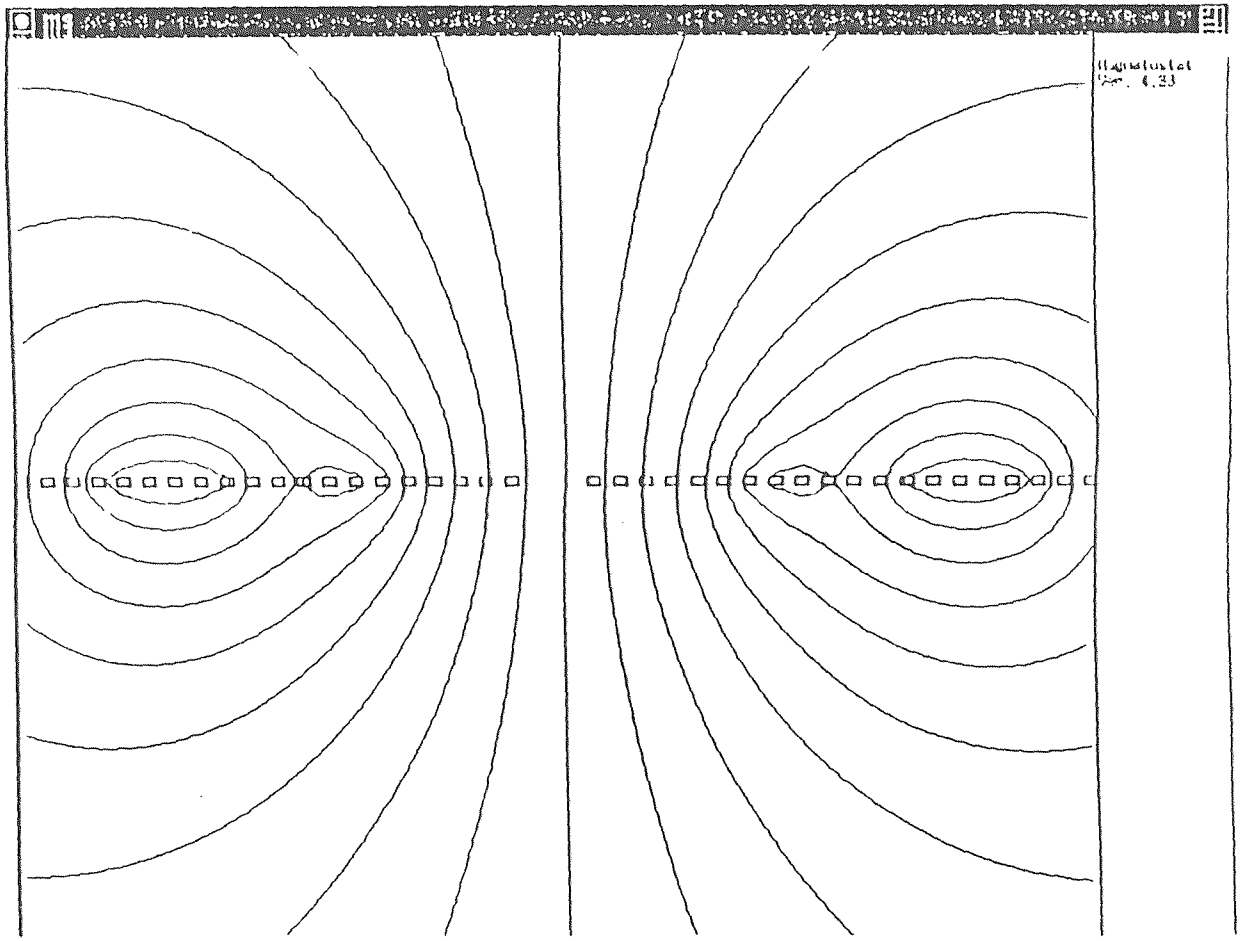

Figure 4.4 Lines of Magnetic flux for inductance calculation

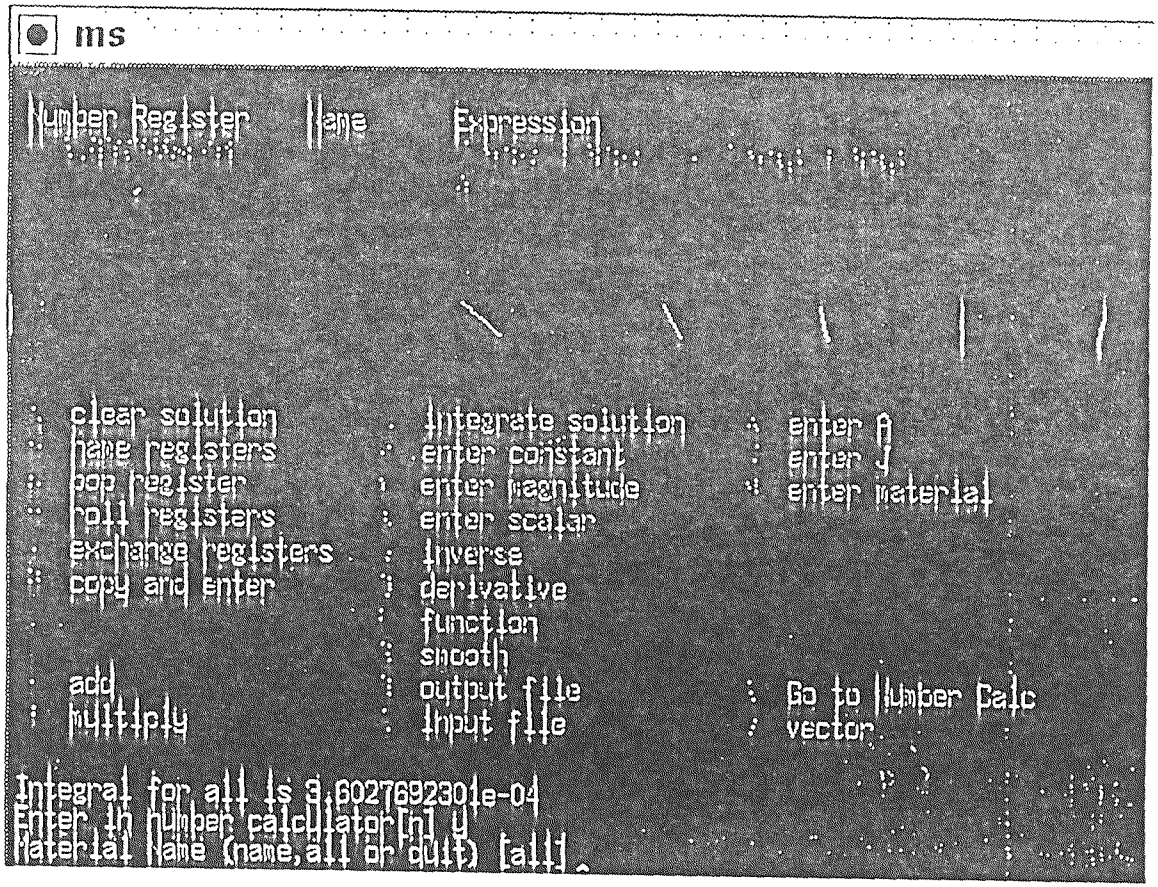

Figure 4.5 Output of result for inductance calculation

The following is a program for calculating inductance using Grover's model as described in section 4.1

```
l0=col(1)*1e-1
w=col(2)*1e-4
t=col(3)*1e-4
n=col(4)
s=col(5)*1E-4
LL(l)=2*l*(ln(2*l/(w+t))+0.50049+((w+t)/3/l))
for k=1 to 20  step 1 do
l(k)=2*LL(l0-w-2*(k-1)*(s+w))+2*LL(l0-w-2*(k-1/2)*(s+w))
col(14)=l0-w-2*(k-1/2)*(s+w)
cell(20,k)=l(k)
end for
L0=total(col(20))
col(6)=L0

G1(d)=d*exp(-((1/12*(w/d)^2)+(1/60*(w/d)^4)))
G(d)=G1(d)*exp(-(1/168*(w/d)^6)-(1/360*(w/d)^8))
Q(l,d)=ln((l/G(d))+(1+(l/G(d))^2)^0.5)-(1+(G(d)/l)^2)^0.5+G(d)/l
MM(l,d)=l*Q(l,d)
for i1=1 to 19 step 1 do
for j1=i1+1 to 20 step 1 do
mm11(i1,j1)=8*(MM((l0-w-(j1-i1)*(s+w)),(j1-i1)*(s+w)))
mm1(i1,j1)=mm11(i1,j1)-8*MM((j1-i1)*(s+w),(j1-i1)*(s+w))
mm22(i1,j1)=8*(MM((l0-w-(j1-i1+1)*(s+w)),(j1-i1)*(s+w)))
mm23(i1,j1)=8*MM((j1-i1)*(s+w),(j1-i1)*(s+w))
```

```
mm2(i1,j1)=mm22(i1,j1)-mm23(i1,j1)
cell(21+i1,j1)=mm1(i1,j1)+mm2(i1,j1)
end for
cell(19,i1)=total(col(21+i1))
end for
m1=total(col(19))
col(7)=m1

for i=1 to 20 step 1 do
for j=1 to 20 step 1 do
mm33(i,j)=16*(MM((l0-w-abs(j-i)*(s+w)),(l0-w-(i-1)*(s+w)-(j-1)*(s+w))))
mm3(i,j)=mm33(i,j)-16*MM((abs(j-i)*(s+w)),(l0-w-(i-1)*(s+w)-(j-1)*(s+w)))
cell(21+i,j)=mm3(i,j)
end for
cell(18,i)=total(col(21+i))
cell(17,i)=2*(l0-w-2*(i-1)*(s+w))+2*(l0-w-2*(i-1)*(s+w)-(s+w))
end for
m2=total(col(18))
col(8)=m2
L=L0+m1-m2
col(9)=L
LE=total(col(17))

RCU=1.67*1E-6*LE/w/t
RAL=2.80*1E-6*LE/w/t
col(10)=RCU
col(11)=RAL
```

col(12)=2*3.1415926*150*1E-3*L/RCU

col(13)=2*3.1415926*150*1e-3*L/RAL

	-1- L(mm)	-2- w(microns)	-3- T(microns)
1	2.0000	30.0000	60.0000

	-4- n(turns)	-5- gap(microns)	-6- L0
1	20.0000	10.0000	37.0099

	-7- Mut. Ind M1	-8- Mut. ind M2	-9- Inductance LT
1	188.2899	-25.2926	136.2700

	-10- R(Cu)	-11- R(Al)	-12- Q(Cu)
1	0.4333	0.7264	296.4221

	-13- Q(Al)
1	176.7946

Table 4.1 Summary of inductor characteristics

CHAPTER 5

SIMULATION RESULTS FOR CAPACITANCE MODELING

5.1 Capacitance Estimate

In biomedical research, the need for small and reliable pressure sensor is without question[8]. It has an urgent need for a small, accurate, stable and low power pressure sensor, which is biocompatible and inexpensive. By taking advantage of the advanced state of the art for integrated circuit processing, silicon diaphragm miniature pressure sensors were developed for biomedical applications.

The two main types of transducers commonly used pressure sensors are piezoresistors mounted on a thin diaphragm that is deflected by pressure, and the capacitive transducer which has two plates one of which is a diaphragm. Both can be made using monolithic silicon technology, but capacitive transducers offer a number of advantages.

An exact method of calculating the capacitance of a plate capacitor has been suggested first by J.J. Thompson and more completely worked by A.E.H. Love[9]. In the present design the fringing effects were not considered. The general formula for calculating the capacitance consisting of a single pair of parallel plates in air is given by:

$$C = \sum_{i=1}^{n} \frac{\varepsilon A_i}{d}$$

where

C = the capacitance between the circular plates

$\varepsilon = 8.85418 * 10^{-14} F/cm$

$A = \pi r^2$ = the area of the modeled capacitance increment

d = the separation between the circular plates

For the following device dimensions,

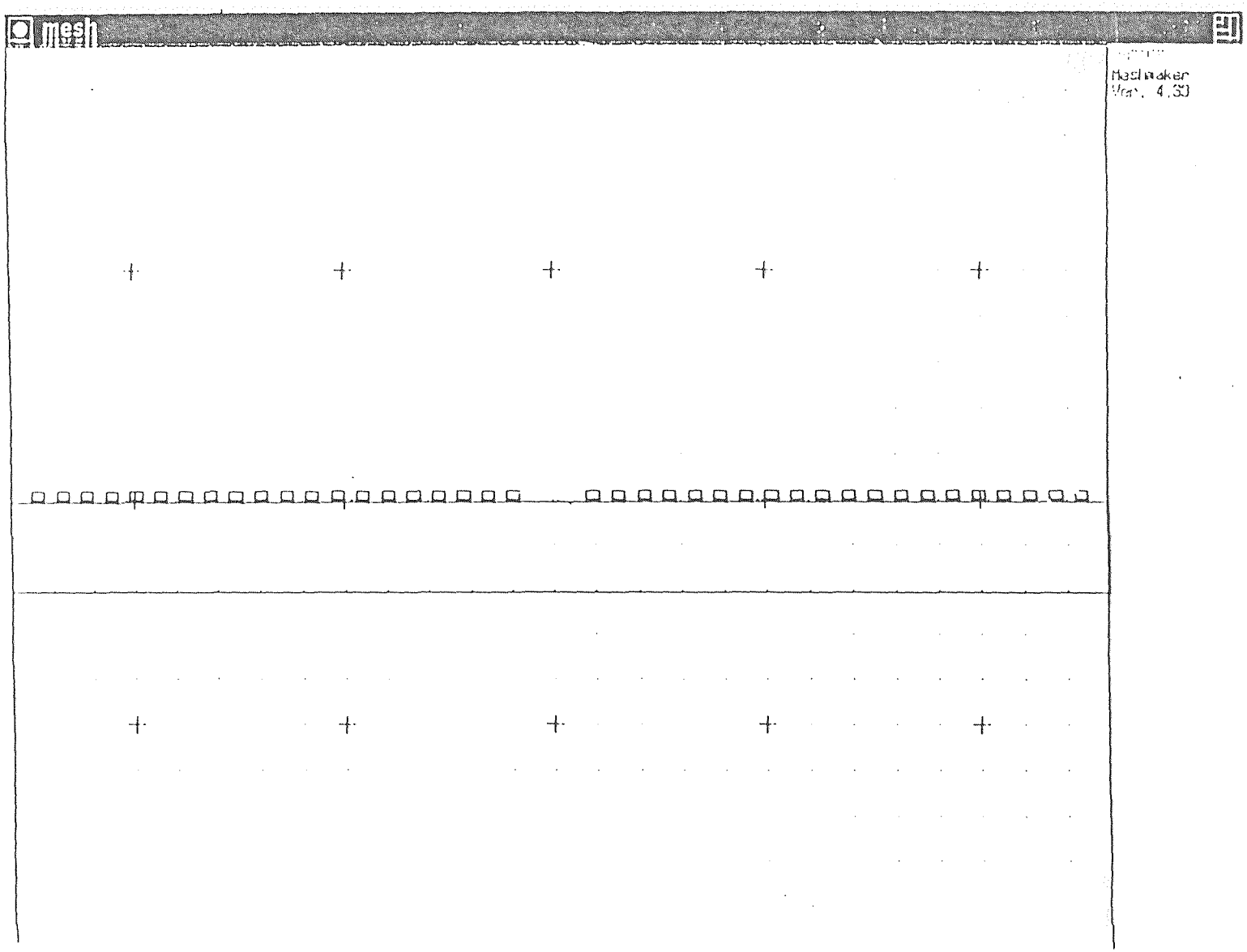

Figure 5.1 Cross section of the capacitance modeling

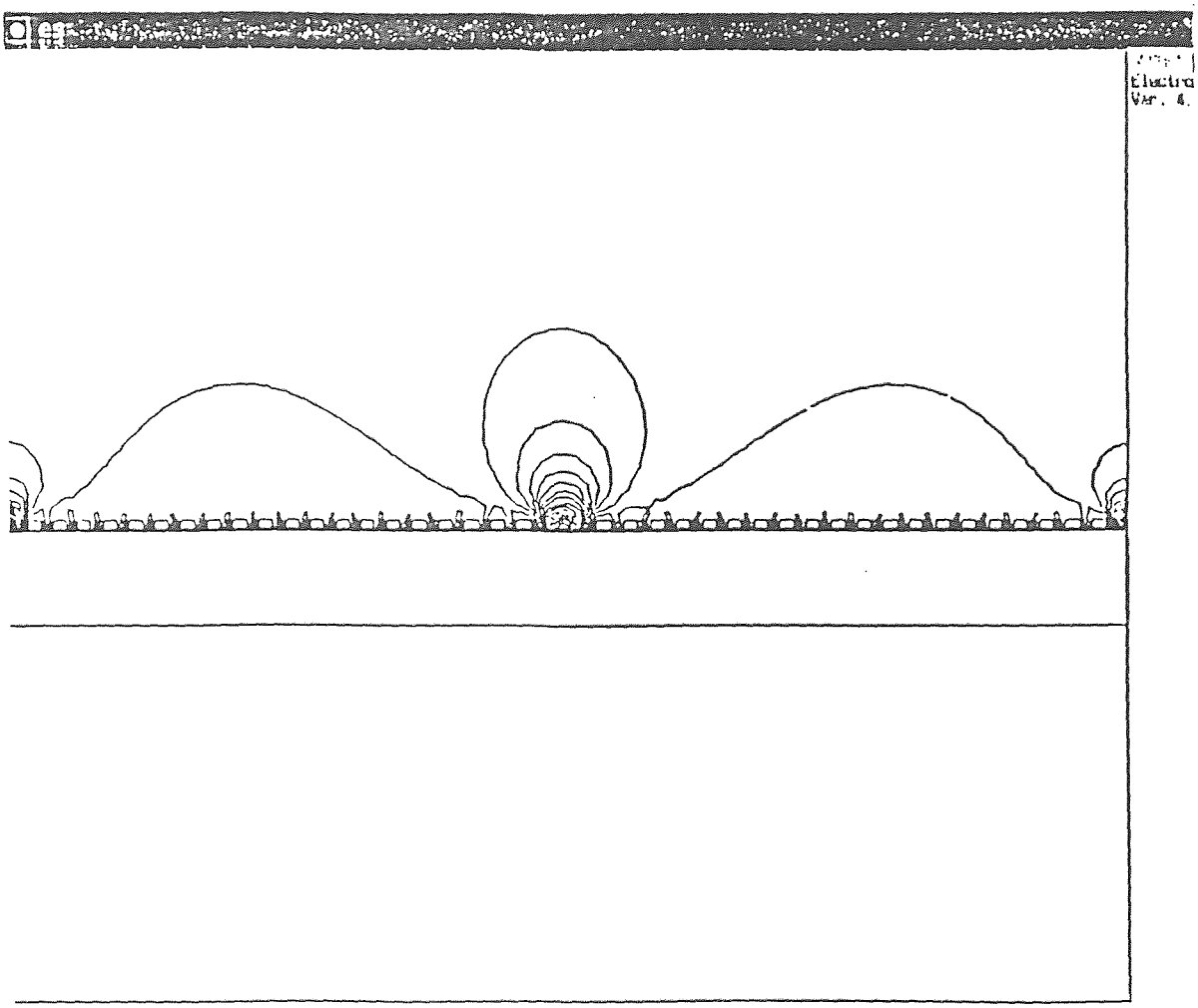

Figure 5.2 Electrostat equi plot

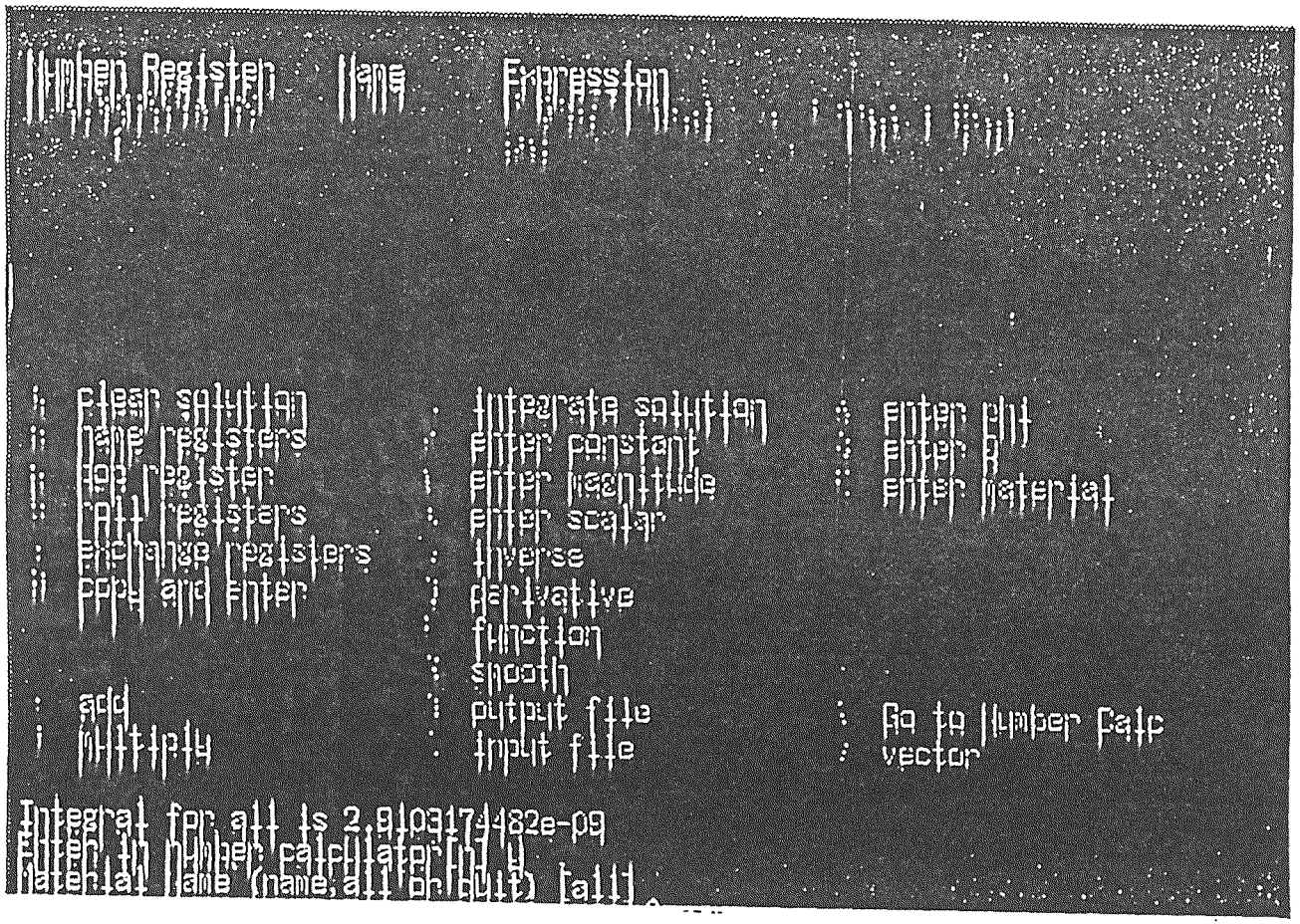

Figure 5.3 Output of result for capacitance calculation

r = 120 μm and d = 0.6 μm the capacitance was found to be 2.9nF/meter.

5.2 Solid Modeling of Capacitance

For my thesis we would like to use a diaphragm type LC resonant sensor that resonates at the lowest practical frequency f_0. Calculate the actual capacitance of these structures Fig. 5.1-5.3. We are interested in obtaining a maximum capacitance per square micro of silicon. This means that the gap should be a minimum consistent with technology used.

5.3 Sigmaplot for Device Dimension Calculation

Resonant RLC devicecs based on silicon technology in which the capacitance varies with external pressure have been report by Collins and Backlund et.. The resonant frequency of the RLC series connected devices varies with as the capacitance diaphragm electrode spacing is varied.

In order to specify the device dimensions for the actual mask set, we us Sigmaplot Fig. 5.3-5.11 to get the relationship between resonant frequency and dimensions of the device. Sigmaplot is the acclaimed scientific graphics software for the PC. It is sophisticated enough to handle the highly specialized grahing needs of scientist and engineers. The program is accessible and easy to use, remarkably simple to operate. If I want analyze the data statistically or apply equations to generate new data. We can accomplish this with the menu options in the View and Math Menus, located approximately halfway across the Menu Bar. Sigmaplot's Transform option offers a full range of mathematical functions and a flexible editing format. I can define any combination of equations and they performed sequentially on the data in any column in worksheet.

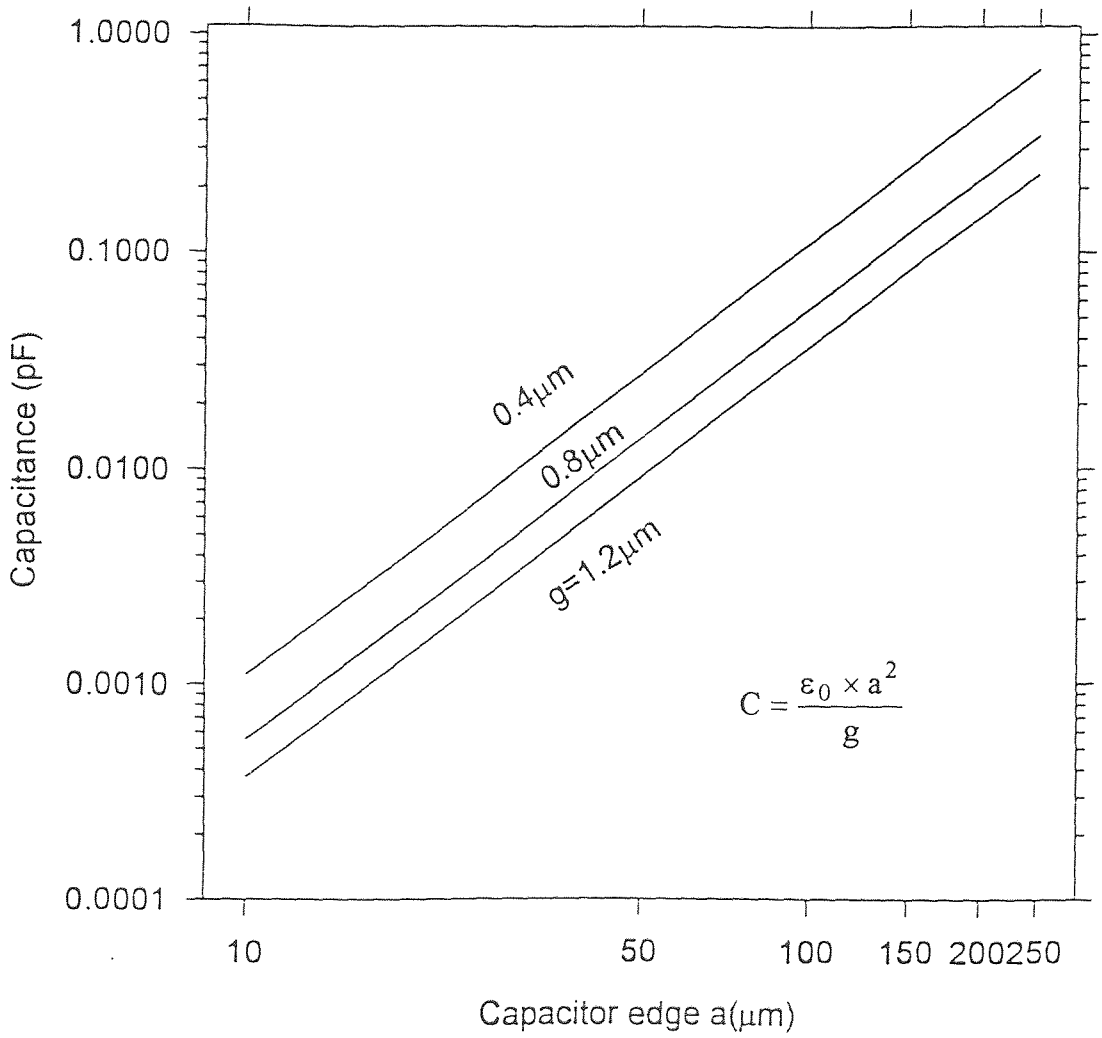

Figure 5.4 Capacitance vs capacitor edge (Device A), Area=a^2.

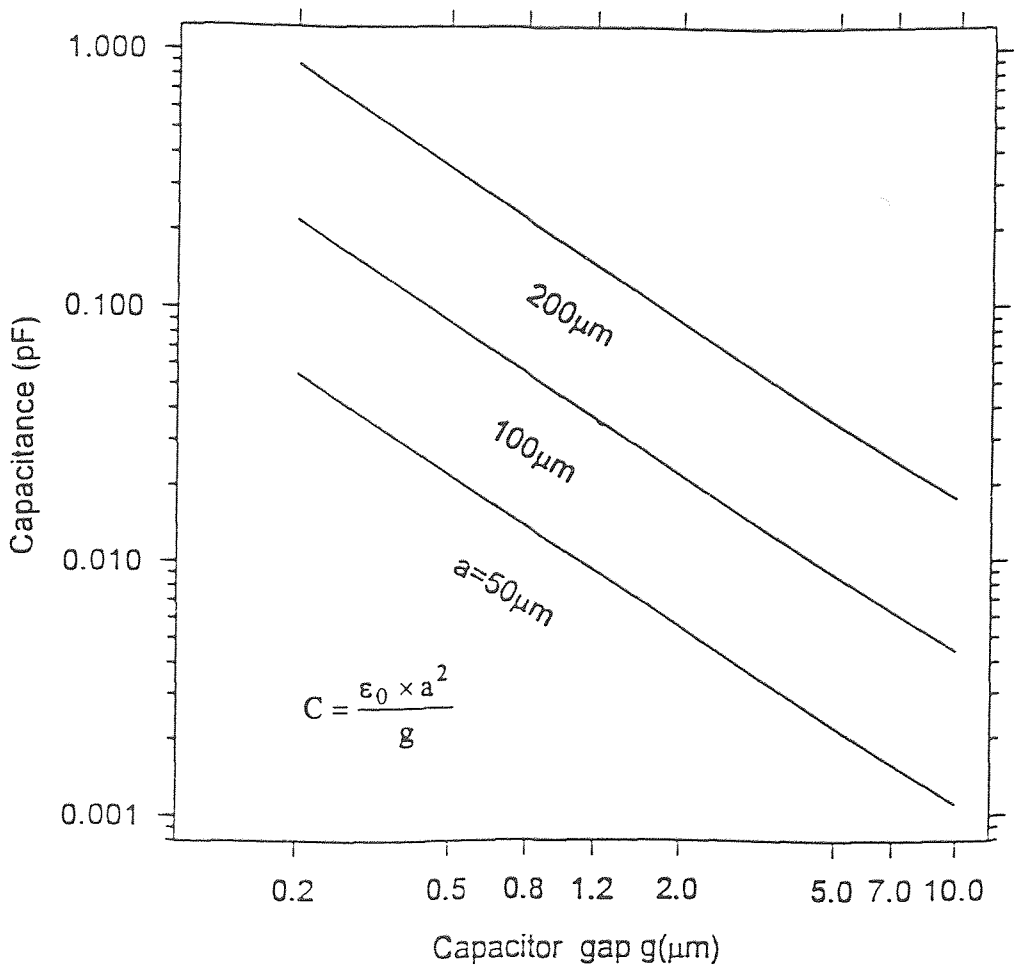

Figure 5.5 Capacitance vs capacitor gap (Device A)

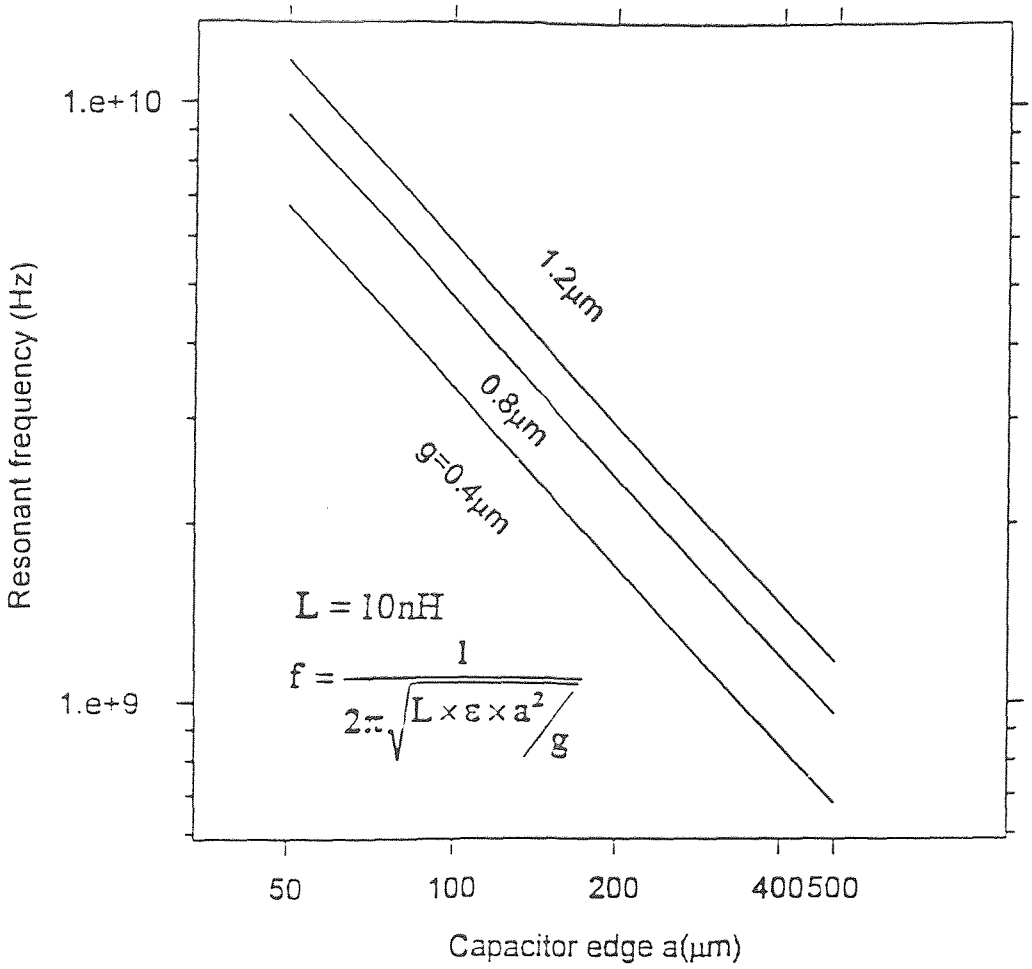

Figure 5.6 Resonant frequency vs capacitor edge (Device A)

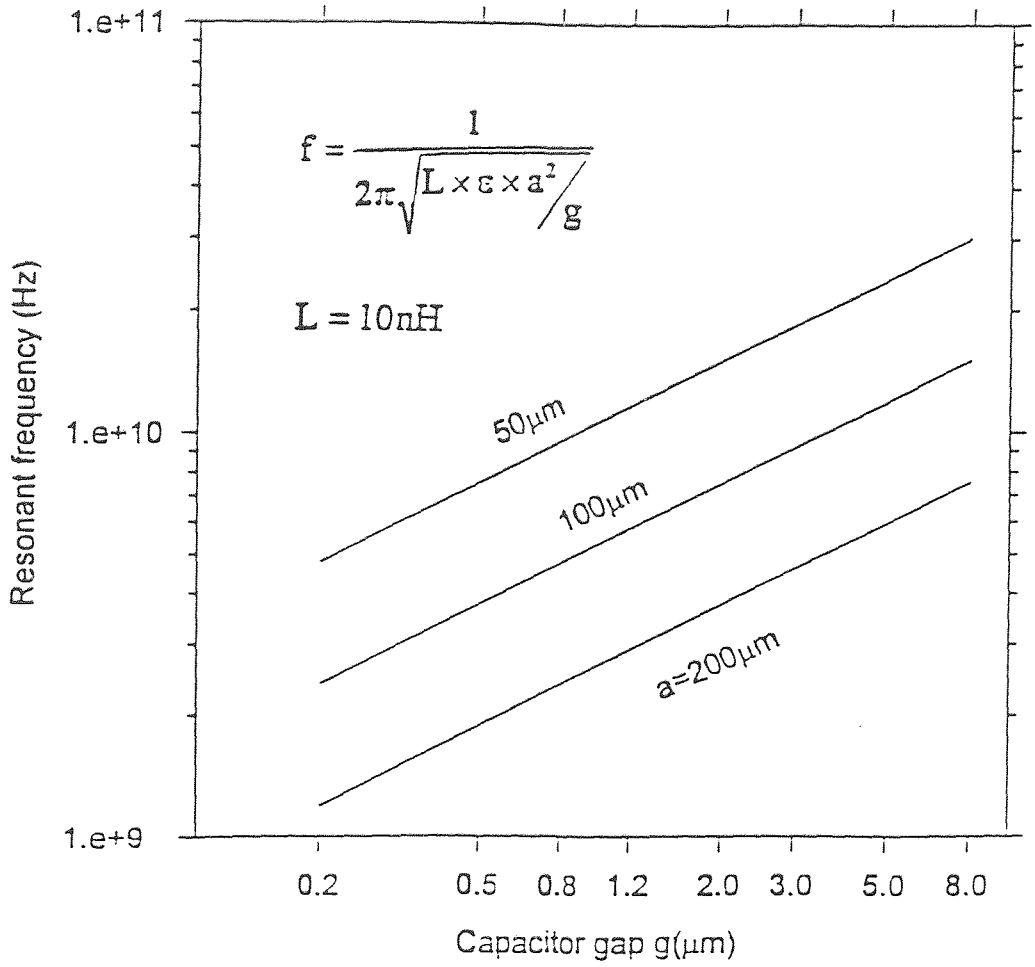

Figure 5.7 Resonant frequency vs capacitor gap (Device A)

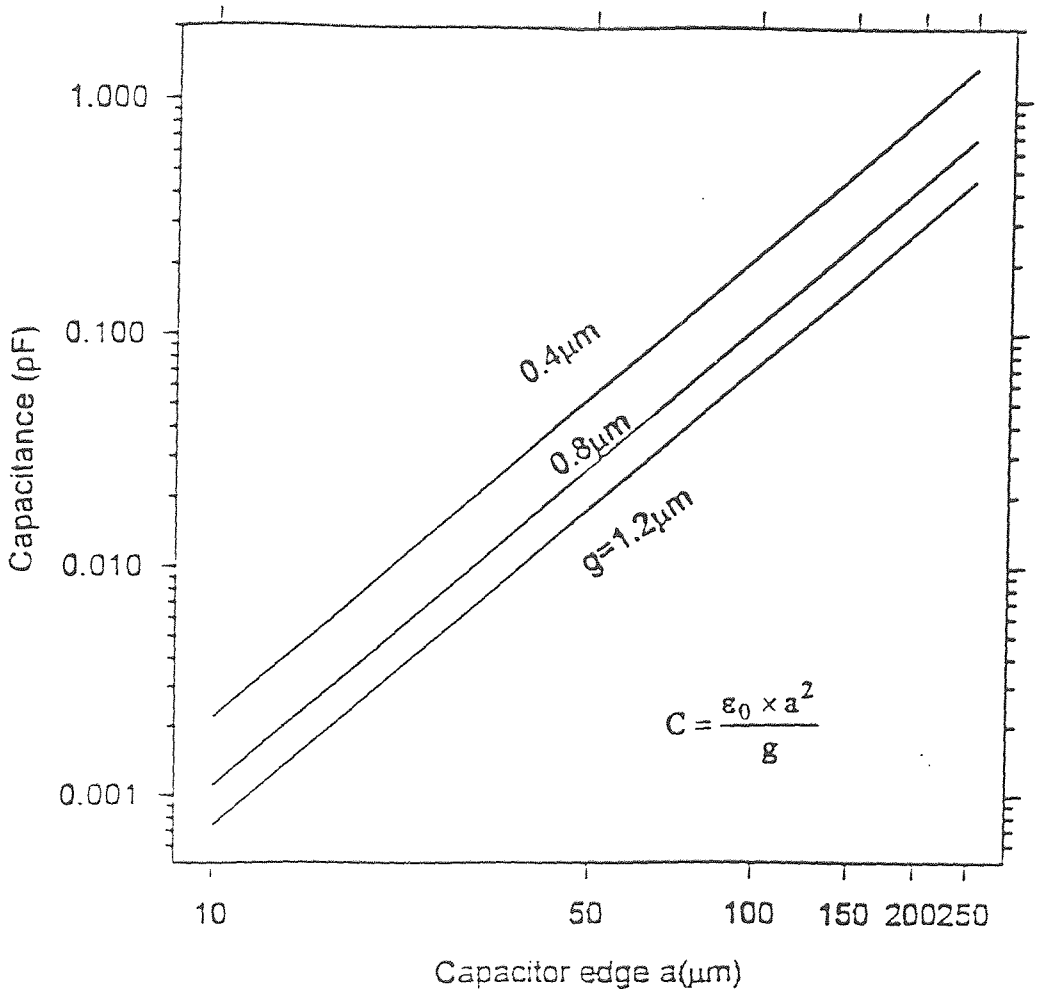

Figure 5.8 Capacitance vs capacitor edge (Device B) Area=a^2

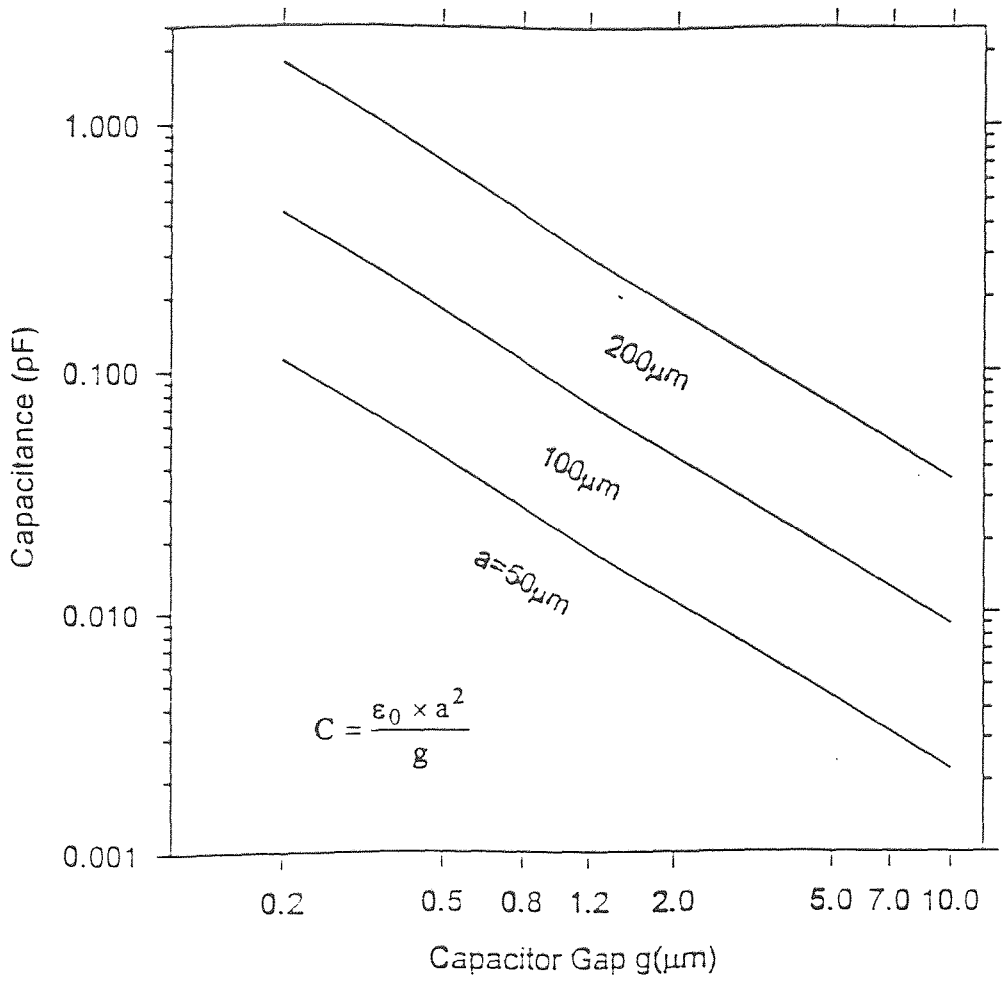

Figure 5.9 Capacitance vs gap (Device B)

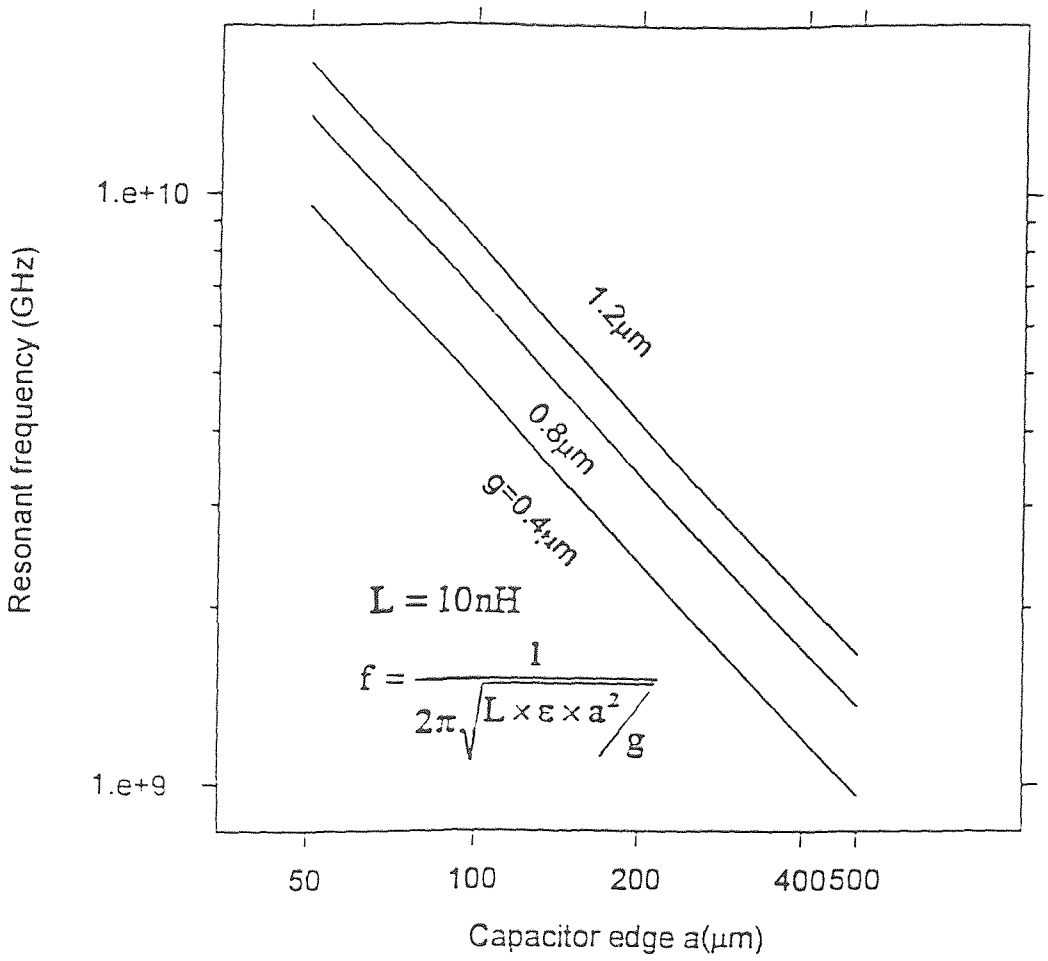

Figure 5.10 Resonant frequency vs capacitor edge (Device B)

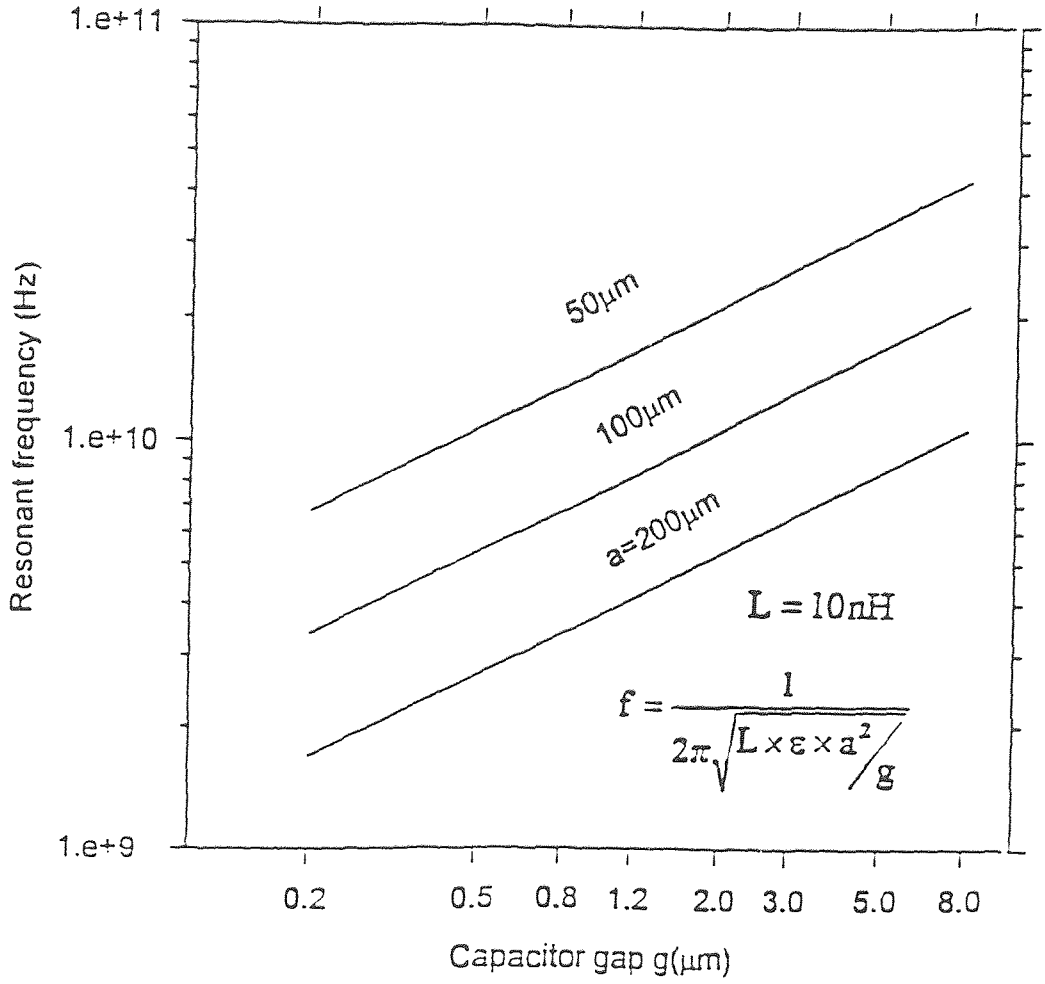

Figure 5.11 Resonant frequency vs capacitor gap (Device B)

CHAPTER 6

SIMULATION RESULTS FOR PSPICE MODELLING

6.1 Introduction

The operational system includes three components: the rf power source, the implanted sensor, and the telemetry receiver shown in Fig. 3.9. The rf power source at frequency f_S consists of a current-driven inductive source which creates the rf magnetic field around the implanted sensor. The implanted sensor which located within the rf magnetic field region contains inductance L which is excited by the magnetic field. The implanted sensor has series-connected capacitance C as shown in Fig. 2.3. and will resonate at the frequency

$$f_0 = \frac{1}{2\pi\sqrt{LC}}$$

When the external power source frequency f_S equals the implanted device resonance of f_0. The external power source sweeps a frequency range

$$f_0 - \Delta\frac{f_\Delta}{2} < f_s < f_0 + \Delta\frac{f_\Delta}{2}$$

near the frequency $f_S=f_0$ the current i flows in the RLC loop of the implanted device and the loading is detected by the telemetry receiver unit. The implanted sensor acts as a passive transponder in this application. A sensitive receiver unit determines the resonant frequency f_0 which is a direct function of capacitance and fluid pressure.

6.2 PSPICE Simulation Result

The equivalent circuit has been simulated (Appendix C) using varied fs and R to get resonant frequency f_0 and the best value of driving frequency. Quality factor is varied with resistance R in Fig. 6.1.

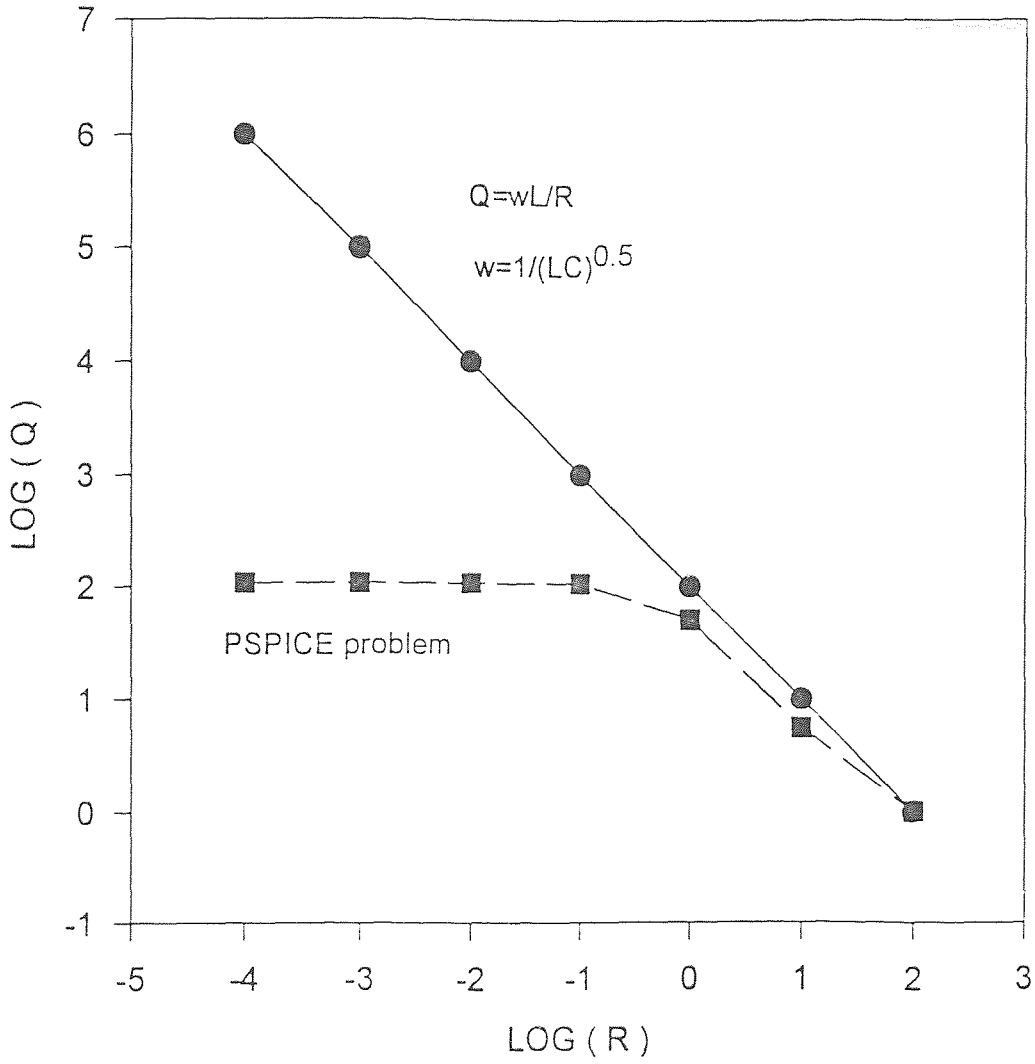

Figure 6.1 Quality factor vs resistance (Device B)

CHAPTER 7

SUMMARY AND CONCLUSIONS

In this thesis we designed four totally implantable passive devices. The basic passive pressure sensor consists of a chemically etched diaphragm with an integral plane coil. The resonant frequency of the RLC series connected device varies with static fluid pressure as the capacitance diaphragm electrode spacing is varied. The capacitive diaphragm for the all types is very sensitive for ICP monitoring. The geometry of the device is simulated using Maxwell 2D solid modeling package. IC station in Mentor Graphic version 8.2 has been used for drawing the physical layout of the device. The geometry is much smaller than previously designed intracranial pressure sensors. The chip dimensions are 2mm by 2mm with an area of $4mm^2$. Inductance of the microsensor is mathematically modeled by the help of Grover's model and simulation is flexible to variety of structures and dimensions of inductance. The PSPICE simulation for all types of devices has broadened the choice of the ICP monitoring. A lumped equivalent circuit is used for modeling to determine the resonant frequency with PSPICE. This thesis demonstrates feasibility, based on detail simulation of a microsensor-based pressure monitoring system with remote readout. The microsensor is a micromachined device using thick film copper interconnects to be fabricated in a Class-10 cleanroom facility at NJIT's Microelectronics Research Center. In accomplishing the readout measurements the coupling coefficient between the transmitter and receiver is observed to be very small thereby posing an experimental challenge. The harmonic analysis of the whole system is done using the Fourier Analysis capability of PSPICE. From the results it is observed that the received signal strength is high when the transmitter is pulsed with a burst of sinusoidal oscillations with $\omega=2f_0$ is twice the resonant frequency of the pressure sensor. So it is suggested for the improvement of the readout remote sensing of ICP that the signal strength of the V_S

(source) has to be high and has to be operated at $2f_0$ twice the frequency of the pressure sensor internal resonance.

The current designed microsensor has variety applications apart from the current ICP measurement application. The other biomedical applications of the sensor include the blood pressure measurement and the monitoring of the fluid pressures of a women during the child birth. Glaucoma patents and postsurgery for many ophthalmology clinical situations can be monitored using this passive sensor as an implanted device. With the further study of the diaphragm characteristics, the pressure sensing mechanism described in this thesis can be applied to more fields including the automotive industry.

APPENDIX A

MAXWELL PROGRAMMING DETAIL

The following is a set of screens of MAXWELL modeling

1 Meshmaker – Draw the geometry of the design and make the mesh

(1) Set up the unit of the screen

In the menu, go to "param"–"Units", and choose the unit you want to use in solving the problem from the sub-menu bar shown on the screen (as shown in Figure A.1).

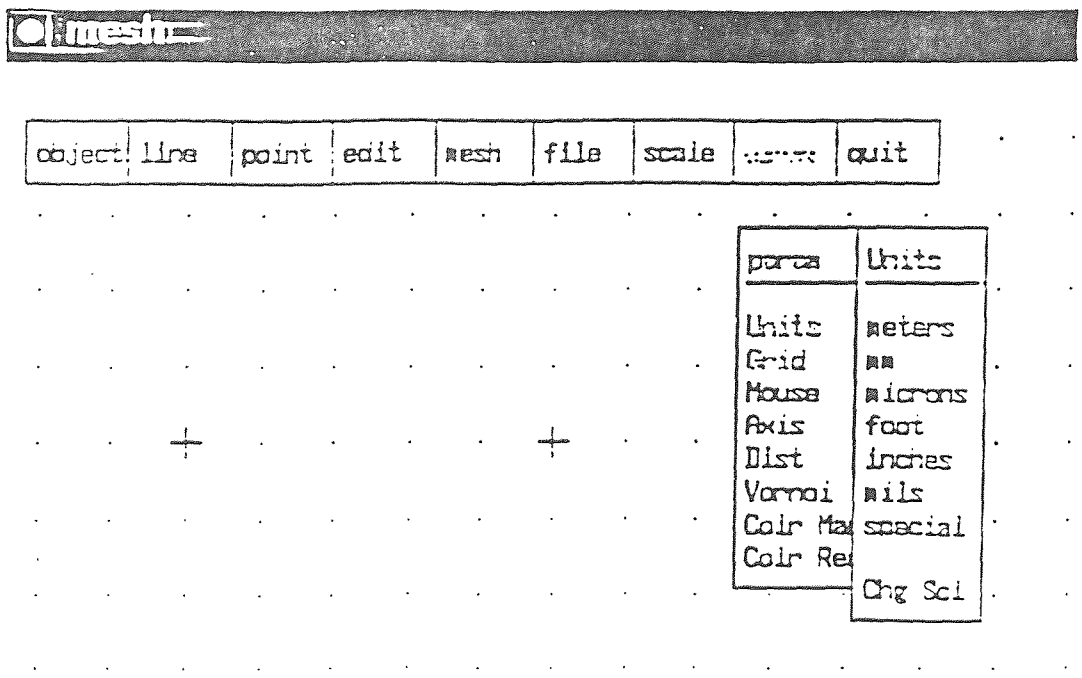

Figure A.1 Screen of setting the unit.

(2) Set up the grid type of the screen

In the menu, go to "param" -- "Grid", it will show the screen (as shown in Figure A.2). There are two kinds of coordinate systems can be chosen: Cartesian or Cylindrical. Either coordinate system can be chosen as for the convenes for drawing the geometry design.

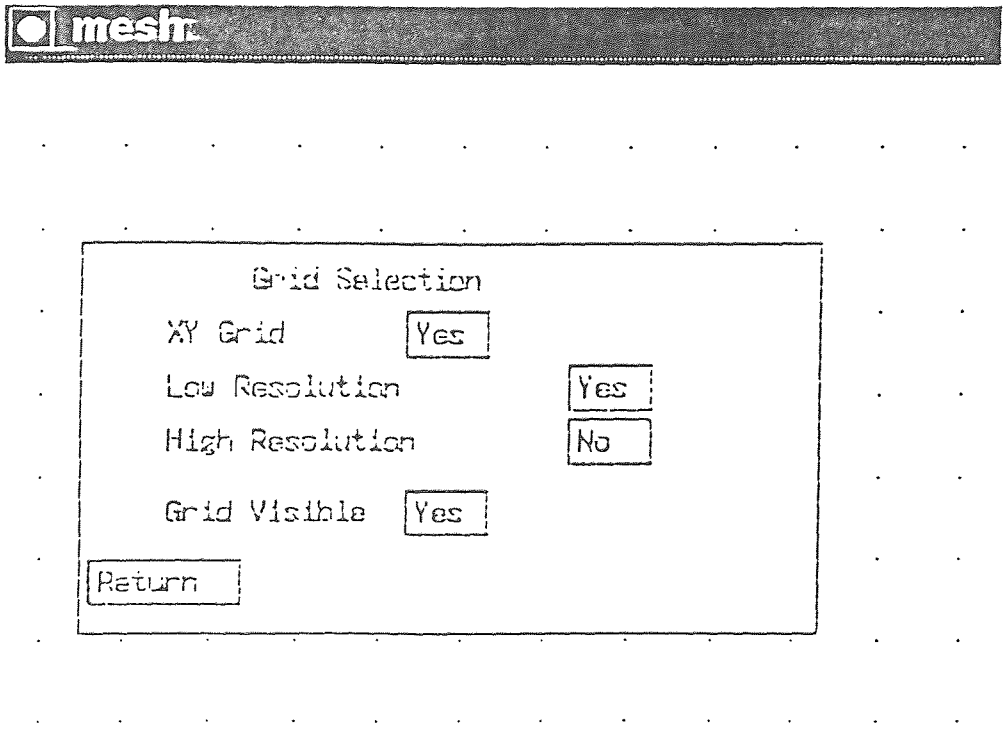

Figure A.2 Screen of setting the grid type.

(4) Draw the problem geometry

In the menu, "object", "line" or "point" sub-menu can be used to draw the problem geometry, whatever the geometry is. A "line" sub-menu is shown in Figure A.4.

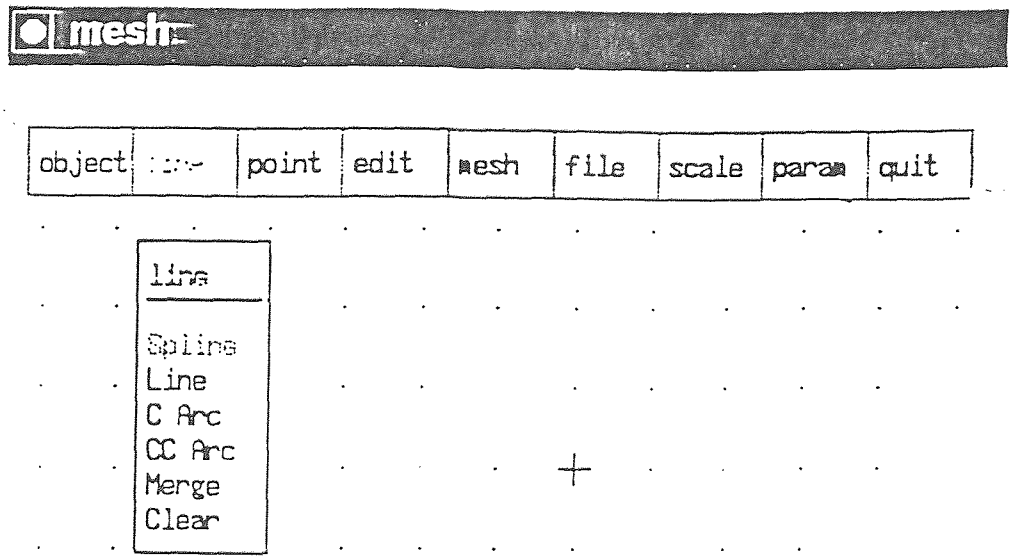

Figure A.4 Screen of "line" sub-menu.

(5) Edit the problem geometry

After the problem geometry has been drawn, the "edit" sub-menu can be used to edit the geometry ("edit" screen is shown in Figure A.5). By using the "edit" sub-menu, part or the whole geometry can be moved, copied or re-sized. And this makes the geometry making much easier.

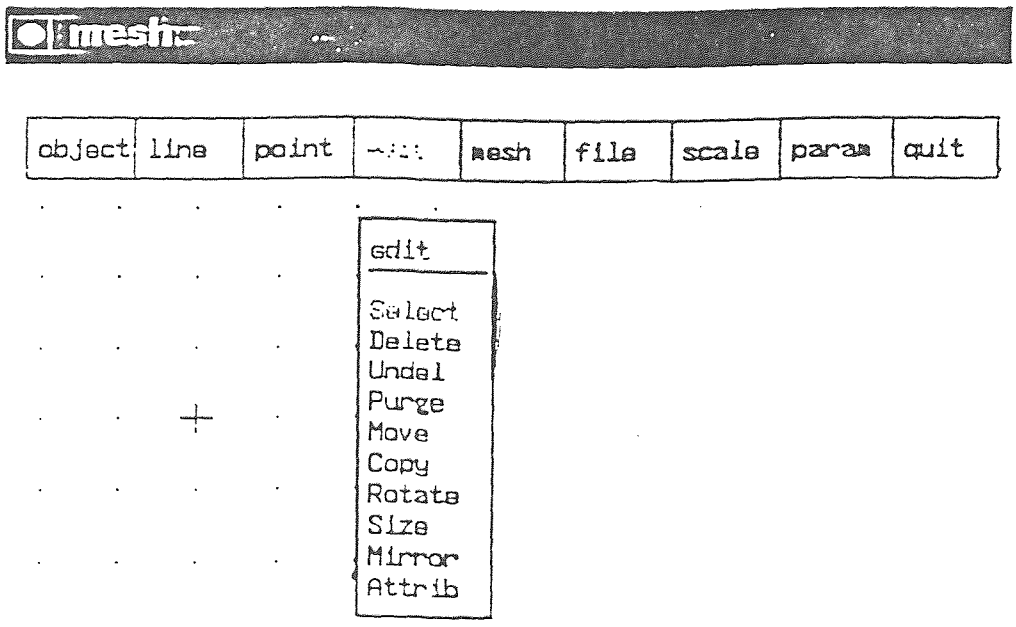

Figure A.5 Screen of "edit" sub-menu.

(6) Do the mesh making

After the geometry is set, mesh making is followed. A screen of "mesh" is shown in Figure A.6. From the menu, choose "Make" to do the initial mesh making. This is the fist step of mesh making.

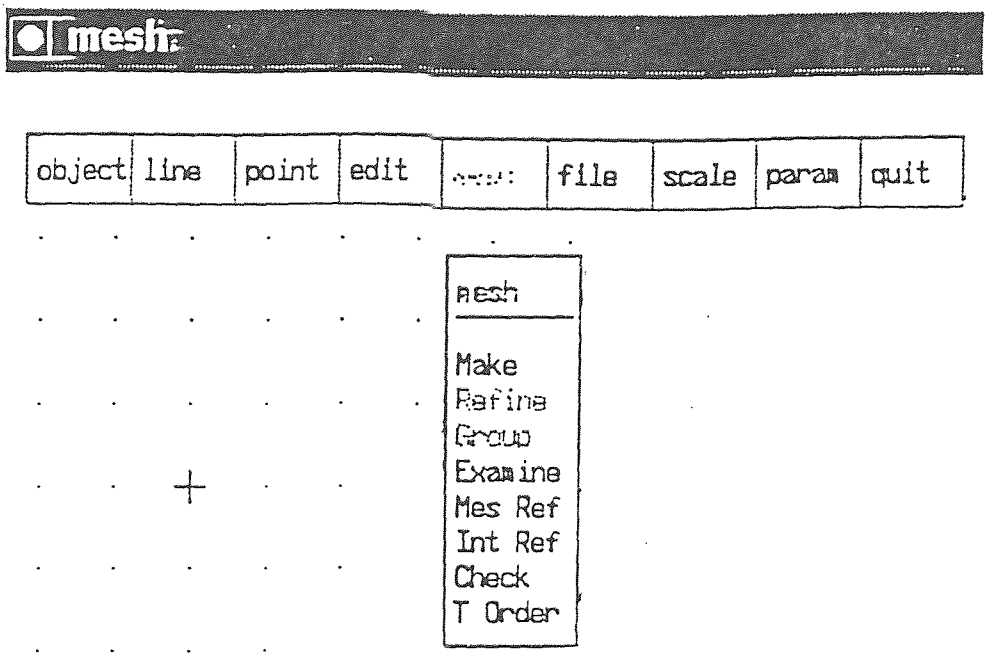

Figure A.6 Screen of "mesh" sub-menu.

(7) Refine the mesh

The initial mesh got from the "mesh" – "Make" is pretty rough, so the refinement of the mesh is necessary. The "mesh" –"Refine" sub-menu is shown in Figure A.7. Different kinds of refinement can be chosen from this sub-menu according to the different geometry refinement required from the problem.

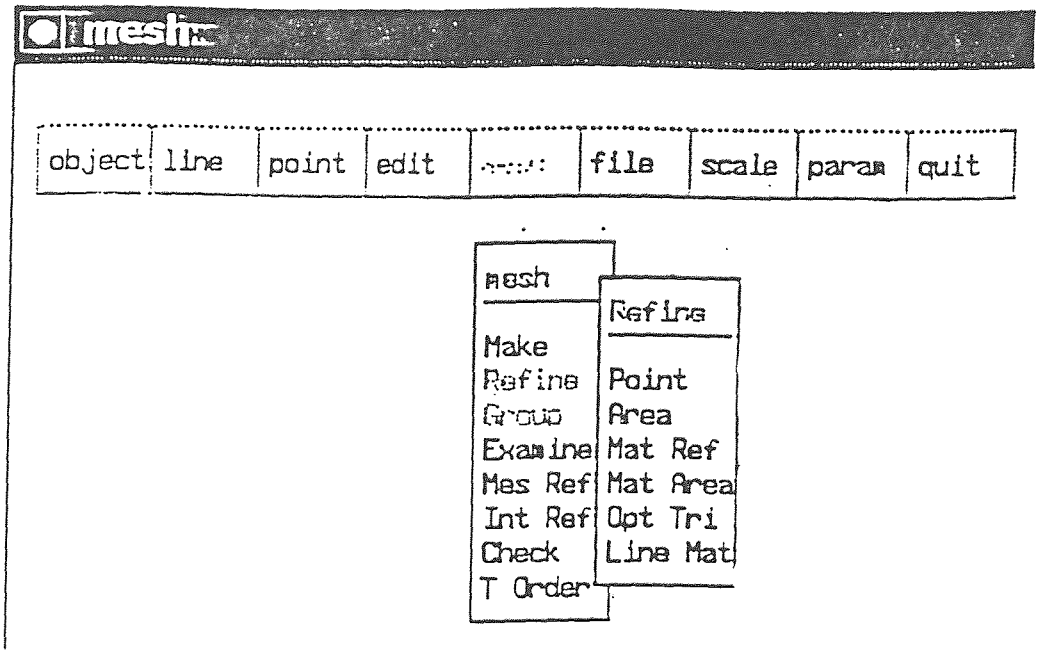

Figure A.7 Screen of "Refine" sub-menu.

After the refinement has been done, the mesh of the whole geometry area for this magnetic micromotor YTMM-5 is shown in Figure A.8.

Figure A.8 Screen of geometry with mesh

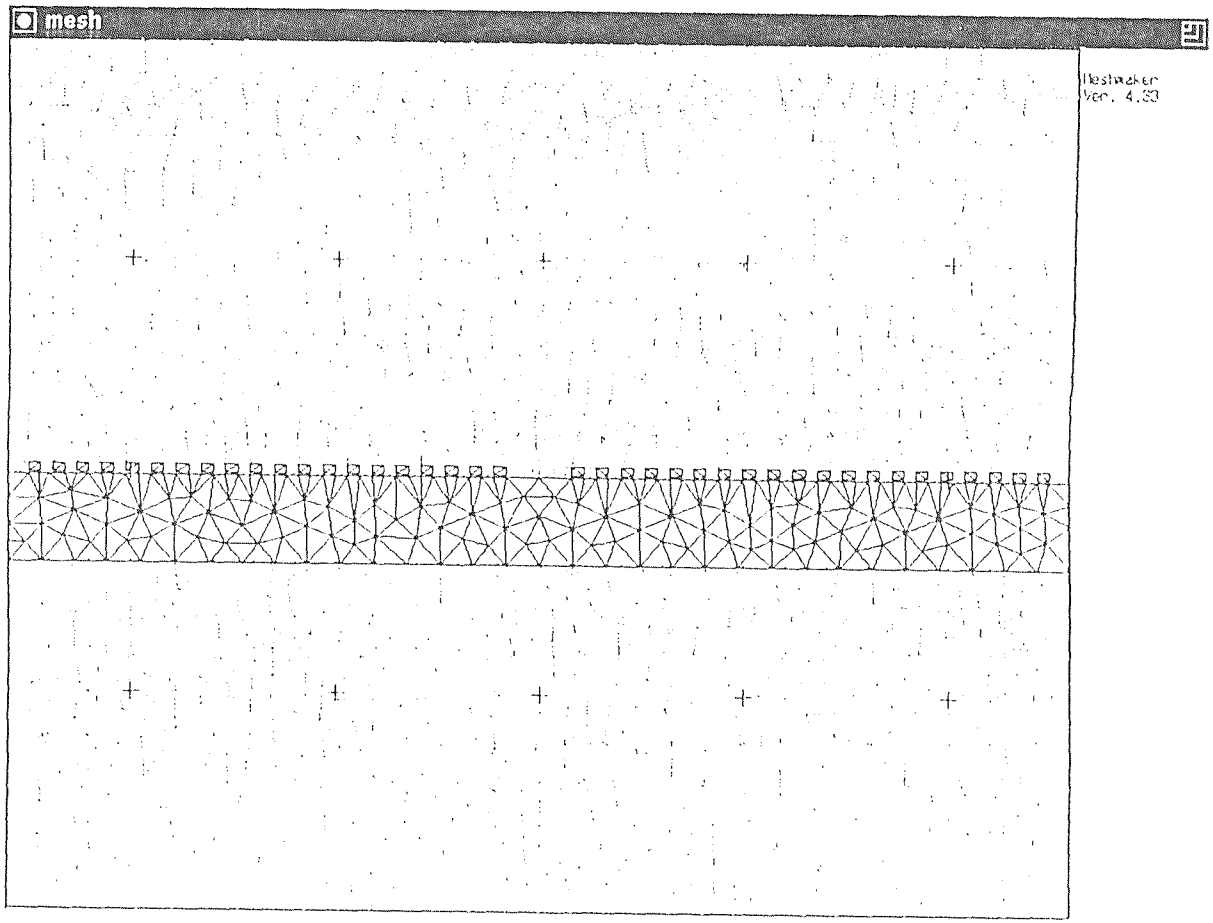

2. Magnetostatic Solver – Solve the problem

(1) Retrieve the file and set up the parameters for the problem

Use the "file" sub-menu and retrieve the file saved in Meshmaker. Then choose the "setup" -- "Att Set" sub-menu (as shown in Figure A.10). If we click and choose this function, a series of screens will appear and the parameters can be set through these screens. These screens are shown as Figure A.11.

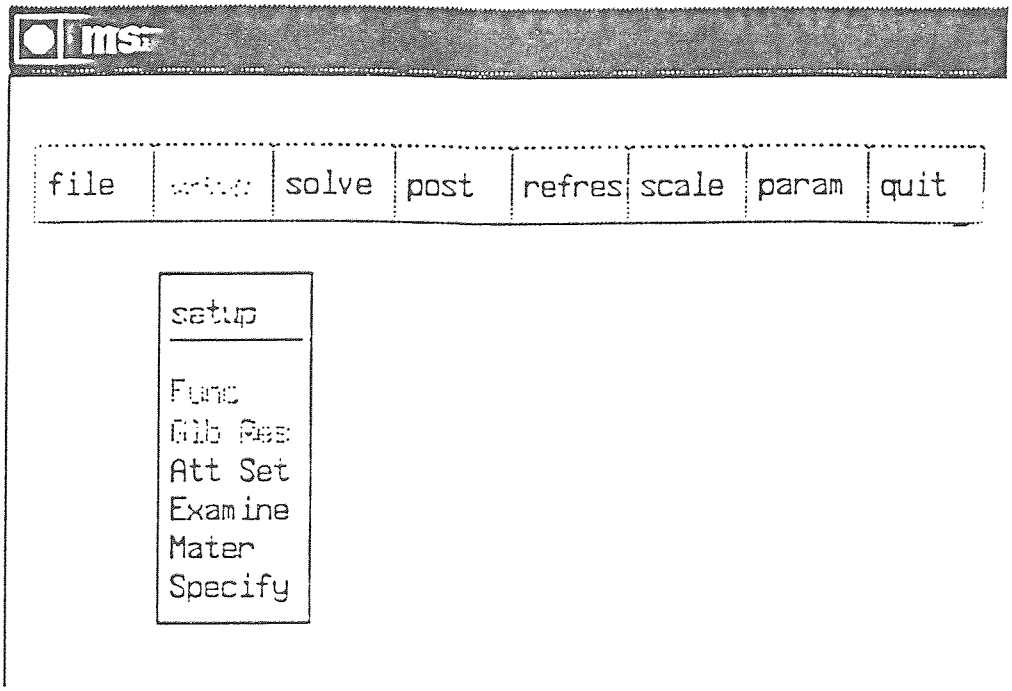

Figure A.10 Screen of "Att Set" sub-menu.

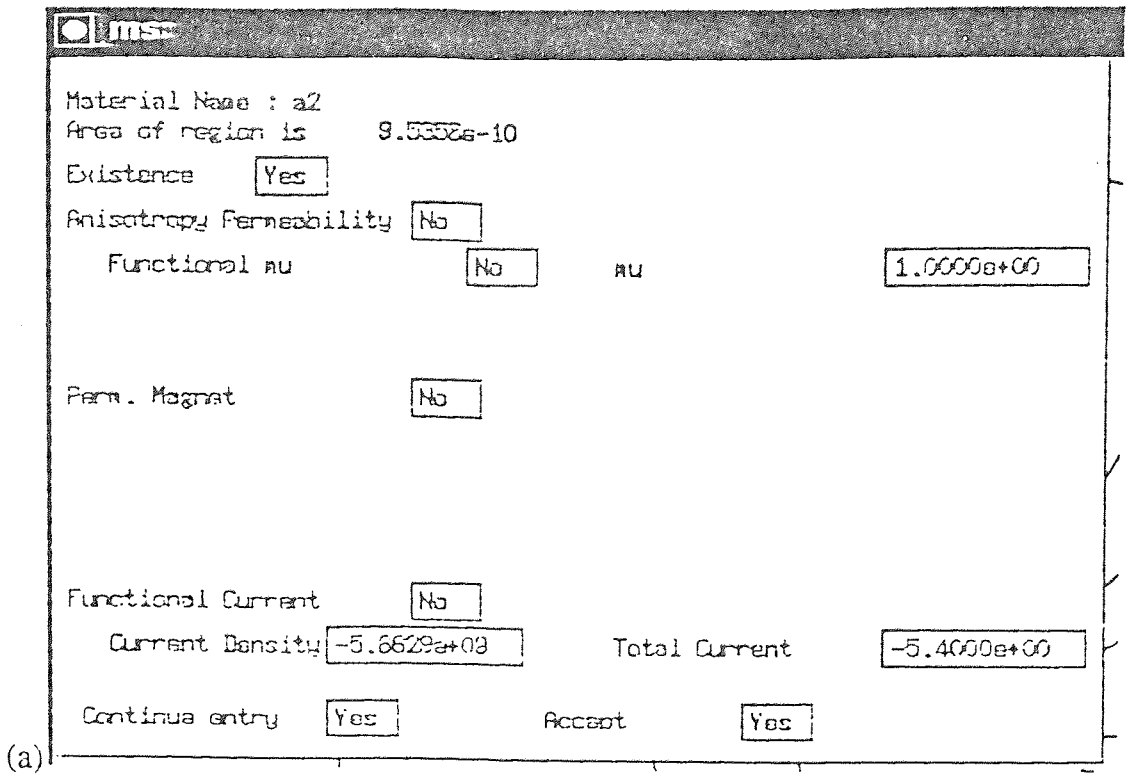
Material Name : a2
Area of region is 9.5358e-10
Existence Yes
Anisotropy Permeability No
Functional mu No mu 1.0000e+00
Perm. Magnet No
Functional Current No
Current Density -5.6629e+09 Total Current -5.4000e+00
Continue entry Yes Accept Yes

(a)

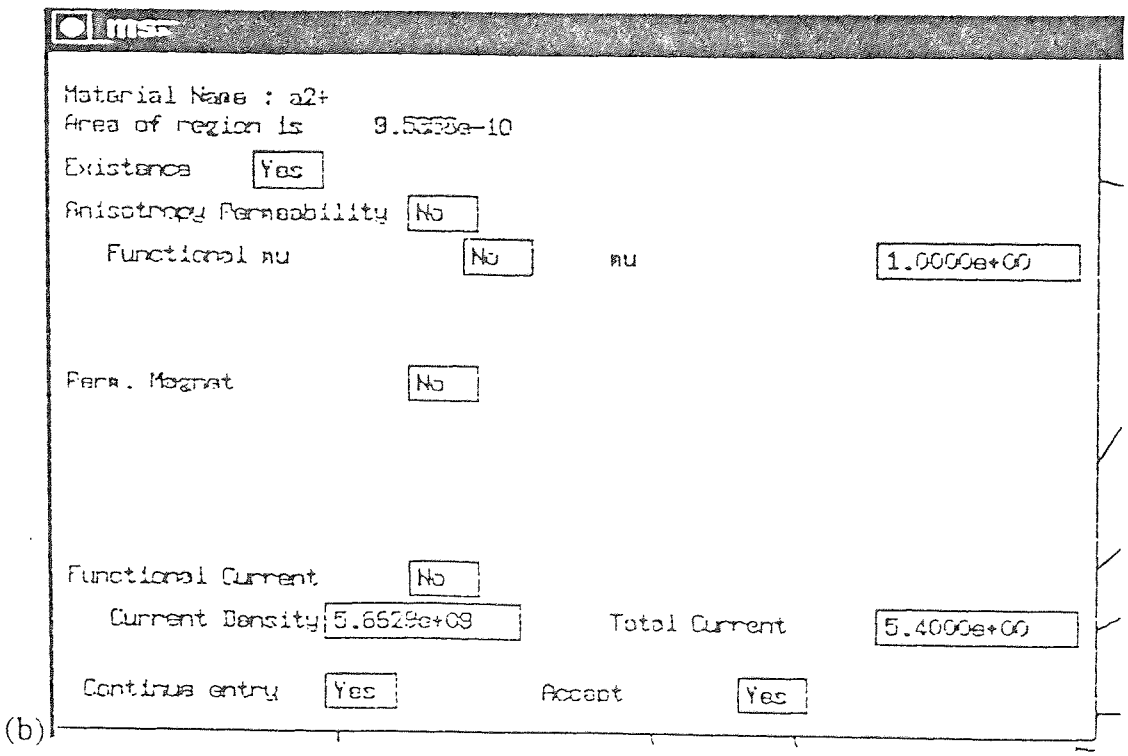
Material Name : a2+
Area of region is 9.5358e-10
Existence Yes
Anisotropy Permeability No
Functional mu No mu 1.0000e+00
Perm. Magnet No
Functional Current No
Current Density 5.6629e+09 Total Current 5.4000e+00
Continue entry Yes Accept Yes

(b)

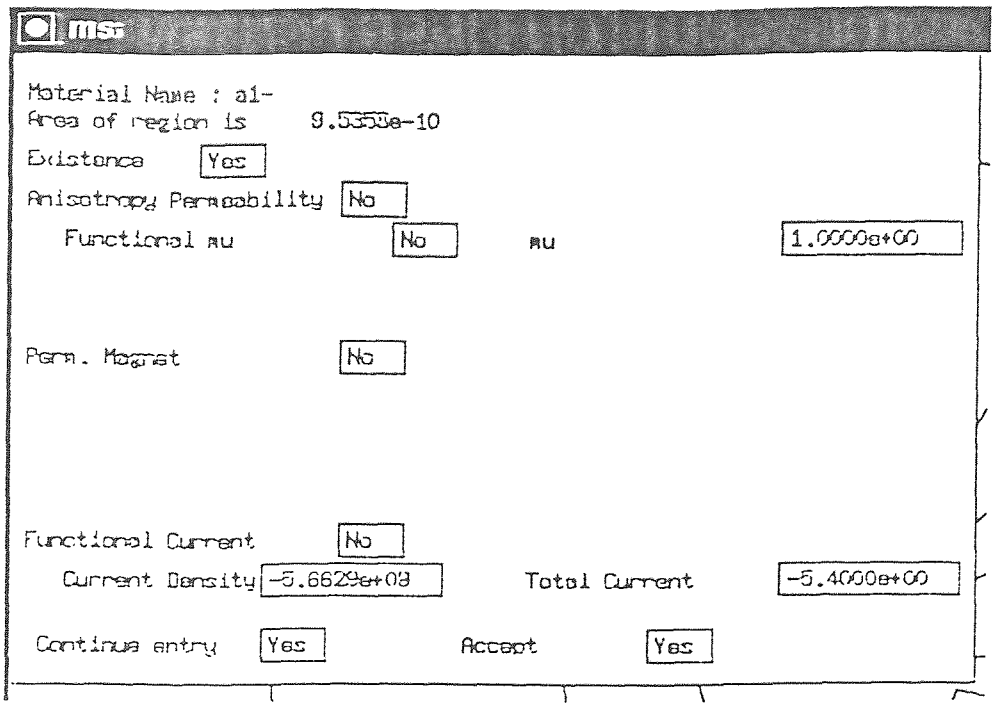
msr
Material Name : al-
Area of region is 9.5355e-10
Existence Yes
Anisotropy Permeability No
Functional mu No mu 1.0000e+00
Perm. Magnet No
Functional Current No
Current Density -5.6629e+09 Total Current -5.4000e+00
Continue entry Yes Accept Yes

(c)

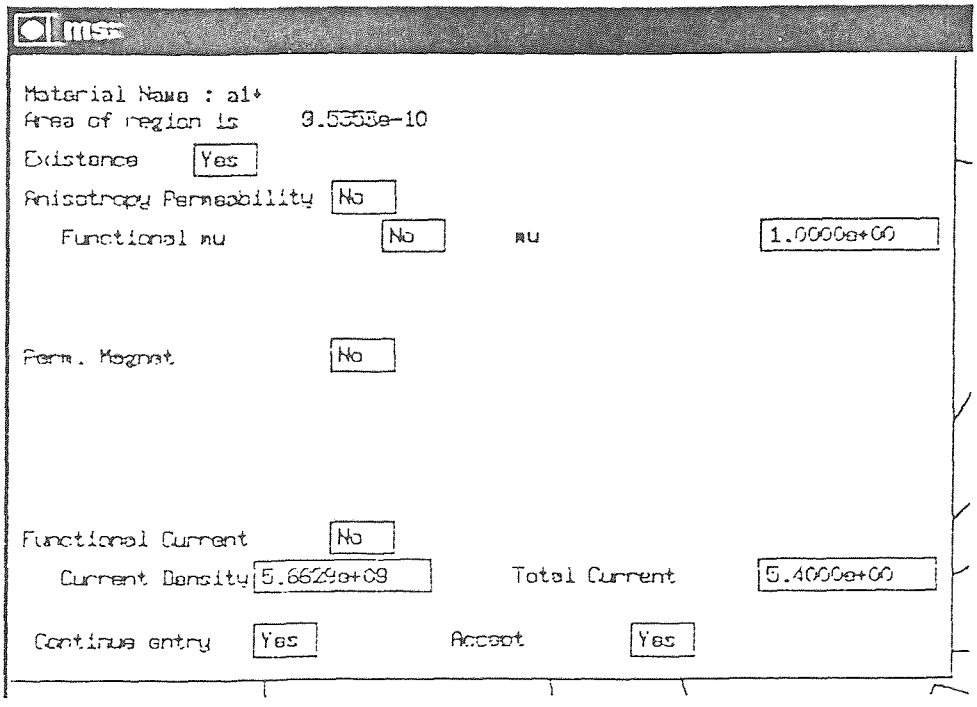
msr
Material Name : al+
Area of region is 9.5355e-10
Existence Yes
Anisotropy Permeability No
Functional mu No mu 1.0000e+00
Perm. Magnet No
Functional Current No
Current Density 5.6629e+09 Total Current 5.4000e+00
Continue entry Yes Accept Yes

(d)

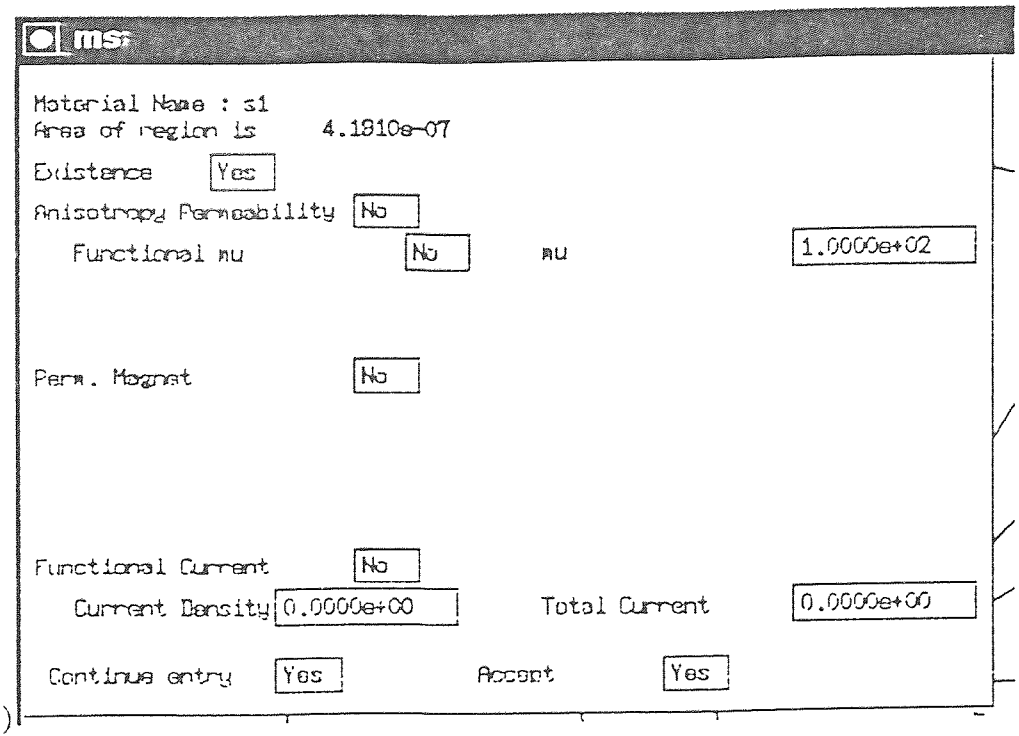
msf
Material Name : s1
Area of region is 4.1310e-07
Existence Yes
Anisotropy Permeability No
Functional mu No
mu 1.0000e+02
Perm. Magnet No
Functional Current No
Current Density 0.0000e+00
Total Current 0.0000e+00
Continue entry Yes
Accept Yes

(e)

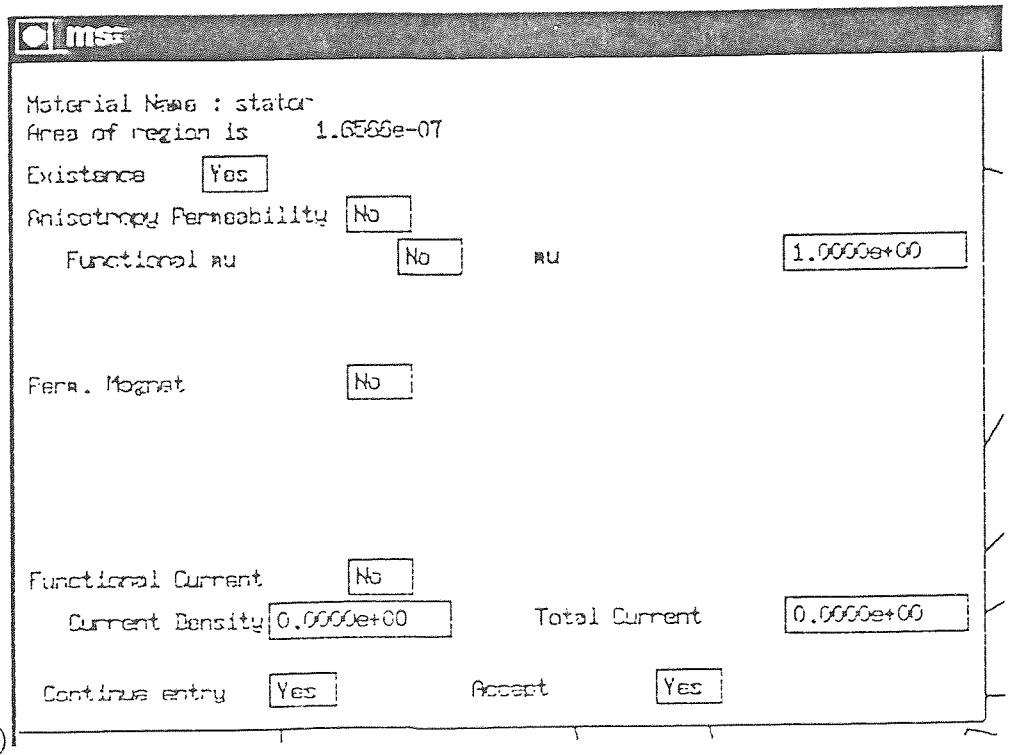
msf
Material Name : stator
Area of region is 1.6566e-07
Existence Yes
Anisotropy Permeability No
Functional mu No
mu 1.0000e+00
Perm. Magnet No
Functional Current No
Current Density 0.0000e+00
Total Current 0.0000e+00
Continue entry Yes
Accept Yes

(f)

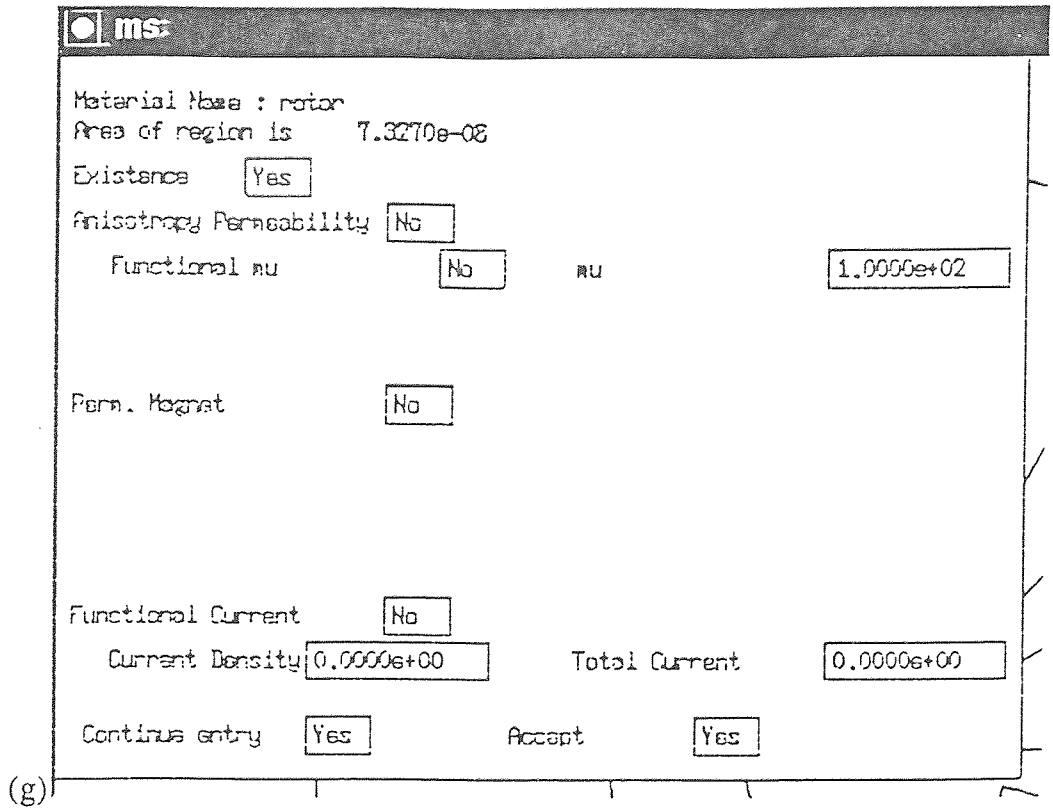

(g)

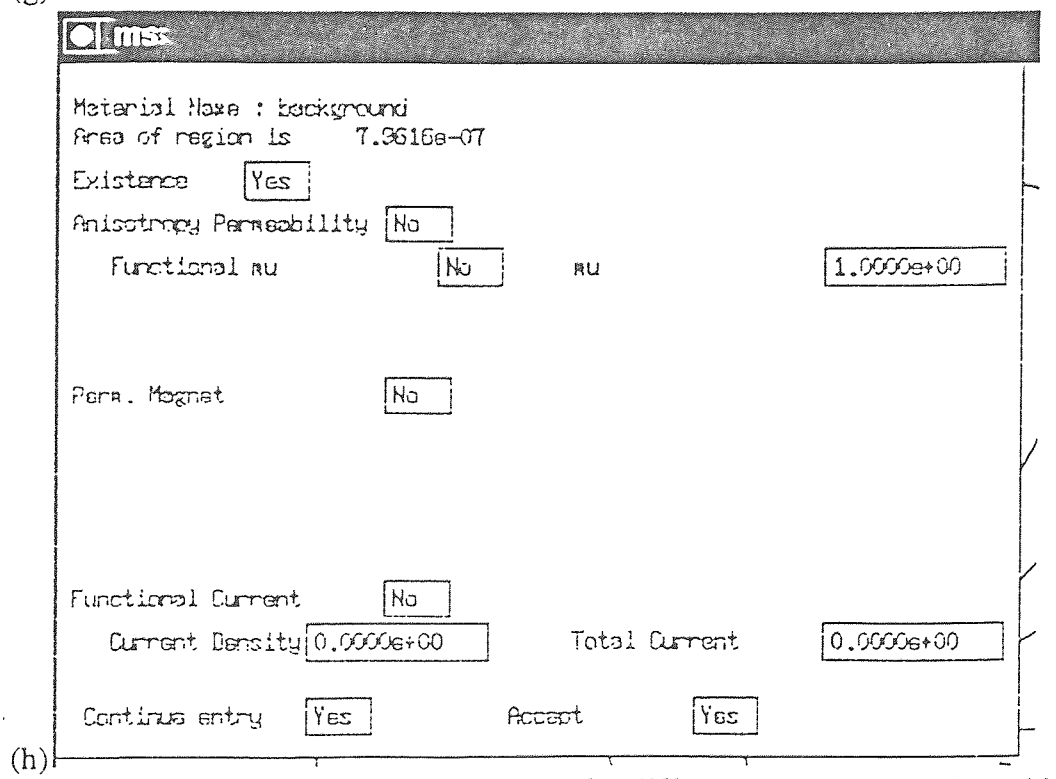

(h)

Figure A.11 Screens of setting the parameters for different materials in this problem: (a), (b), (c), (d) set the currents to the coils wrapped around one stator pole pair; (e) set the relative permeability μ_r to the stator (yoke and poles); (f) set the parameters for the area between the stator and rotor; (g) set the relative permeability μ_r to the rotor; (h) set the parameters to the program running background.

(2) Pick the boundary for solving the problem

Go to the "solve" -- "B Pick" sub-menu (as shown in Figure A.12), choose any command and set up a boundary for this problem.

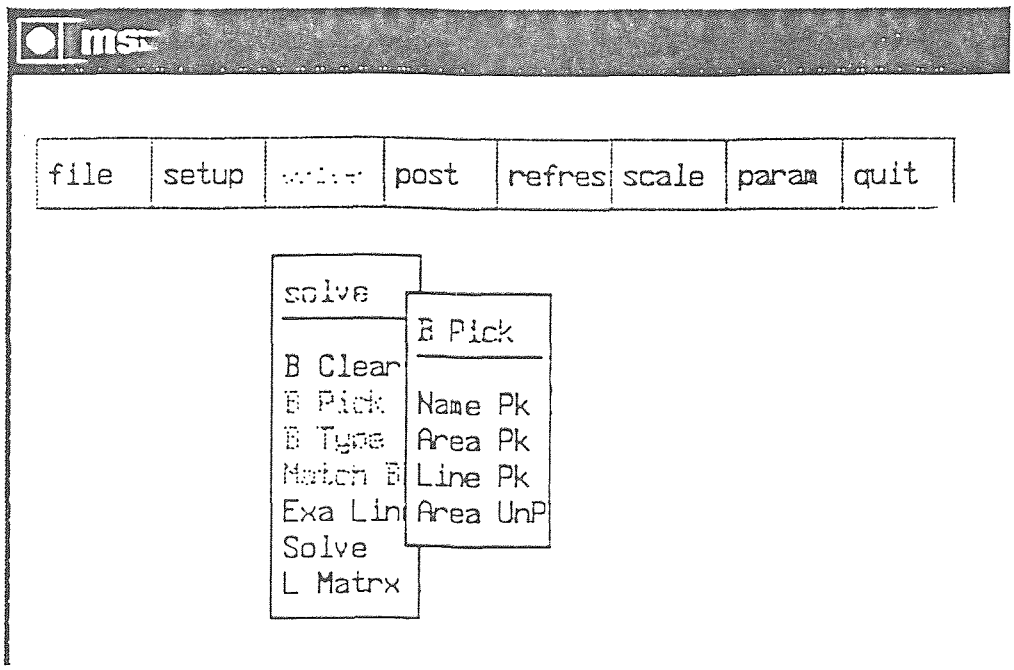

Figure A.12 Screen of "B Pick" sub-menu.

(3) Define the type of the boundary chosen before

After choosing the boundary, then to define the type of this boundary. A "B Type" sub-menu is shown in Figure A.13. "Balloon" is chosen as the boundary for solving this problem.

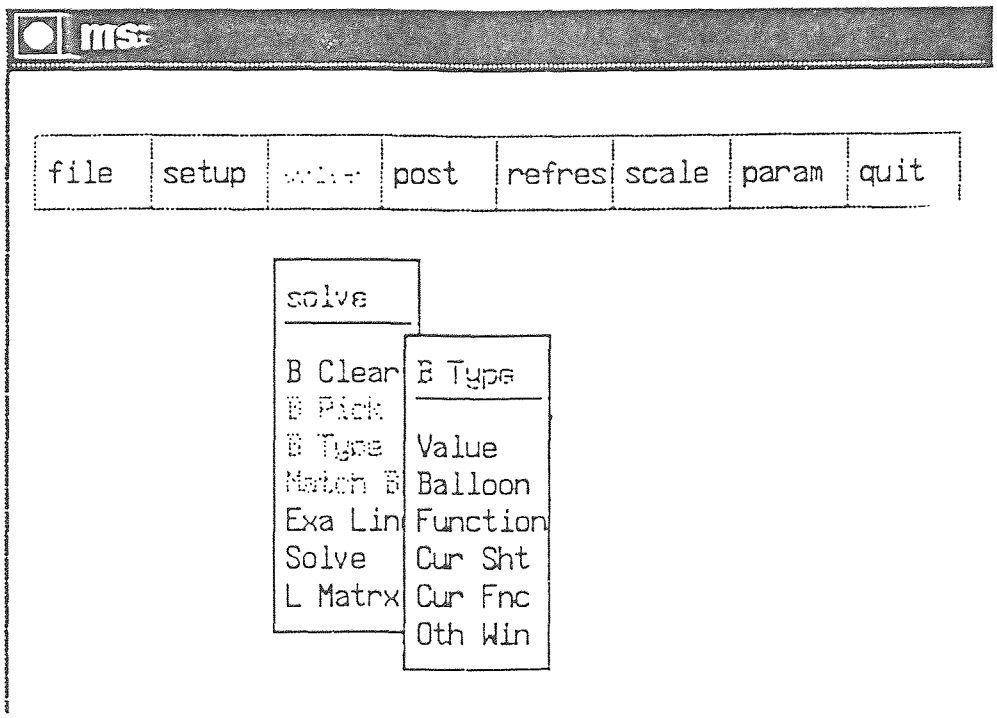

Figure A.13 Screen of "B Type" sub-menu.

(4) Solve the problem

Go to "solve" -- "Solve" and solve the problem. A screen of "Solve" sub-menu is shown in Figure A.14. After the "solve" has finished, some unknown parameters such as torque can be calculated.

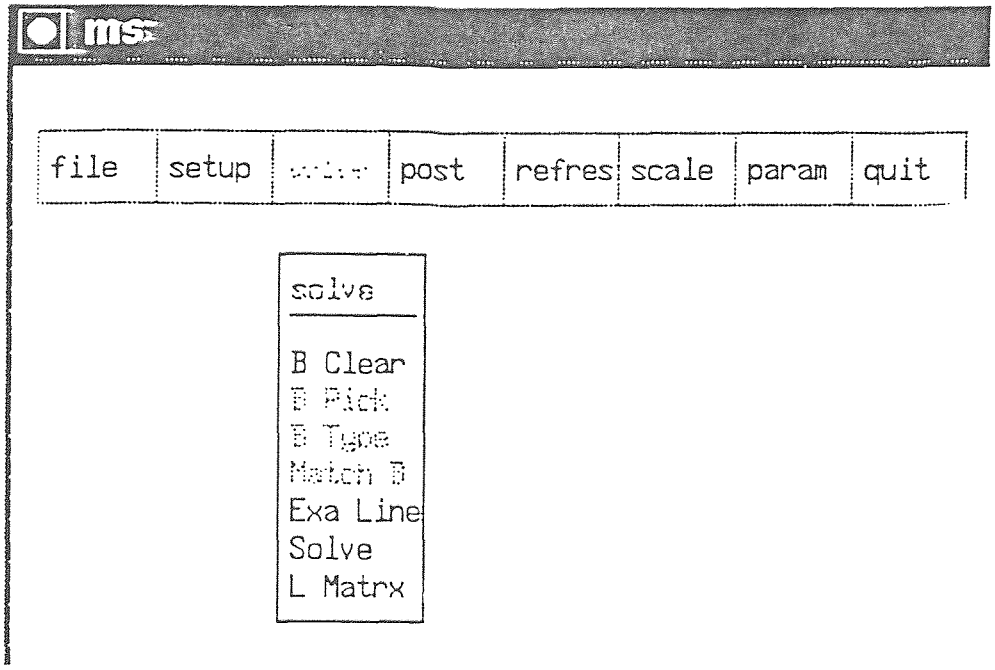

Figure A.14 Screen of "Solve" sub-menu.

(5) Calculate some unknown parameters

Once the solve has completed, go to "post" -- "line" sub-menu (as shown in Figure A.15). First, use "Enter", "Crc Line" or "Obj Line" to choose a line for calculation.

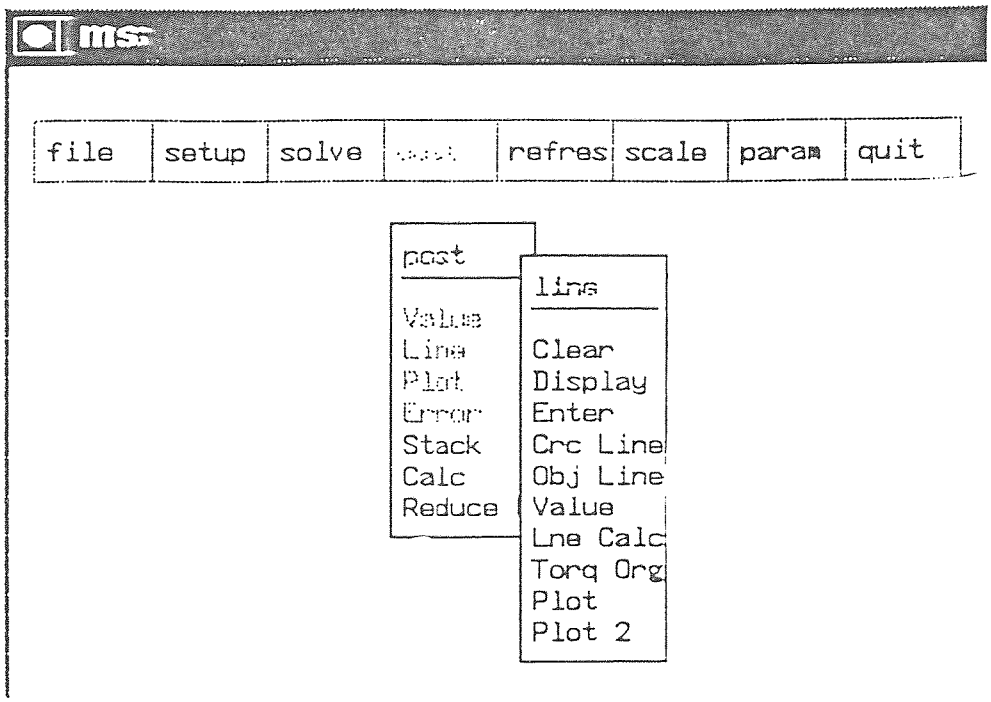

Figure A.15 Screen of "post" -- "line" sub-menu.

Then go to "Lne Calc" sub-menu (as shown in Figure A.16) to calculate some unknown parameters like torque. If calculate the torque, press "t", then key in the "Number of points". Then, press "Return" key to start calculating the torque.

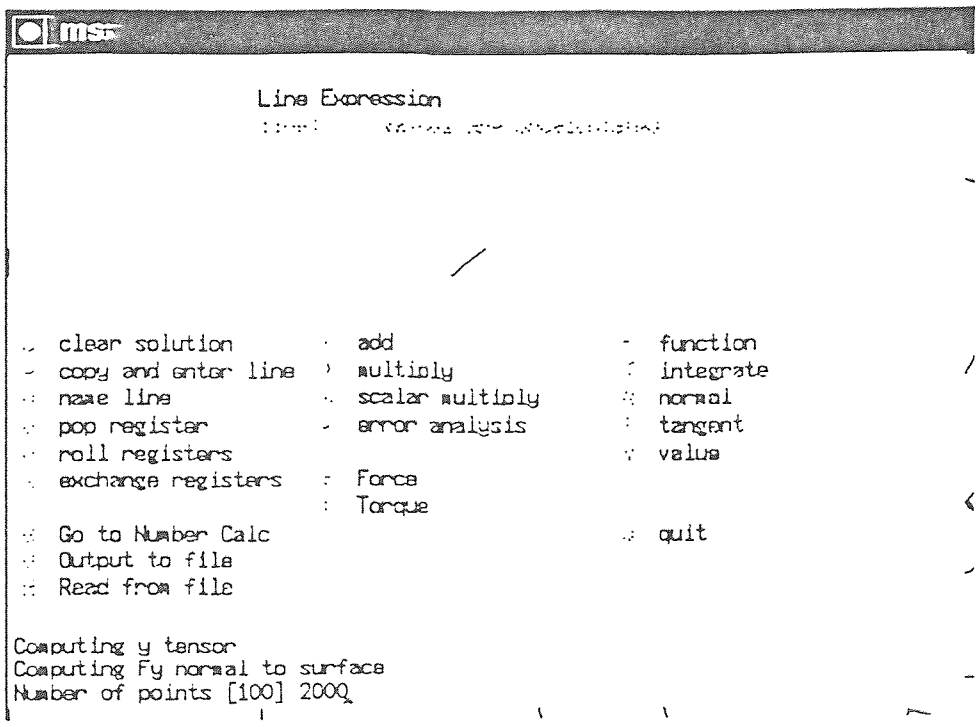

Figure A.16 Screen of "Lne Calc" sub-menu.

The calculating result of the torque is shown in Figure A.17, and the calculating expression is also shown in the figure. The result here is MKS unit, so the unit for the torque is Nt•m. The "-" sign of the torque just means the direction of this torque is counter-clockwise.

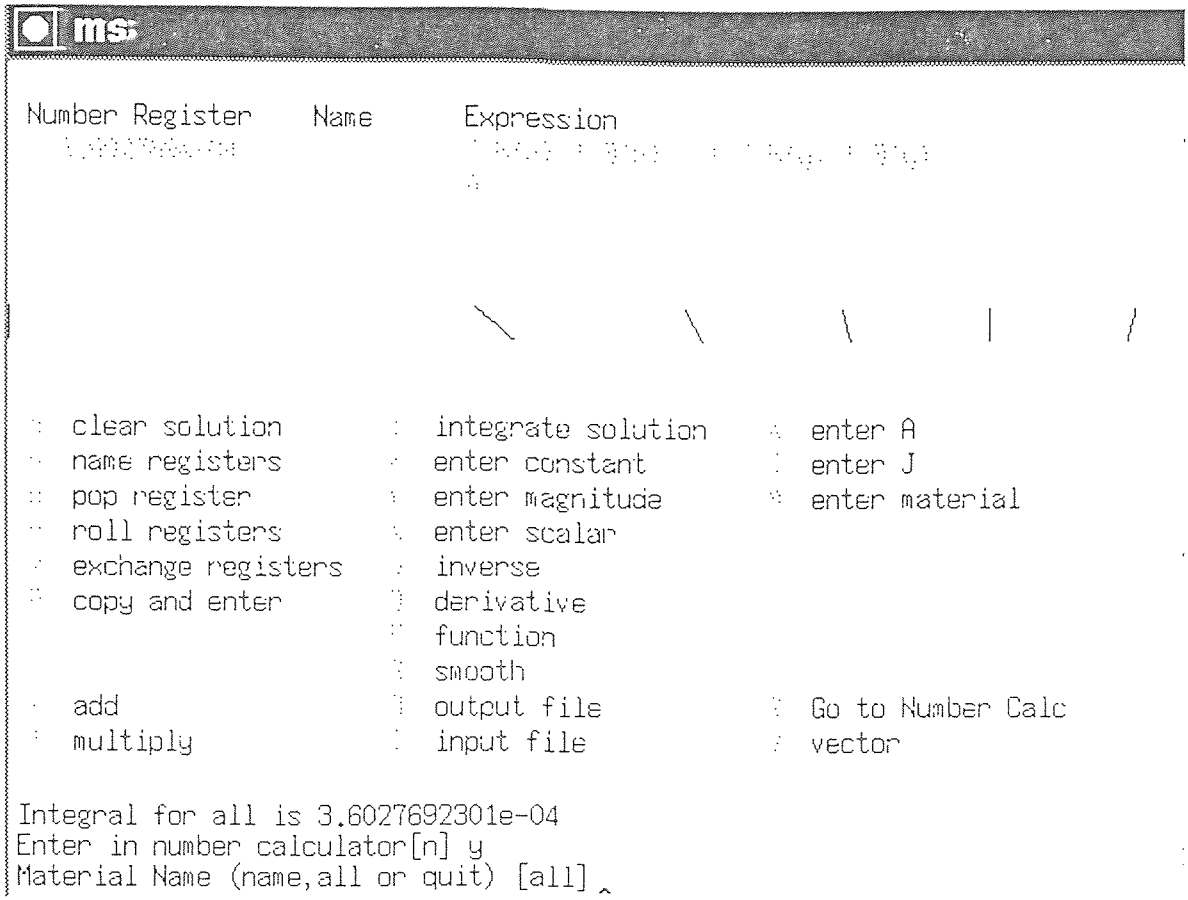

Figure A.17 Screen of "Lne Calc" sub-menu with calculating result.

APPENDIX B

SIMULATION RESULTS FOR CAPACITANCE MODELLING

B.1 Generating and Analyzing a Solution with Electrostat

This section describes how to calculate the capacitance. My goals are to:

- Run the electrostat module and read the mesh
- Generate a solution for the sample problem. The electrostat module calculates electric potential
- Plot lines of equal potential
- Calculate capacitance

The electrostat module contains a special command for capacitances and capacitance matrices. However, for the purpose of illustrating the use of the module, the capacitance will be calculated from the energy of the system.

B.2 Run Electrostat

This section describes how to run the electrostat module in a PC.

(1) Load the Mesh

The same mesh that was read into magnetosta can be read into electrostat. To read in the mesh by using 'file/Read' command, now the mesh is read into the solver.

(2) Overview of the Capacitance Problem

To calculate the capacitance, you will

- Apply 1 volt to the upper side
- Apply 0 volt to the down side assuming that they are both grounded.
- Calculate the total energy of the system using this equation

$$U = \frac{1}{2}\int E \bullet D dv$$

(4) Generate the Solution

Choose solve/solve and accept the default 1.0000 e -4 for final solver residual.

(5) Analyzing the Problem

Plot lines of equal potential. The electrostat module computes the electric potential field. To plot contours of this field, choose post/plot/Equi and accept all of the defaults in the dialog box. The plot drawn as shown in Fig B.2.

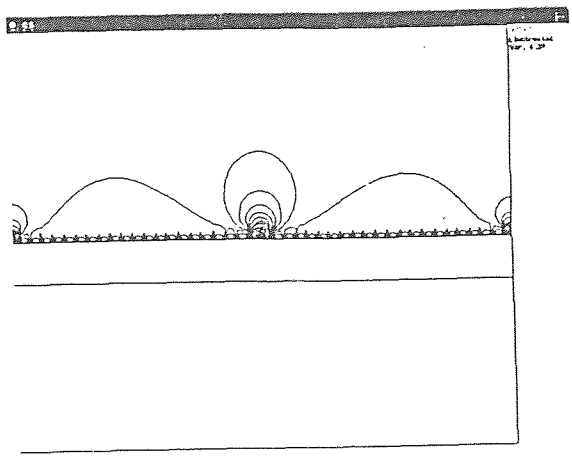

Figure B.2 Electrostat equal potential line

(6) Calculate Capacitance

My goal is to find capacitance by first calculating the energy in the system using this equation:

$$C = \frac{2U}{\Delta V^2}$$

But since ΔV is 1, use following equation:

$$C = \int E \bullet D dv$$

Choose post/calc and a panel appears as shown in Fig B.3. Look at the top portion of the panel and note that phi is the field quantity in the top register.

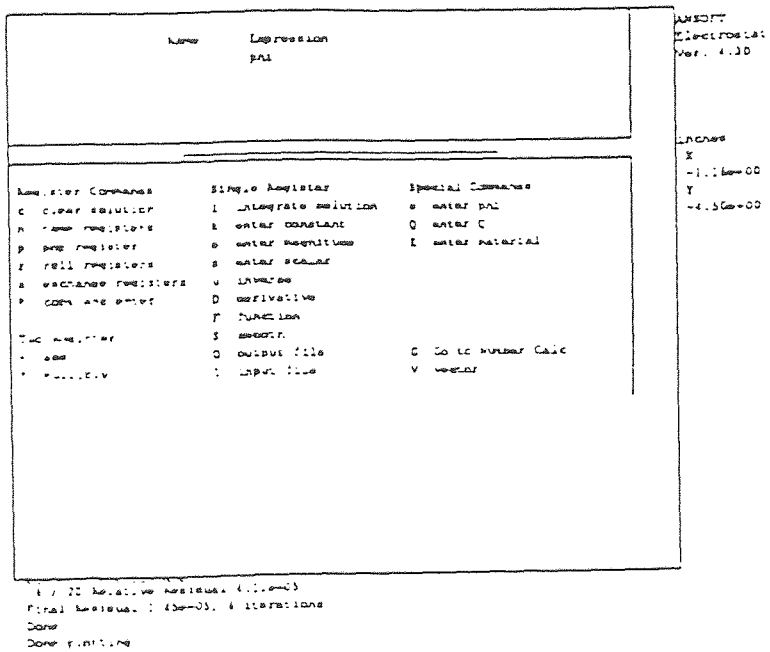

Figure B.3 2D calculator panel for electrostat

(7) Save the Solution

Save the solution to a file. Choose file/S Write. At the File Name Busbar prompt, enter a name other than busbar-don't overwrite the solved files for the magnetostat module.

APPENDIX C

RESULTS OF PSPICE SIMULATION

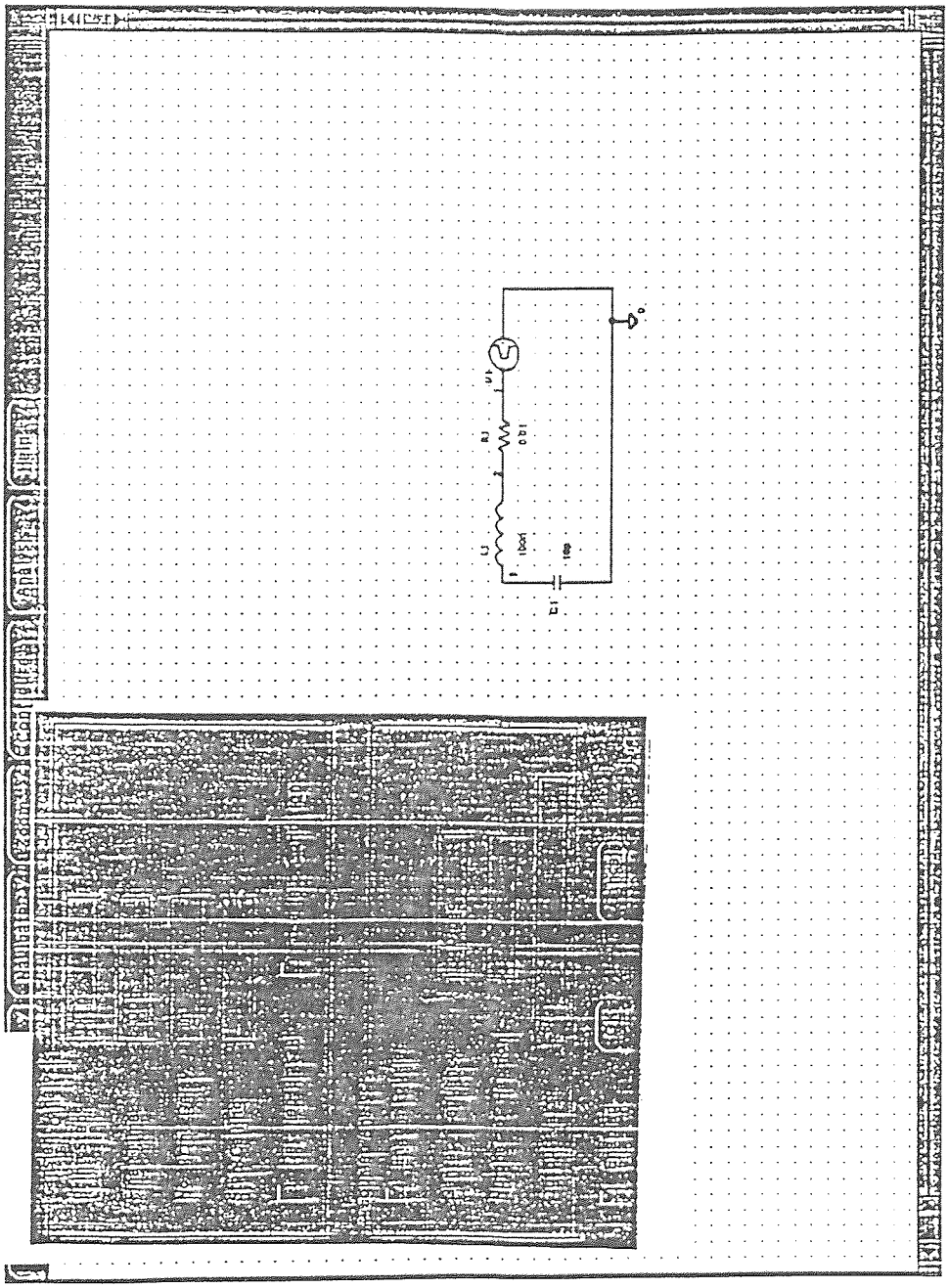

Figure C.1 PSPICE equivalent circuit for resonant frequency

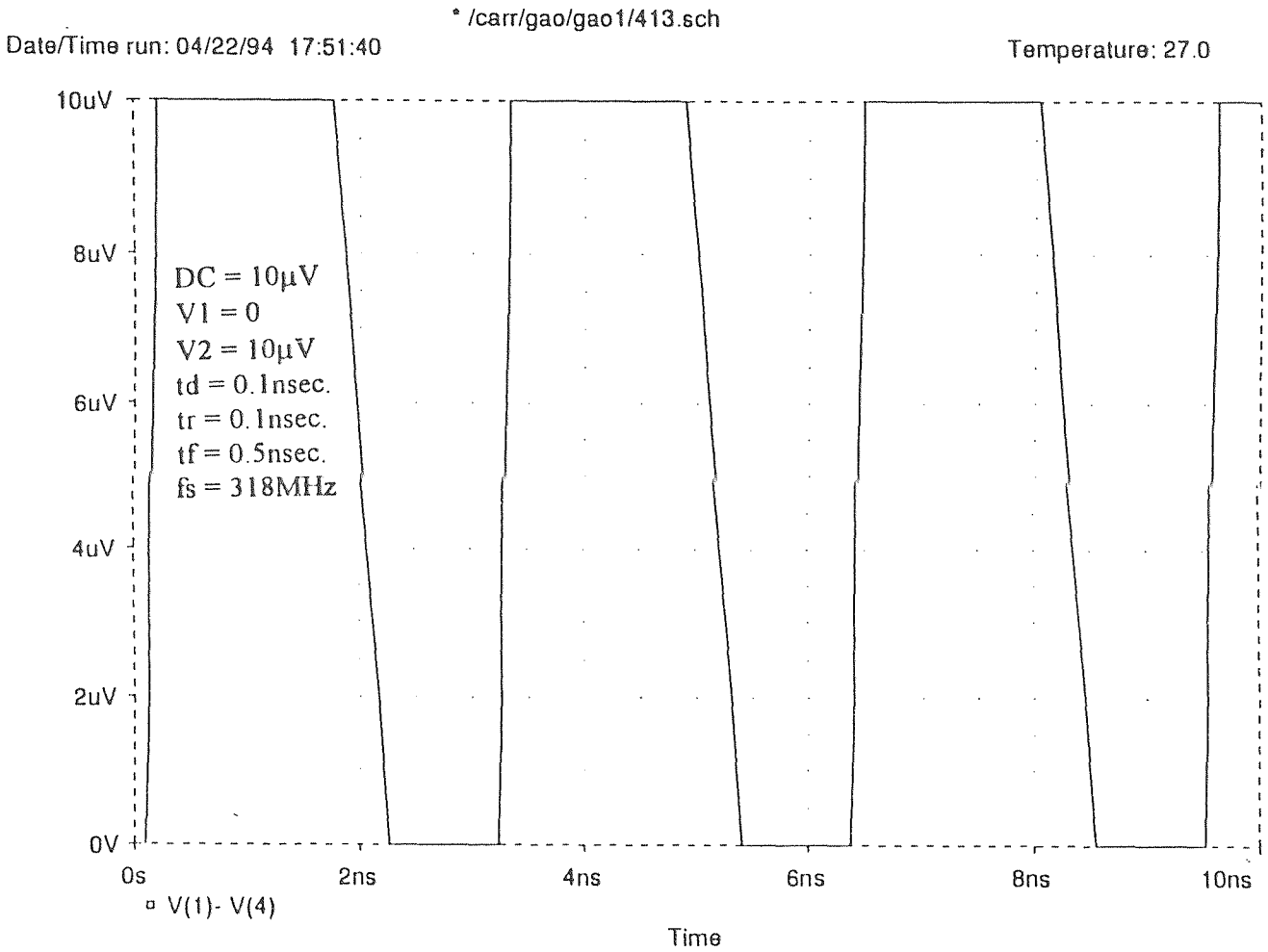

Figure C.2 Plot of pulsed input (the number of input pulses ≈ 17)

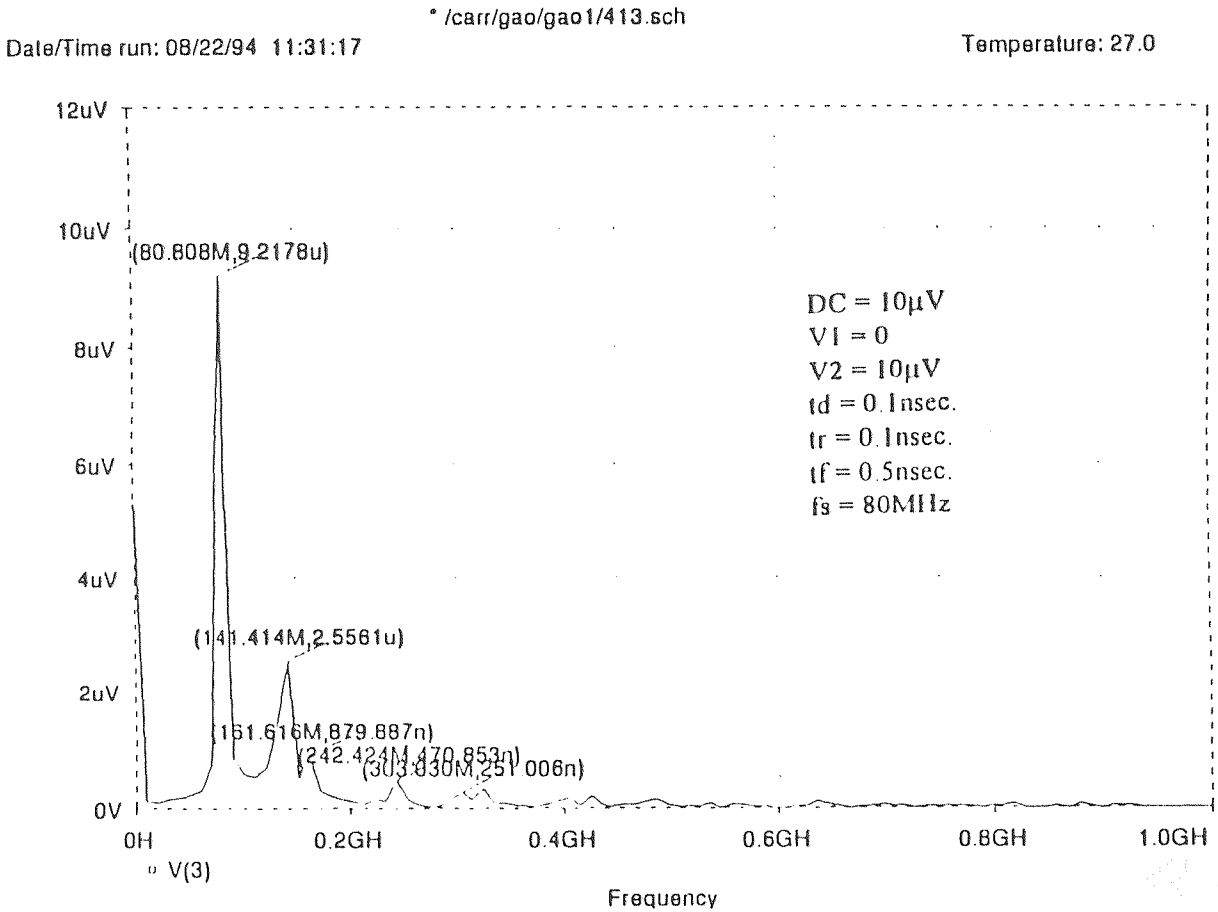

(a)

R=0.01Ω (a) fs=80MHz (b) fs=161MHz (c) fs=242MHz (d) fs=323MHz

fs=318MHz (e) R=0.001Ω (f) R=0.01Ω (g) R=0.1Ω (h) R=1Ω (i) R=10Ω

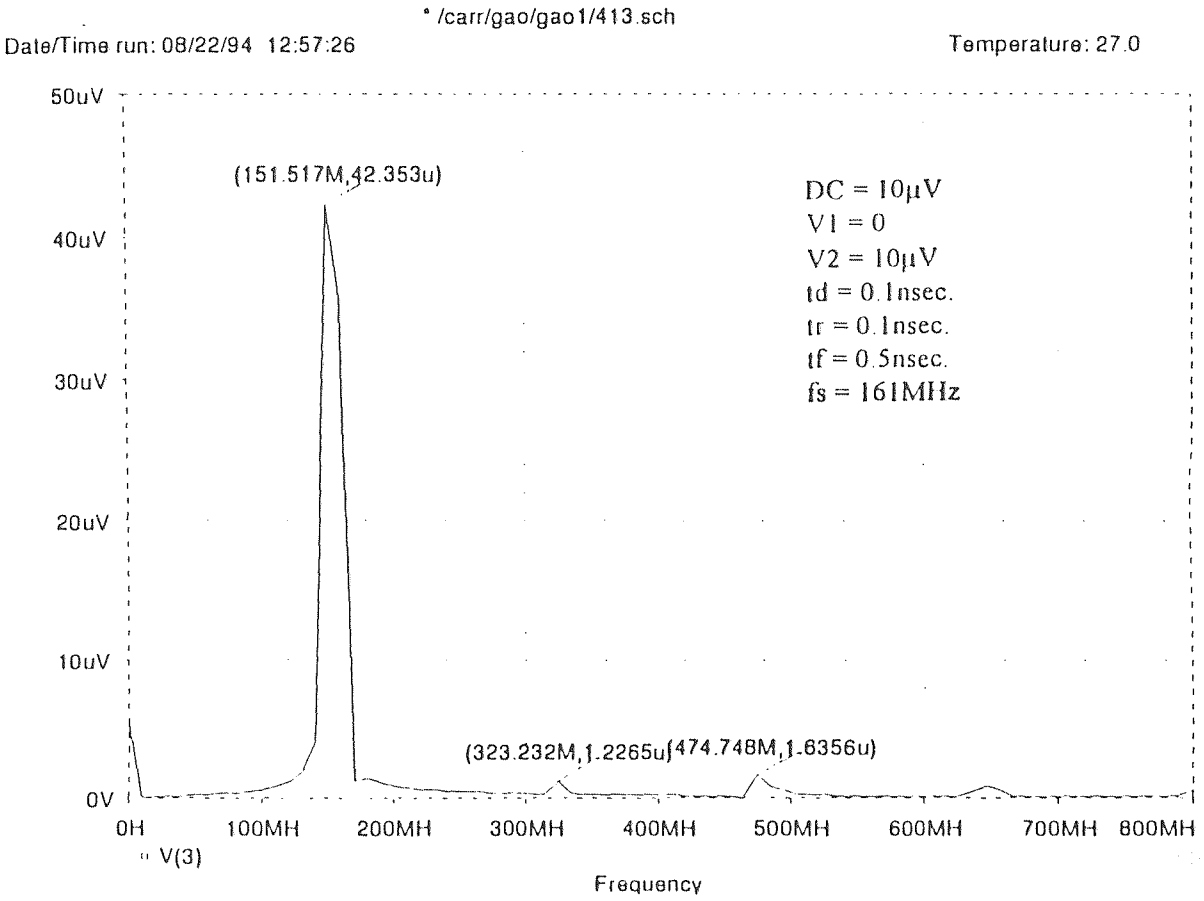

(b)

R=0.01Ω (a) fs=80MHz (b) fs=161MHz (c) fs=242MHz (d) fs=323MHz

fs=318MHz (e) R=0.001Ω (f) R=0.01Ω (g) R=0.1Ω (h) R=1Ω (i) R=10Ω

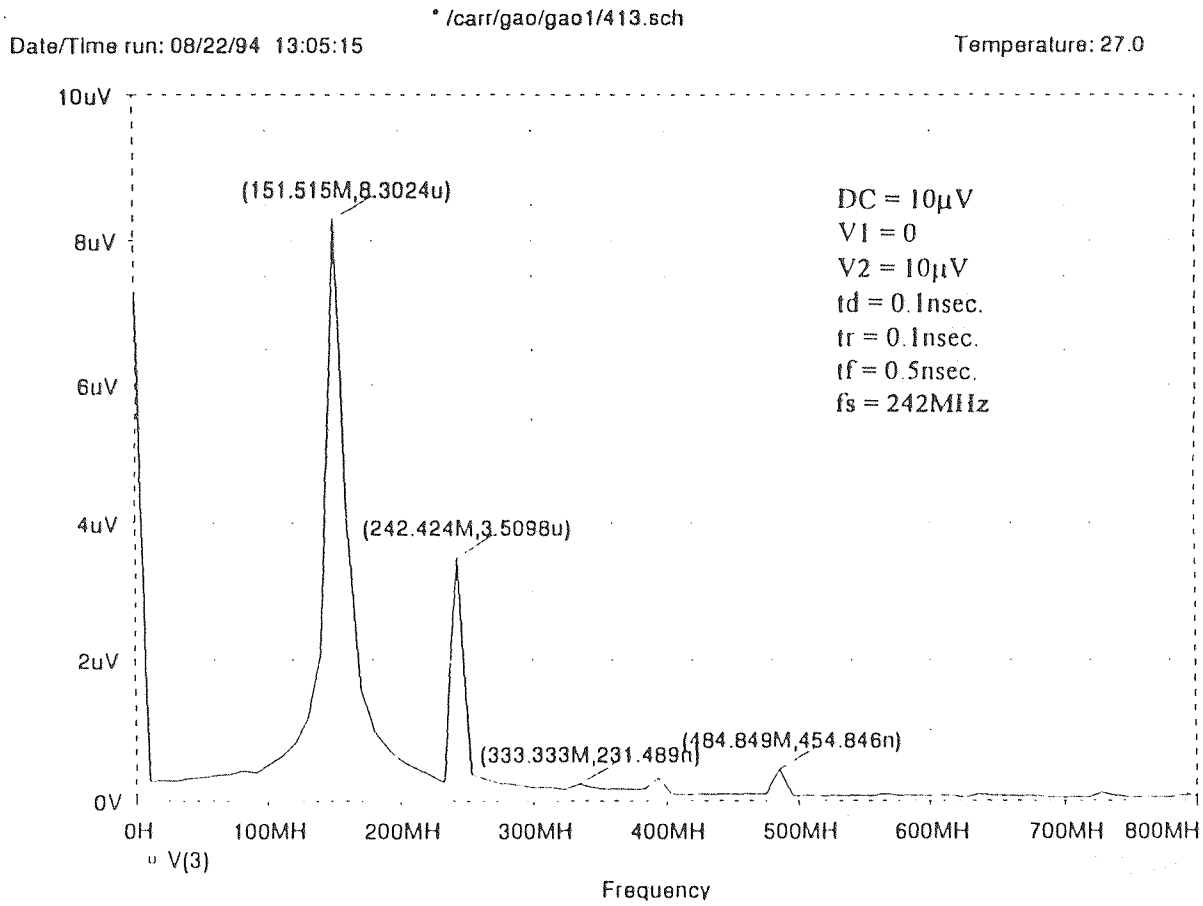

(c)

R=0.01Ω (a) fs=80MHz (b) fs=161MHz (c) fs=242MHz (d) fs=323MHz

fs=318MHz (e) R=0.001Ω (f) R=0.01Ω (g) R=0.1Ω (h) R=1Ω (i) R=10Ω

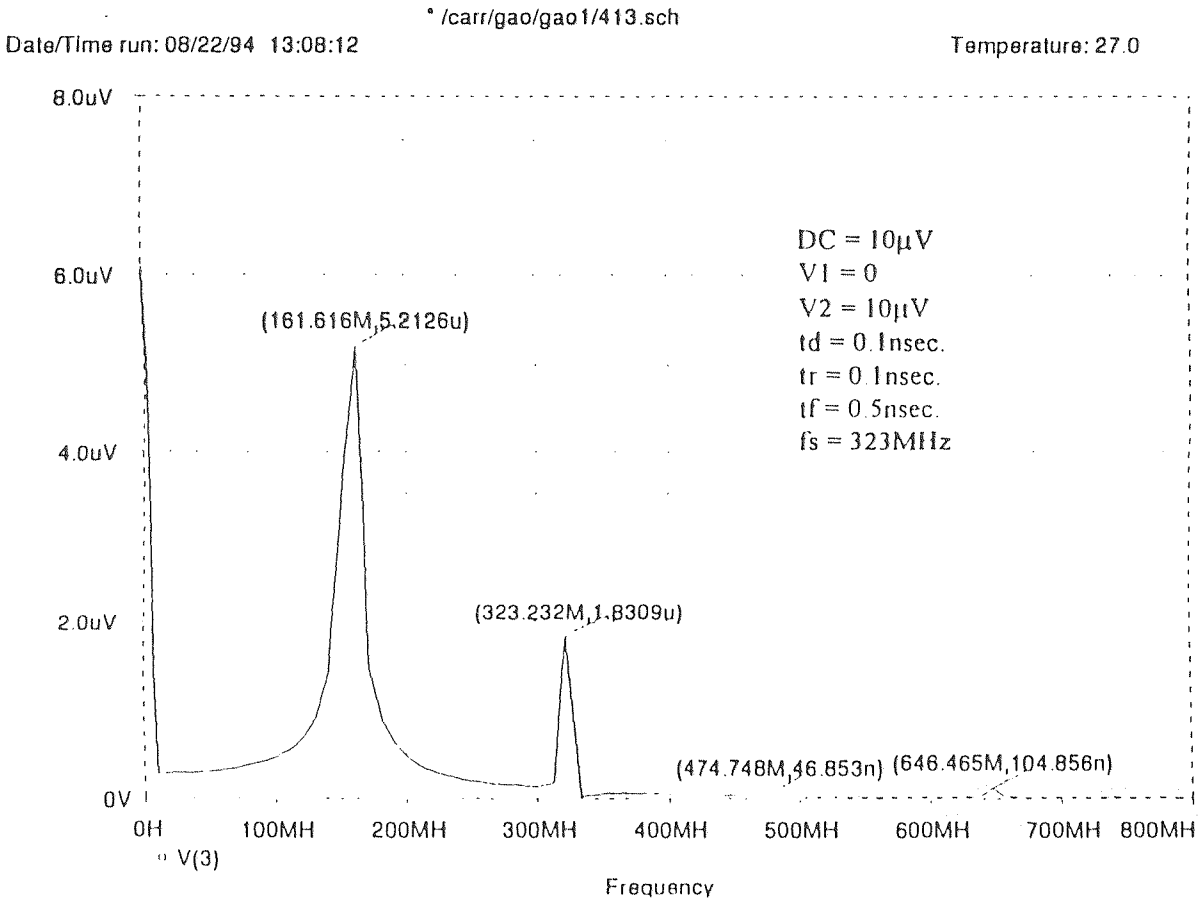

(d)

R=0.01Ω (a) fs=80MHz (b) fs=161MHz (c) fs=242MHz (d) fs=323MHz

fs=318MHz (e) R=0.001Ω (f) R=0.01Ω (g) R=0.1Ω (h) R=1Ω (i) R=10Ω

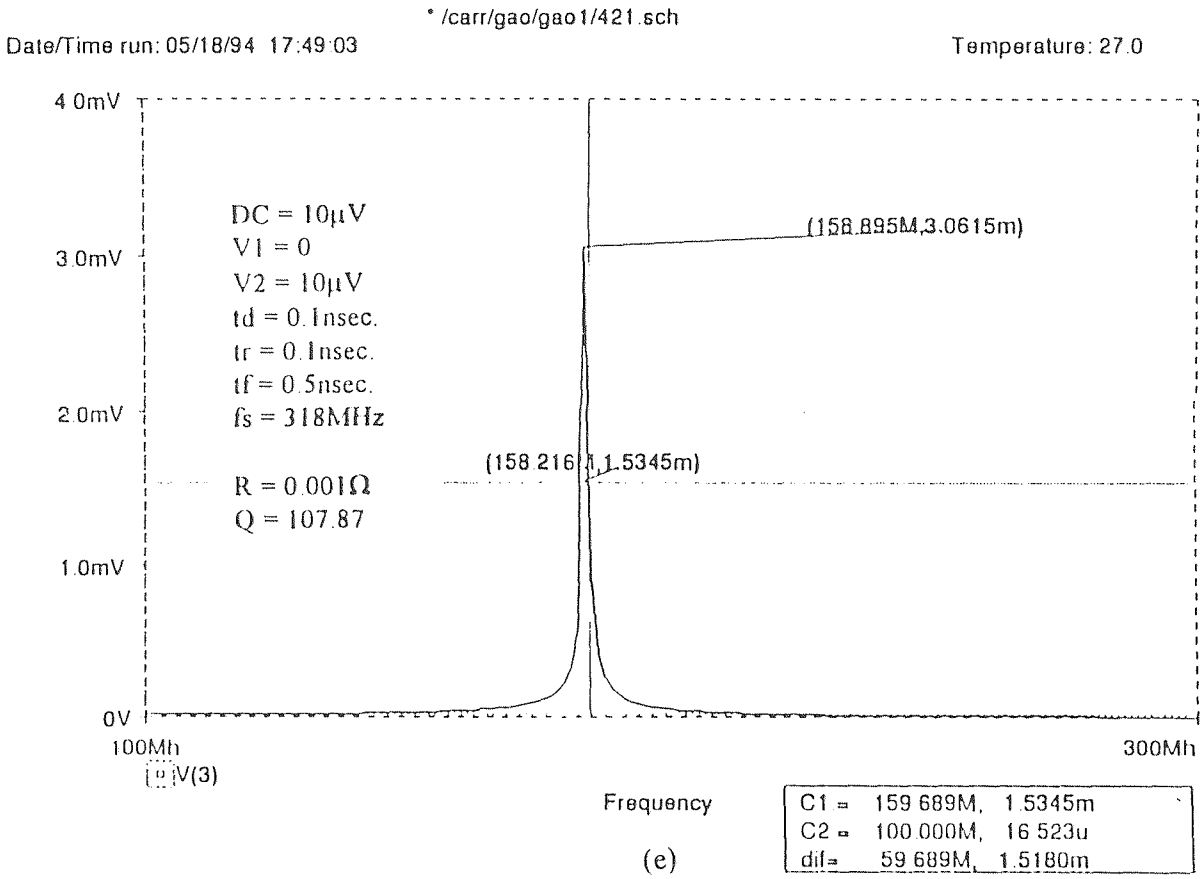

R=0.01Ω (a) fs=80MHz (b) fs=161MHz (c) fs=242MHz (d) fs=323MHz

fs=318MHz (e) R=0.001Ω (f) R=0.01Ω (g) R=0.1Ω (h) R=1Ω (i) R=10Ω

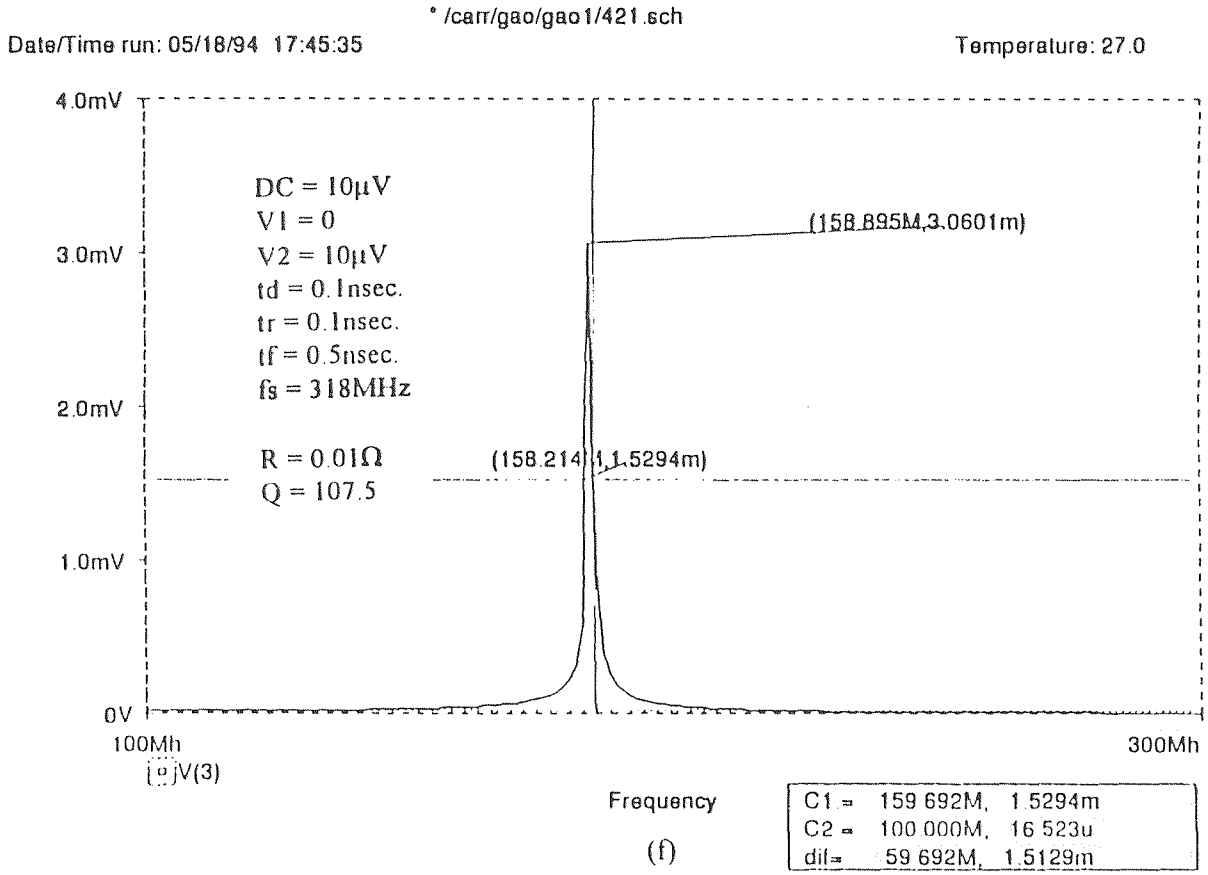

R=0.01Ω (a) fs=80MHz (b) fs=161MHz (c) fs=242MHz (d) fs=323MHz

fs=318MHz (e) R=0.001Ω (f) R=0.01Ω (g) R=0.1Ω (h) R=1Ω (i) R=10Ω

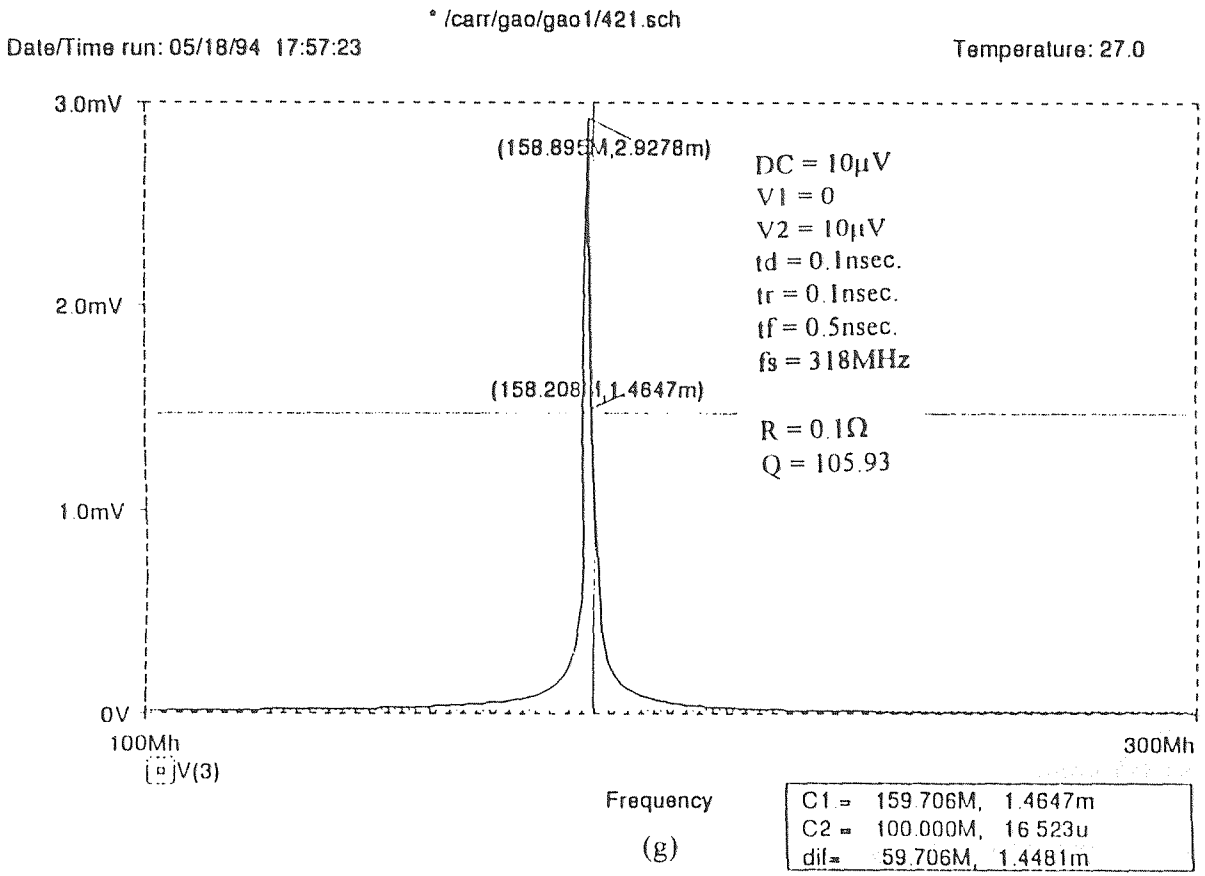

(g)

R=0.01Ω (a) fs=80MHz (b) fs=161MHz (c) fs=242MHz (d) fs=323MHz

fs=318MHz (e) R=0.001Ω (f) R=0.01Ω (g) R=0.1Ω (h) R=1Ω (i) R=10Ω

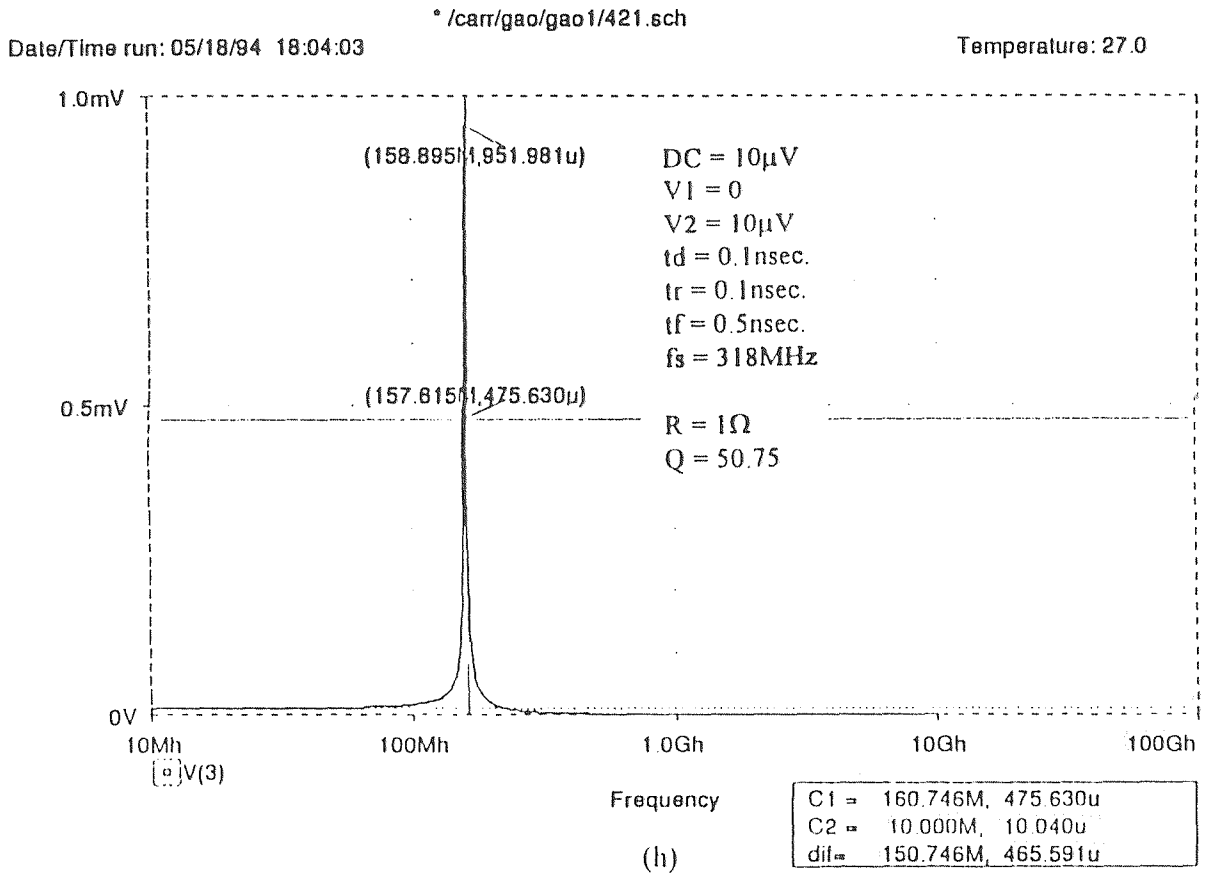

(h)

R=0.01Ω (a) fs=80MHz (b) fs=161MHz (c) fs=242MHz (d) fs=323MHz

fs=318MHz (e) R=0.001Ω (f) R=0.01Ω (g) R=0.1Ω (h) R=1Ω (i) R=10Ω

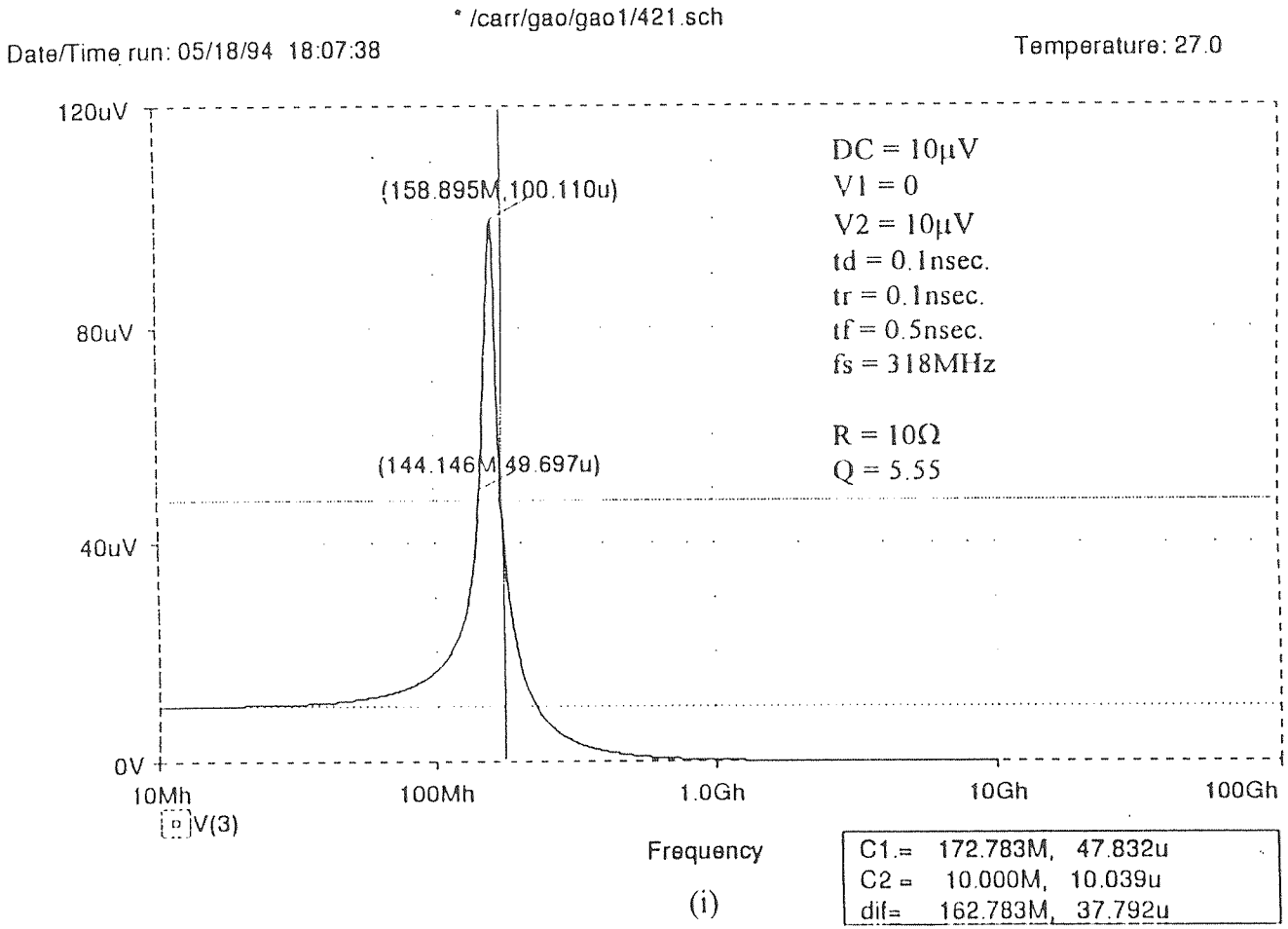

(i)

Figure C.3 Device B plot of output voltage vs frequency for pulsed input burst Vs

R=0.01Ω (a) fs=80MHz (b) fs=161MHz (c) fs=242MHz (d) fs=323MHz

fs=318MHz (e) R=0.001Ω (f) R=0.01Ω (g) R=0.1Ω (h) R=1Ω (i) R=10Ω

```
**** 08/22/94 13:08:12 ******** PSpice 5.2a (Nov 1992) ******** ID# 61746 ****

 * /carr/gao/gaol/413.sch

 ****     CIRCUIT DESCRIPTION

*******************************************************************************



* Schematics Version 5.2 - July 1992
* Mon Aug 22 13:08:09 1994

* From [SCHEMATICS NETLIST] section of msim.ini:
.LIB

.INC "/carr/gao/gaol/413.net"

**** INCLUDING /carr/gao/gaol/413.net ****
* Schematics Netlist *

R_R1      2 1 0.01
L_L1      3 2 100n
C_C1      0 3 10p
V_V1      1 0 dc 0.00001v ac 0.00001
+PULSE 0 0.00001v 0.1n 0.1n 0.5n 1.545n 3.09n

**** RESUMING /carr/gao/gaol/413.cir ****
.INC "/carr/gao/gaol/413.als"

**** INCLUDING /carr/gao/gaol/413.als ****
* Schematics Aliases *

.ALIASES
R_R1          R1(1=2 2=1 )
L_L1          L1(1=3 2=2 )
C_C1          C1(1=0 2=3 )
V_V1          V1(+=1 -=0 )
_     _(1=1)
_     _(2=2)
_     _(3=3)
.ENDALIASES


**** RESUMING /carr/gao/gaol/413.cir ****

** Analysis setup **
.tran 0.1ns 100ns 1n UIC
.four 160meg 8 v([3])



.END
```

**** 08/22/94 13:08:12 ******** PSpice 5.2a (Nov 1992) ******** ID# 61746 ****

* /carr/gao/gao1/413.sch

**** FOURIER ANALYSIS TEMPERATURE = 27.000 DEG C

****

FOURIER COMPONENTS OF TRANSIENT RESPONSE V(3)

DC COMPONENT = 5.926134E-06

HARMONIC NO	FREQUENCY (HZ)	FOURIER COMPONENT	NORMALIZED COMPONENT	PHASE (DEG)	NORMALIZED PHASE (DEG)
1	1.600E+08	6.332E-06	1.000E+00	-1.497E+02	0.000E+00
2	3.200E+08	1.815E-06	2.866E-01	-8.985E+01	5.980E+01
3	4.800E+08	4.893E-08	7.727E-03	1.668E+02	3.165E+02
4	6.400E+08	9.330E-08	1.473E-02	1.162E+02	2.658E+02
5	8.000E+08	4.933E-08	7.791E-03	-1.086E+02	4.102E+01
6	9.600E+08	3.862E-08	6.099E-03	-1.590E+02	-9.381E+00
7	1.120E+09	5.669E-08	8.953E-03	-1.248E+02	2.484E+01
8	1.280E+09	7.859E-08	1.241E-02	-1.315E+02	1.811E+01

TOTAL HARMONIC DISTORTION = 2.876676E+01 PERCENT

JOB CONCLUDED

TOTAL JOB TIME 4.05

APPENDIX D

PHYSICAL LAYOUT

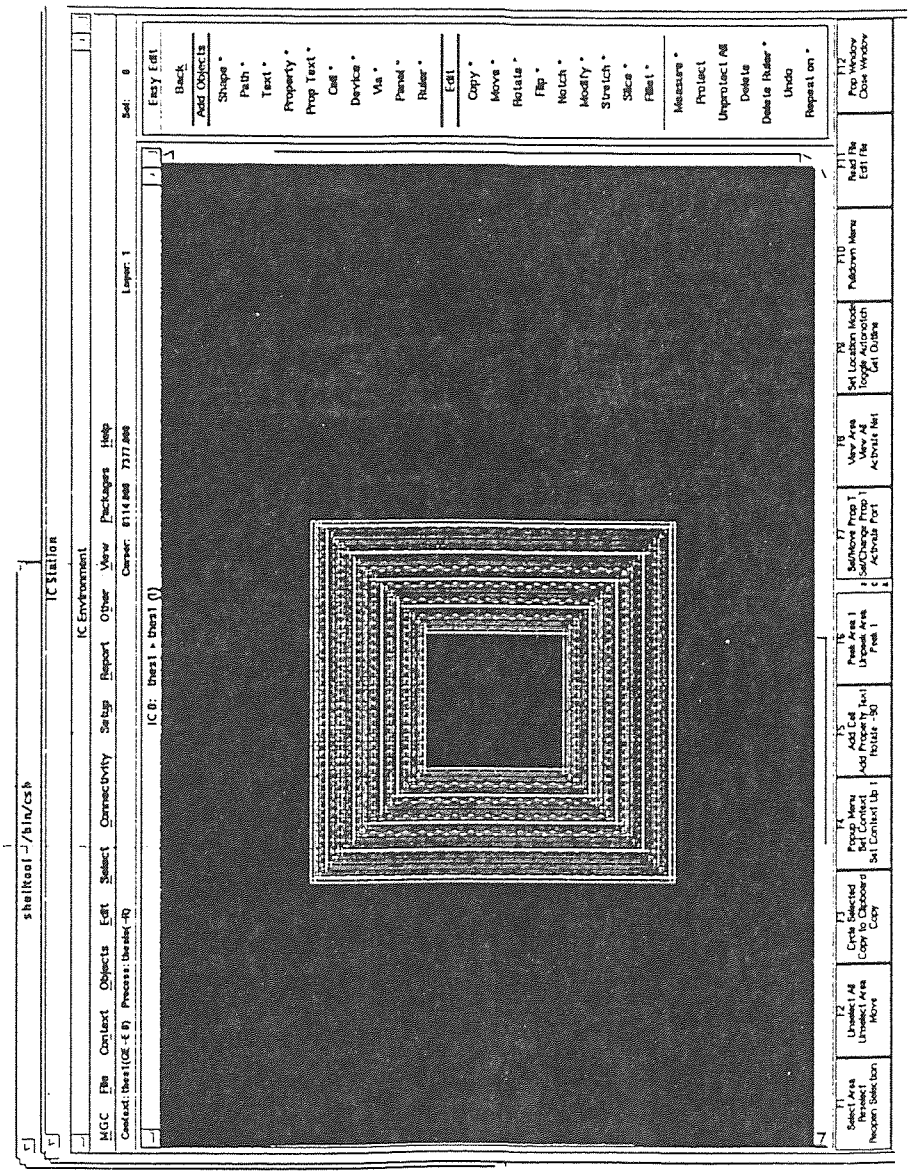

(a)

w=30μm S=10μm L=2mm n=20 thichness=10μm

Figure D.1 Layout of the pressure sensor (a) bottom wafer-metal1

(b) bottom wafer via (c) top wafer-metal2

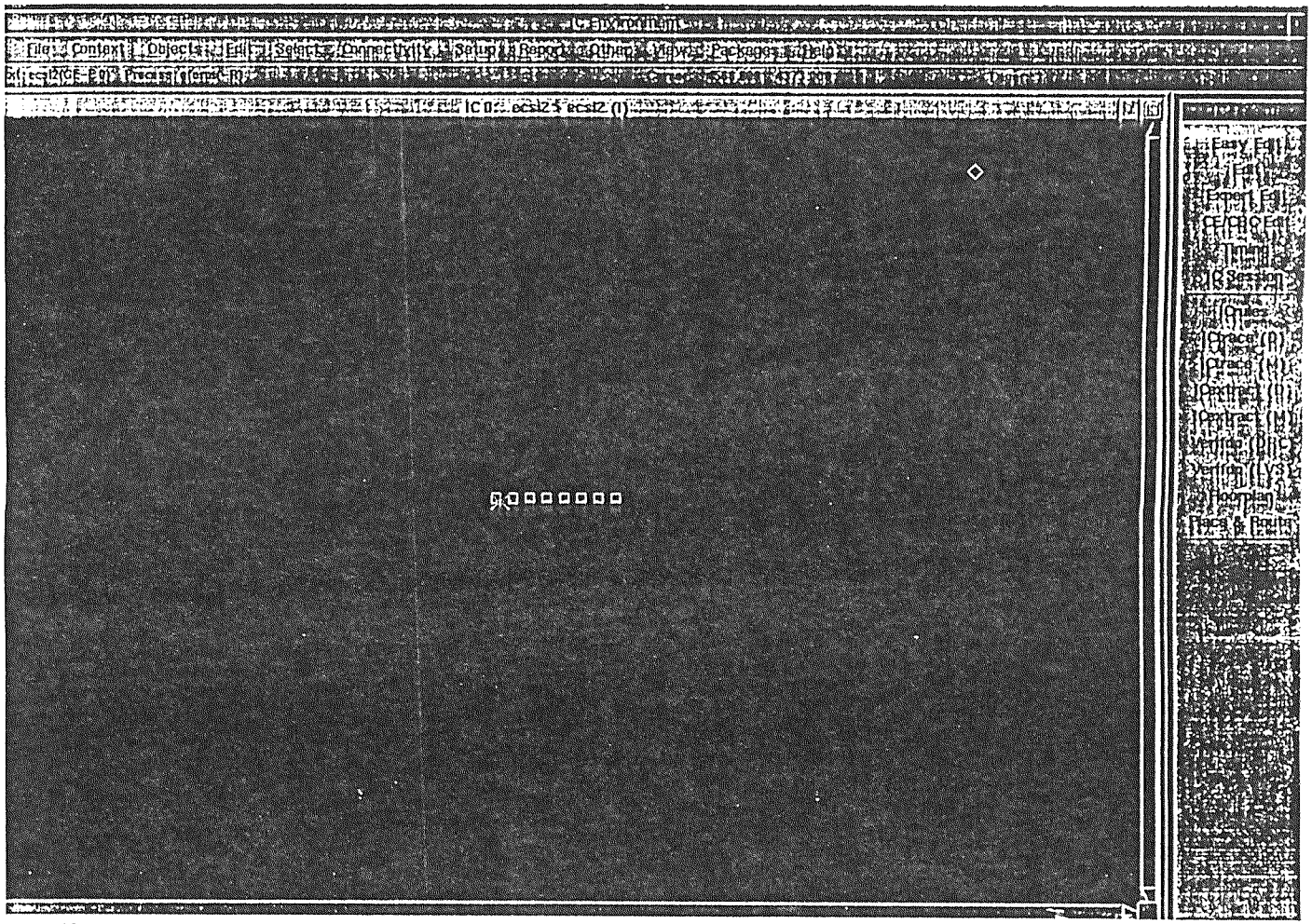

(b)

Figure D.1 Layout of the pressure sensor (a) bottom wafer-metal1

(b) bottom wafer via (c) top wafer-metal2

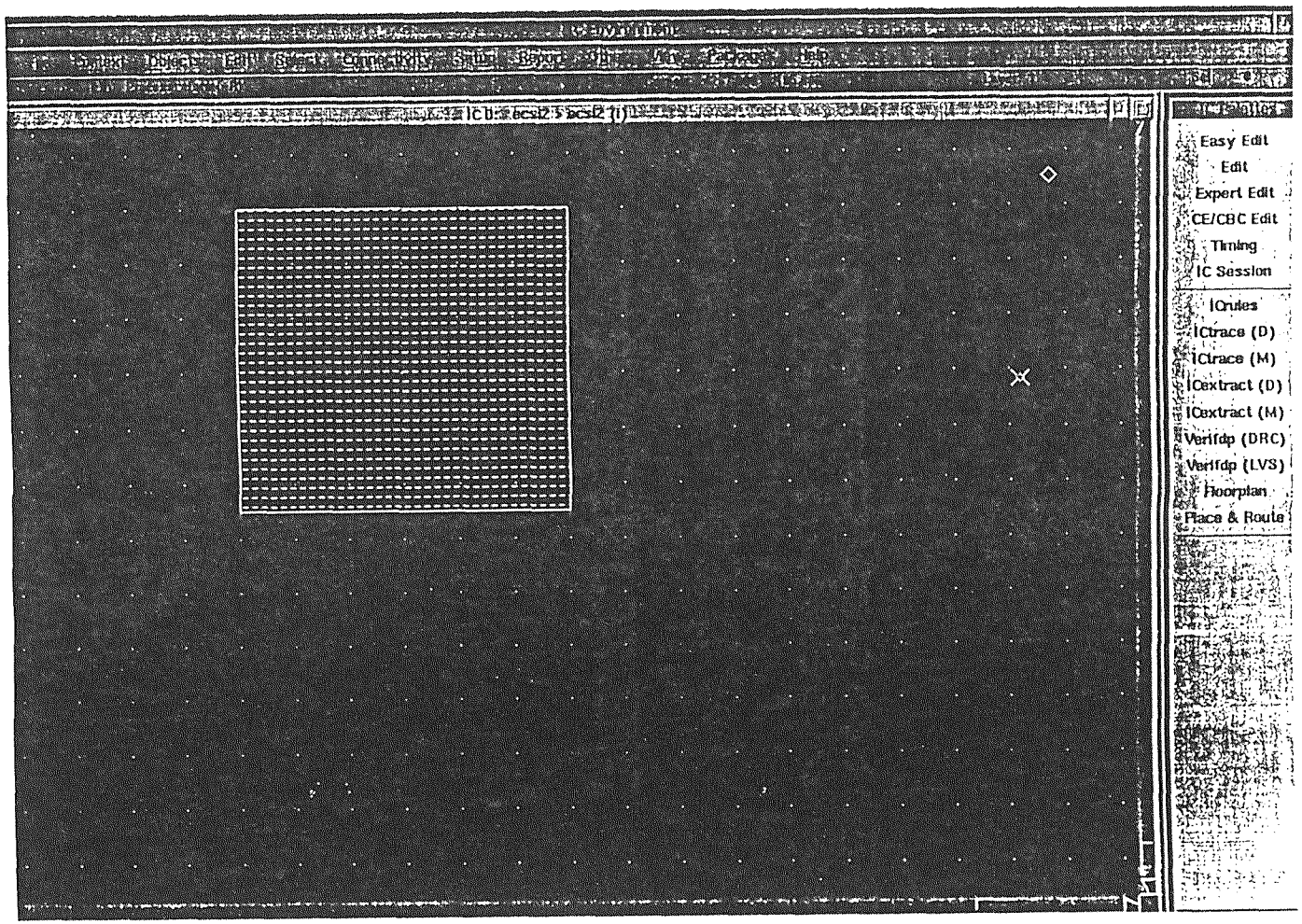

(c)

Figure D.1 Layout of the pressure sensor (a) bottom wafer-metal1

(b) bottom wafer via (c) top wafer-metal2

REFERENCES

1. Jacob Kline, *Handbook of Biomedical Engineering*, Academic Press Inc.: London, pp. 472, 1988.

2. Stuart R. Mackay, *Biomedical Telemetry*, John Wiley & Sons, Inc.: New York, NY, pp. 298, 1970.

3. C. C. Collins, "Miniature Passive Pressure Transensor for Implanting in the Eye," *IEEE Transactions On Bio-Medical Engineering*, vol. BME-14, Vul No.2, April, 1967.

4. Peggy Hollingsworth, "Heart & Lung," *Journal of Critical Care*, vol. 17, pp. 111-117, March 1988.

5. Cesar A. Caceres, *Biomedical Telemetry*, Academic Press Inc.: London, pp. 3, 1965.

6. Anshumat Parasar, *Design and Analysis of an Intracranial Pressure and Temperature Sensor Telemetry System*, M.S. Thesis, New Jersey Institute of Technology, 1989.

7. H. M. Greenhouse, "Design of Planar Rectangular Microelectronic Inductors," *IEEE Trans. Parts, Hybrids, and Packaging*, vol. PHP-10, pp. 101-109, June 1974.

8. Michael J. Smith, "Analysis, Design and Performance of a Capacitive Pressure Sensor IC," *IEEE Trans. Biomedical Engineering*, vol. BME-33, pp. 163-174, Feb. 1986.

9. A. E. H. Love, *A Treatise on the Mathematical Theory of Elasticity*, Dover Publications, New York, NY, pp. 495,1944.

10. F. R. Gleason, "Thin-Film Microelectronic Inductors," *Proceedings of the National Electronics Conference 20*, pp. 197-198, 1964.

11. H. G. Dill, "Designing Inductors for Thin-Film Applications," *Electronic Design*, pp. 52-59, 1964.

12. Wolf D. Frobenius, "A Microminiature Solid-state Capacitive Blood Pressure Transducer with Improved Sensitivity," *IEEE Trans. Biomedical Engineering*, pp. 312-314, July 1973.

13. Fred J. Weibell, *Biomedical Instrumentation and Measurements*, Prentice-Hall, Inc.: New Jersey, NJ, pp. 316, 1980.

14. Masaki Hirata, "Diaphragm Thickness Control in Silicon Pressure Sensors Using an Anodic Oxidation Etch-Stop," *Journal of Electrochemical Society*, vol. 134, No.8, Aug. 1987.

15. Ylva Backlund, "Passive Silicon Transensor Intended for Biomedical, Remote Pressure Monitoring," *Abstracts of Transducers*, 89 COMST Publishers, Lausanne, Switzerland, June 25-30, 1989.

16. Wen H. Ko, "A High-Sensitivity Integrated Circuit Capacitive Pressure Transducer," *IEEE Trans. Electronic Devices*, vol. ED-29, pp. 48-56, Jan. 1982.

17. Harold A. Wilkinson, *Journal of Neurosurgery*, vol. 1, No.2, pp. 139-141, 1977.

18. S. Timoshenko, *Theory of Plates and Shells*, McGraw Hill Book Company, New York, NY, pp. 55, 202, 1987.

19. Masayoshi Esahi, "Fabrication of Catheter-Tip and Sidewall Miniature Pressure," *IEEE Trans. Electronic Devices*, vol. ED-29, pp. 57-60, Jan. 1982.

20. Frederick W. Grover, *Inductance Calculations, Dover Publications*, Inc.: New York, NY, 1973.

21. Ewald Pettenpaul, "CAD Models of Lumped Elementson GaAs up to 18 GHz," *IEEE Trans. Microwave Theory and Tech.*, vol. 36, No.2, Feb. 1988.

22. Probhakar Gorty, *Endoradiosonde Pressure Sensor System for Chronic Biomedical Monitoring*, M.S. thesis, New Jersey Institute of Technology, 1990.

23. Gorty Prabhakar and William N. Carr, *Proc. of the IEEE 12th Annual Conf. on Engineering in Medicine and Biology*, Philadelphia, USA, Nov. 1-4, 1990.